2016

Building and Optimizing a Spectroelectrochemical System for the Study of Shewanella Putrefaciens

Jonathan Muscolino
Loyola University Chicago

LOYOLA UNIVERSITY CHICAGO

BUILDING AND OPTIMIZING A SPECTROELECTROCHEMICAL SYSTEM FOR THE STUDY OF *SHEWANELLA PUTREFACIENS*

A THESIS SUBMITTED TO

THE FACULTY OF THE GRADUATE SCHOOL

IN CANDIDACY FOR THE DEGREE OF

MASTER OF SCIENCE

PROGRAM IN CHEMISTRY

BY

JONATHAN MUSCOLINO

CHICAGO, IL

DECEMBER 2016

ACKNOWLEDGMENTS

I would like to thank my mother and father for supporting me during my time at Loyola University and Dr. Alanah Fitch for giving me the opportunity to advance my knowledge and for introducing me into the world of electrochemistry.

TABLE OF CONTENTS

LIST OF TABLES

LIST OF FIGURES

LIST OF ABBREVIATIONS

Abbreviation	Definition
ATR	Attenuated total reflection
CEC	Cation exchange capacity
CME	Clay modified electrode
CPE	Controlled potential electrolysis
CR	Capacitance ratio
CV	Cyclic voltammogram
DET	Direct electron transfer
DI	Deionized
DIRB	Dissimilatory iron-reducing bacterium
E_i	Initial/starting potential
E_{pa}	Anodic peak potential
E_{pc}	Cathodic peak potential
E_{sw}	Switching potential in a cyclic voltammogram
EA-IOW	Electroactive integrated optical waveguide
i_o	Oxidative current
i_r	Reduction current
I_{oCPE}	Reference light spectra taken at beginning of CPE
I_{oCV}	Reference light spectra taken at beginning of a CV

I_{pa}	Anodic peak current
I_{pc}	Cathodic peak current
IOW	Integrated optical waveguide
IR	Infrared
ITO	Indium tin oxide
MET	Mediated electron transfer
MFC	Microbial fuel cell
MIR	Mid-infrared
OD_{650}	Optical density at 650nm
OTE	Optically transparent electrode
RI	Refractive index
$[Ru(bpy)_3]^{2+}$	Tris(2,2'-bipyridyl)ruthenium(II) chloride hexahydrate
SWy-1	Standard Wyoming Montmorillonite
TIR	Total internal reflection
TSB	Tryptic soy broth
UV-Vis	Ultraviolet-Visible spectroscopy

ABSTRACT

Shewanellaceae are among the most widely studied electroactive microorganisms. This study reports on *Shewanella putrefaciens* under anaerobic conditions during applied potential while monitored by spectroscopy. The attachment of the microbe *Shewanella putrefaciens* onto an indium tin oxide electrode was found to occur after 2 hr of +0.2 V applied potential. Microbial detachment occurred with a 5 mV/s scan rate cyclic voltammogram from +0.2 V to -0.5 V to +0.2 V. This was confirmed through use of a spectroelectrochemical apparatus utilizing a standard 3 electrode setup with evanescent wave spectroscopy.

CHAPTER 1

INTRODUCTION

Microbial transfer of electrons to substrates in the environment (iron oxides, primarily) or in a microbial fuel cell (an electrode) is a field of contemporary interest. Our goal in this study is to help elucidate mechanisms of electron transfer by application of planar waveguide evanescent wave spectroelectrochemistry.

Electrochemically active microbes have become increasingly studied as an alternative energy technology with the call for renewable resources and other "green" technologies to replace fossil fuels. Some of the potential applications for these microbes are to generate electricity (*e.g.* microbial fuel cells) and bioremediation (*e.g.* wastewater treatment). However this research is still in its infancy as studies pursue to understand the processes used by these microbes.

Chapter 1 begins with background information about microbial fuel cells and electron transferring microorganisms. Electrochemical and evanescent wave spectroscopy methods used are also introduced.

Microbial Fuel Cells

A microbial fuel cell (MFC) is an electrochemical device which converts the chemical energy of fuel (such as organic substrates) to electrical energy (*i.e.* current) by the catalytic actions of microorganisms. [1-4] Several types of fuel cells

including microbial fuel cells and enzymatic biofuel cells have been well documented in literature. [5,6] Various microbial or biochemical fuel cells have been developed using different bacteria such as *Desulfovibrio desulfuricans, Proteous vulgaris, Escherichia coli, Pseudomonas* species and redox enzymes as biocatalysts. [6]

A microbial fuel cell system can be used for various purposes including bacterial activity monitoring, electricity generation in a local area, or wastewater treatment processes by using organic contaminates in wastewater as fuel [7]. Microbial fuel cells have not been commercialized yet, and this may be due to difficulties in using mediators at a commercial scale. [3,6]

In a typical microbial fuel cell, the microorganisms oxidize a substrate and generate a potential by making the substrate electrons available to the electrode. The current generation of a microbial fuel cell has been found to be dependent on the bacterial cell concentration and on the electrode surface area. These results suggest that the electron transfer from the bacterial cells to the electrode also depends on physical contact between the cells and the electrode. [7-9]

Though the direct transfer of electrons from microbial cells to electrodes has been demonstrated, this process is oftentimes inefficient both in terms of the proportion of electron transferred (*i.e.* the Coulombic yield) and the rate of electron transfer (*i.e.* the current generation) [3,6,10,11]. For this reason it has been suggested that electrochemical mediators are essential for the microbial fuel construction. This is discussed in the section comparing direct electron transfer (DET) and mediated electron

transfer (MET). However, this does not preclude the design and use of a mediator-less microbial fuel cell should the right mix of microbes and substrates be used. [7]

For general use of microbial fuel cells, electrochemically active microbes with the ability to use wide range of electron donors are needed in pure cultures or in consortia. When the microbes are first injected into the MFC they are known to attach to surfaces and form a biofilm. The length of time required for full microbial attachment varies on the type of electrode surface, MFC, and consortia of microbes used. It is believed that useful mediator-less microbial fuel cell systems could be obtained by modifying and improving the fuel cell formats and electrodes. Studies are also being done to obtain microbial cultures which metabolize complex organic contaminants in the microbial fuel cell. [12]

Pure culture MFCs tend to have a high substrate specificity compared to mixed culture systems [13] while mixed culture MFCs generally need a longer time to obtain a stable power output compared to pure culture MFCs. [14]

S. putrefaciens IR-1 has been tested in a microbial fuel cell and has been found to produce a potential of up to 0.5 V. [12] Electron donors used by *S. putrefaciens* under anaerobic conditions are limited to few organic acids including lactate and pyruvate. [15] For this reason the microbial fuel cell using *S. putrefaciens* cannot be used to convert complex organic fuels into electricity, though this microbial fuel cell can be used as a lactate biosensor with low specificity. [9]

However, the applied electrode potential on an anodic mixed culture derived biofilm determines the microbial composition. [16] This effect also allows pure culture biofilms to be influenced by applied potential. An example is that the chronoamperometric biofilm growth of *Shewanella oneidensis* MR-1 decreased the lag period from 90 days at 0 mV to 5 days at +500 mV (vs Ag/AgCl). [17] The decrease may be related to the impact of potential on bacterial behavior and/or migration.

Attachment of the bacterium *Shewanella putrefaciens* to an electrode is expected to increase efficiency of electron transfer due to a minimal distance between the microbe and the electrode. Application of a positive potential is believed to attract *S. putrefaciens* due to the outer membrane of the microbe having a net negative charge [18]. Literature reports increased current when a positive potential is applied (see above discussion). [19]

S. oneidensis MR-1 is believed to show some motility towards electrodes and thus the availability of its cellular appendices (wires, pili and flagella) clearly determines its electron transfer performance. [20] Likewise an increase in cell swimming speed when whole cells of *Shewanella* species (*S. oneidensis* MR-1, *Shewanella amazonensis* SB2B and *S. putrefaciens* CN32) were exposed to varying electrode potentials. [21] The effect of applied potential was experimented on *Shewanella loihica* PV-4 (from -400 mV to +200 mV vs. Ag/AgCl), which showed an activity increase for potentials greater than -220 mV vs Ag/AgCl. [22] Another experiment [23] with *S. oneidensis* MR-1 and *S. loihica* PV-4 demonstrated that depending on the potential of bacteria cultivation, the electron

transfer pathways can be switched from DET to MET and the formal potential of the DET [22] is also triggered by the redox-conditions during cultivation.

Wang *et al*. [14] reported that applying a +200 mV potential vs Ag/AgCl reduced the MFC start up time from 59 to 35 days. Likewise the current output was increased from 0.42 to 3 mA during the start up time. The results were verified with current recovery tests, electrochemical impedance spectroscopy analysis, and polarization tests. The experiments showed that charge transfer resistance decreased and power output increased when positive potential was applied on the anode, indicating that positive potential could increase the electrochemical activity of anodic biological community during start-up. When the experimental and control MFCs (*i.e.* with and without applied potential during start-up) generated reproducible power stably, similar power outputs were obtained. This indicates that applying potential can reduce the total start-up time but will not affect the final output once a biofilm is established. Similar results (no change in power output once a MFC was established) were reported when anode potentials were poised at negative potentials (versus Ag/AgCl) [24]. It has also been noted that microbes can be incubated on the surface of anode by using a controlled anode potential over a range from −58 to 680 mV versus Ag/AgCl [8,25]

The microbe *Shewanella putrefaciens*

The evolution of the electron transfer process from a microbe to an outside electron sink resulted in what has been referred to as dissimilatory iron-reducing bacterium (DIRB). DIRB are known to reduce solid minerals containing Fe(III) or Mn(IV).

[26] DIRB genomes also encode for an unusually large number of c-type cytochromes [27,28] (membrane-bound, heme-containing proteins best known for their role in electron transport). Some of these are known to be expressed on the outer surface of the outer membrane [29-32] and so may act as terminal reductases for electron transfer to mineral surfaces. [5,33-35]

Shewanella putrefaciens is a gram negative facultative microbe [19] known for its ability to use a variety of compounds, such as nitrate, fumarate, Fe(III), and Mn(IV), in the absence of oxygen. [36] Because of its ability to transfer electrons to extracellular material the *Shewanella* family has been studied in microbial fuel cells. [37] Electron transfer from the microbe to an electron sink occurs either through direct electron transfer, via direct attachment or microbial nanowire [19,26], or from mediated electron transfer. [19,26,38]

Outer membrane cytochrome c proteins are believed to facilitate the DET in the *Shewanella* genus. [7,12,19,26,38] The majority of membrane bound cytochromes (~80% [12,17]) are in the outer membrane when *S. putrefaciens* is grown anaerobically [7], higher than the amount in aerobically grown cells. [38] MET has been found to play a minor role in *S. putrefaciens* as DET dominates, in contrast to other species of the *Shewanella* family such as *S. oneidensis* MR-1. [19]

Shewanella putrefaciens is a facultative microbe, meaning that it is capable of growing with or without the presence of oxygen. [7] When oxygen is present in an aerobic environment then the *S. putrefaciens* shows minimal or no electron transfer

when undergoing electrochemical experiments. [12] The presence of oxygen results in the lack of production of outer membrane cytochromes. [7] Without these cytochromes the *S. putrefaciens* is unable to undergo direct electron transfer to an electrode.

When no oxygen is present (in an anaerobic environment) then *S. putrefaciens* is forced to use alternative electron acceptors and becomes electrochemically active. [7,12] This results in a greater amount of cytochromes in the outer membrane. [7] These cytochromes allow for direct electron transfer as the electron can now travel through the outer membrane.

Exposure to air by anaerobically grown (*i.e.* electrochemically active) *S. putrefaciens* will reversibly inactivate the electrochemical activity. [7] Kim *et al.* found that if lactate is added and the *S. putrefaciens* undergoes applied potential of +200 mV vs an Ag/AgCl reference electrode then the electrochemical activity will be restored. [7] Literature, however, does not state if the restored electrochemical activity increases or decreases compared to a purely anaerobic growth.

Cells of *S. putrefaciens* are shown to be electrochemically active through the use of cyclic voltammetry (CV) when anerobically grown. [7,12,19] Kim *et al.* suggests that cells grown aerobically prevents the synthesis of outer membrane cytochromes, leading to a loss of activity in CV scans. [7]

Direct and Mediated Microbial Electron Transfer

Electron transfer from a microbe to an electron sink occurs through either direct or mediated contact. A microbial cell is inherently electrochemically inactive due to the

cell wall and other surface structures being naturally nonconductive. [7,39] Likewise literature also states that while a large number of redox proteins are electrochemically active, the direct electron transfer between a redox protein and an electrode is hindered by the peptide chain adjoining the active redox center of the protein. [7] However if a connecting peptide chain or redox protein, such as cytochrome c, is connected through or located in the outer membrane then it allows for electron transfer through the cell wall and to an outside electron sink, such as an electrode. [39] Anaerobic *Shewanella* has a redox activity around -0.2 V vs Ag/AgCl reference electrode. [7,12]

Direct electron transfer happens either through membrane bound redox enzymes [26,40-43] touching the electron sink or when a 'nanowire' pili [44-47] extends from the microbe and provides direct contact. In the microbe *S. putrefaciens* it is believed that cytochromes are responsible for the direct electron transfer that occurs between the microbe and external electron sinks. [19,48] The effect of DET in *S. putrefaciens* NCTC 10695 was noted in literature as the dominant electron transfer method and that planktonic cells (*i.e.* cells floating in culture not attached to anything) only play a minor role. [19] The dominance of DET in that experiment was ascribed by Carmona-Martinez *et al*. to the low concentration of mediator in the medium and thus fast establishment of a biofilm at the electrode. [19]

Other types of biofuel cells, including microbial fuel cells and enzymatic biofuel cells, have been well documented in literature. [6] They, however, require an

electrochemical mediator to produce efficient electron transfer between microbial cells and an electrode. [3,10,49] Known mediators for some of these fuel cells include thionine, methyl viologen, 2-hydroxy-1,4-naphtoquinone, and neutral red among others. [6,49]

Mediated electron transfer uses a mediator [26,50-52] such as a secondary microbial metabolite serving as a temporary electron sink. The molecule is reduced from the microbe then diffuses to the electron sink (*e.g.* electrode) where it is then oxidized by transferring the electron to the sink. The re-oxidized molecule then diffuses back to the microbe ready to be reduced again, as both the oxidized and reduced forms of the mediator are permeable to the microbial membrane. [7] In essence, the mediator simply shuttles electrons between the microbial cells and the electrode. [7,12]

The effect of a mediator has been noted in literature. Kim *et al*. found that a microbial fuel cell containing *E. coli* NCBI 10772 showed no increase in potential following the addition of glucose as fuel. However when methylene blue was added as a mediator the potential increased, indicating the effect of MET on a microbe that is incapable of DET. [12]

Even though *S. putrefaciens* primarily uses DET, the MET of *Shewanellaceae* is able to exploit redox shuttles including humic substances [53,54], melanin [55,56], menaquinone [57], as well as riboflavin [58], flavinmononucleotide [59,60] and their derivatives. The use of mediators does not preclude the use of cytochromes for extracellular electron transfer. [51,59,61] Some strains of the *Shewanella* family (*e.g. S.*

oneidensis MR-1 [51,58,62], *S. loihica* PV-4 [63], *S. baltica* Os155 and Os195 [58], *S frigidimarina* NCIMB400 [58], and *S. decolorationis* NTOU1 [64]) can biosynthesize these mediators under aerobic and anaerobic cultivation. The ability to synthesize suitable amounts of these electron shuttles (especially for anaerobic conditions, where energy for biosynthesis is limited) is not unequivocally established for all *Shewanella* species [58]. Because of the wide range of parameters expressed by cytochrome c on the outermembrane and/or production of mediators it is of crucial importance to consider the exact conditions during biofilm growth and development. [65]

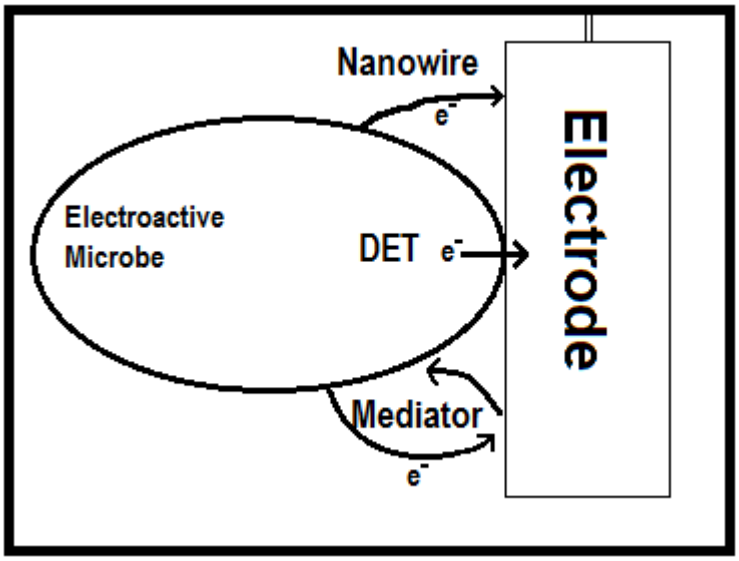

Figure 1: Diagram of electron transfer between a microbe and an electrode. Direct electron transfer is shown through direct contact with the outer cell membrane and through contact with a nanowire extending from the microbe. Mediated electron transfer is shown via a mediator moving between the microbe and the electrode.

Faradaic Processes

Microbial fuel cells are based on electrochemical processes. In this section some electrochemical basics are reviewed.

Current is the result of charge transfer across the microbe-electrode interface when the *Shewanella putrefaciens* undergoes electrochemical reactions at the electrode surface. In other words, electron transfer reactions at an electrode surface occur when electrons residing in a high energy state find a path to a low energy state. Such electron transfer can occur between molecules (whether in a microbial membrane or in solution) or between electrodes and molecules. In electrochemistry, energy is applied to a solution in the form of an electrode potential and current is subsequently measured.

$$\Delta G = -nFE \quad (1)$$

where ΔG is the energy applied in joules (coulomb-volts), n is the number of equivalents (electrons per mole), F is the Faraday constant (9.64846×10^4 C/eq), and E is the applied voltage (V). The number of equivalents, n, is shown in a reduction reaction:

$$Ox + ne \leftrightarrow Red \quad (2)$$

In electrochemistry, an electrode consisting of some charge conducting material is placed into a conductive media. A second electrode is connected through a voltage (energy) source. Before ΔG (energy) is applied to the electrode surface, the solution is in equilibrium with a Boltzman-like distribution of ions in the oxidized and reduced states.

$$[Red] = [Ox] exp^{\frac{-\Delta G_{soln,eq}}{RT}} \quad (3)$$

where T is the temperature, R is the molar gas constant, and $\Delta G_{soln,eq}$ is the free energy of the solution in its equilibrium state.

This equation can be rearranged to:

$$ln\left(\frac{[Red]}{[Ox]}\right) = \frac{-\Delta G_{soln,eq}}{RT} \quad (4)$$

$$\frac{nFE_{soln,eq}}{RT} = ln\left(\frac{[Red]}{[Ox]}\right) \quad (5)$$

At standard state conditions, E_{soln} = E° and [Red] = [Ox]. At other conditions

$$E_{soln,eq} = E° - \frac{\mathrm{RT}}{\mathrm{nF}}\ln\left(\frac{[\mathrm{Red}]}{[\mathrm{Ox}]}\right) \quad (6)$$

Equation 6 is known as the Nernst equation.

Three factors that give rise to the strengths and weaknesses of electrochemical methods include heterogeneity of the solution, time scale of the primary event (rate of electron transfer event), and the coupling of chemical processes. Voltammetric techniques have all the advantages of the above mentioned factors and cyclic voltammetry, to be precise, is the method of choice by most electrochemists. Cyclic voltammetry, for instance, has the capability of rapidly observing redox behavior over a wide potential and kinetic range.

Voltammetry

Voltammetry comprises a group of electroanalytical methods in which information about the analyte is derived from the measurement of current as a function or applied potential obtained under conditions that encourage polarization of an indicator, or working, electrode. In order to enhance polarization, the working electrodes are microelectrodes having surface areas of a few square millimeters at the most and in some applications, a few square micrometers or less.

In voltammetry, a variable potential excitation signal elicits a characteristic current response upon which the method is based. Cyclic voltammetry is used as a tool for fundamental and diagnostic studies that provides qualitative information about electrochemical processes under various conditions. It is a most versatile electroanalytical technique for the study of electroactive species (species that undergo reduction and oxidation). It has become an important tool for the study of mechanisms and rates of oxidation/reduction processes since it usually reveals the presence of intermediates in the oxidation/reduction processes.

Cyclic Voltammetry

In cyclic voltammetry, the current response of a small stationary electrode in an unstirred solution is excited by a triangular potential waveform (Figure 2). A supporting electrolyte must be present to repress migration of charged reactants and products. For an oxidized substrate, the potential scan is in the negative direction and starts from a value more positive to its formal potential. As the potential approaches the formal potential, a Faradaic current, due to the reduction of the substrate at the electrode surface, is observed in the cyclic voltammogram (Figure 3). The electrode surface is eventually depleted of oxidized species and a diffusion layer forms. This causes the current to tail off and a peak shape forms. When the potential scan is reversed, Faradaic current of opposite sign appears as the substrate is regenerated through an oxidation reaction.

Important parameters in cyclic voltammetry are cathodic peak current, i_{pc}, anodic peak current, i_{pa}, cathodic peak potential, E_{pc}, and anodic peak potential, E_{pa}, as illustrated in Figure 3. For a reversible reaction, anodic and cathodic peak currents are approximately equal in absolute value, but opposite in sign. One method of measuring the peak current involves extrapolation of a baseline current as shown in Figure 3.

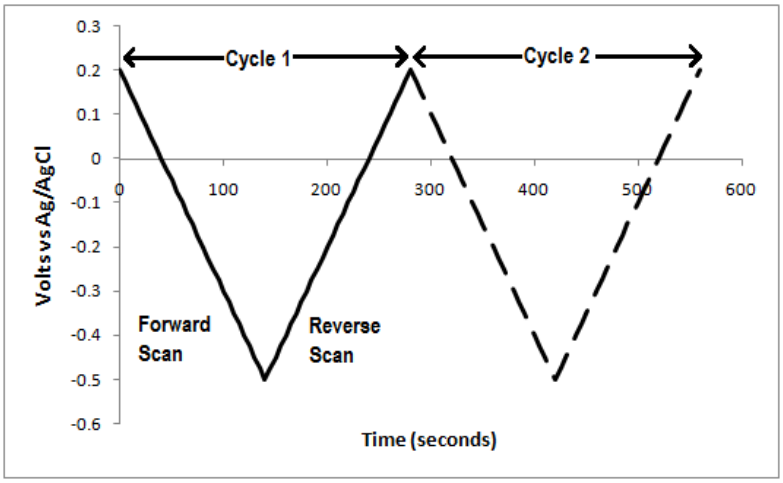

Figure 2: Representative excitation signal for cyclic voltammetry (a triangular potential waveform with switching potentials at 0.2 and -0.5 V versus Ag/AgCl).

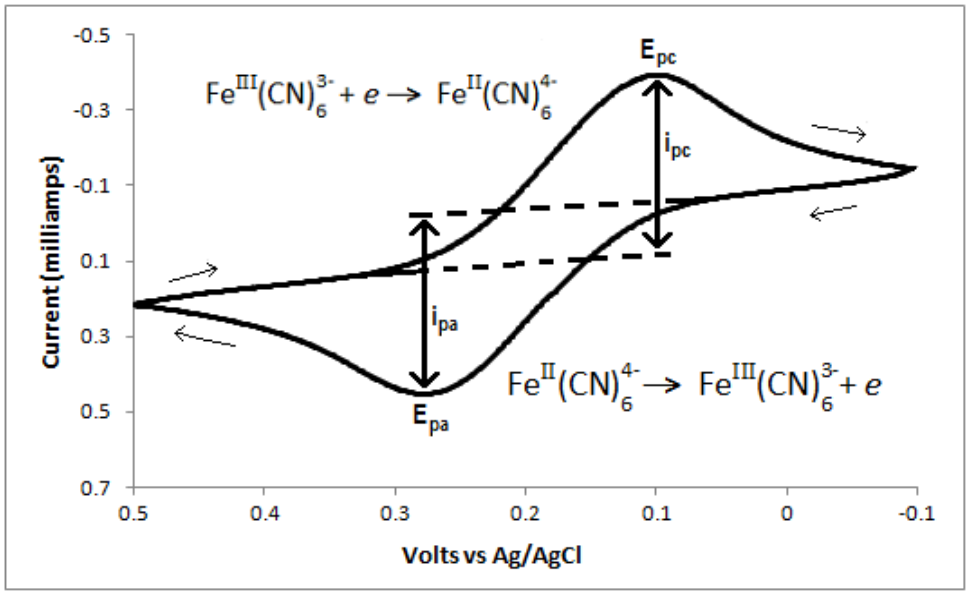

Figure 3: Cyclic voltammetry of 3 mM $Na_3Fe(CN)_6$ in N_2 purged 30 g/L tryptic soy broth. Scan initiated at 0.5 V versus Ag/AgCl in negative direction at 5 mV/s.

The formal reduction potential (E°) for a reversible couple is centered between E_{pa} and E_{pc}.

$$i.e.\ E° = \frac{E_{pa} + E_{pc}}{2} \quad (7)$$

where E_{pa} is the anodic (oxidative) peak potential and E_{pc} is the cathodic (reductive) peak potential.

The number of electrons transferred in the electrode reaction (n) for a reversible couple can be determined from the separation between the peak potentials, which at ambient temperature is:

$$\Delta E_p = E_{pa} - E_{pc} = \frac{0.059}{n} \quad (8)$$

The peak current for a reversible system is described by the Randles-Sevcik equation for the forward sweep of the first cycle as:

$$i_p = (2.69 \times 10^5) n^{3/2} A D^{1/2} C v^{1/2} \quad (9)$$

where C is the concentration of solution species (mol/cm^3), *v* is the scan rate (V/s), A is the area of the electrode (cm^2), and D is the diffusion constant (cm^2/s).

When a CV is not chemically reversible, several other possible processes may be taking place. One of such processes is the conversion of the oxidized or reduced species to an alternative form. An example is known as an EC mechanism, which involves an electron transfer followed by a chemical reaction.

$$A^+ + e^- \leftrightarrow A \Rightarrow B \quad (10)$$

where B is a new chemical species.

Likewise a CE mechanism is also possible and involves a chemical reaction prior to electron transfer.

$$B^+ \Rightarrow A^+ + e^- \leftrightarrow A \qquad (11)$$

Both of these processes can generate CVs that are irreversible.

Electrodes intentionally modified with adsorbed species, which can promote irreversibility, have been developed. These adsorbed species include polymers, inorganic layers, organics, and biological molecules. Applications include electrocatalysis for fuel cells and batteries, analytical sensors, molecular electronic devices, and electrode protection. Modified electrodes can be utilized to study reaction rates in the coating itself.

Applied Potential via Controlled Potential Electrolysis

The principle behind the Controlled Potential Electrolysis (CPE) experiment is very simple, as it applies a predetermined potential for a known time and measured the output current. For example, if only the oxidized species is initially present then the potential is set at a constant value sufficiently negative to cause rapid reduction and is maintained at this value until only the reduced species is present in solution. The current approaches zero as all of the oxidized species becomes reduced. The total charge passed during the CPE experiment is calculated by integrating the current either visually from the graph produced by the program in use or through Faraday's law:

$$Q = nFN \qquad (12)$$

where Q is the total charge transferred, n is the number of electrons transferred per molecule, F is Faraday's constant (96485 C mol^{-1}), and N is the amount of material electrolyzed (mol). Therefore, if one or the other of n or N is known, the other can be calculated.

The value of the applied potential is determined based on the redox potential of the analyte, which can be initially measured by cyclic voltammetry. For a reduction, the ideal potential is around 200 mV more negative than the redox potential so that the rate of electrolysis is controlled by the rate of mass transport to the working electrode. However, it is not always possible to use a potential too far removed from the redox potential due to electrolysis of other electroactive materials (*e.g.*, electrolyte, solvent , or other components of the solution mixture).

The size of the electrodes required for CPE is significantly different than those used for other electrochemical experiments (in which only a very small fraction of the electroactive molecule of interest is electrolyzed). Other electrochemical experiments may prefer the use of microelectrodes whereas CPE is enhanced with increased surface area from larger electrodes (both working and counter electrodes). Stirring the solution also increases the rate of mass transport. The counter electrode must be isolated from the working electrode to prevent species that are electrogenerated at the counter electrode from interfering with electrolysis at the working electrode. However, care must be taken when choosing the material used to isolate the counter electrode from

the working electrode, since high resistance material may affect the efficiency of the electrolysis.

Spectroelectrochemistry

Electrochemistry can be combined with a quite different technique, spectroscopy, for studying the redox chemistry of inorganic, organic, and biological molecules. Oxidation states are changed electrochemically by addition or removal of electrons at an electrode while the spectral measurements are made simultaneously. This technique is a convenient way of obtaining spectra of electrogenerated species and redox potentials and for observing subsequent chemical reactions of electrogenerated species. Frequently used optical techniques in spectroelectrochemistry are absorption spectroscopy in the ultraviolet, visible, and infrared regions. UV and visible spectroelectrochemistry are quite commonly employed for the identification of electrode reaction products and intermediates. Fiber optics have been used for the illumination and collection of light near electrode surfaces. A fiber-optic absorbance probe in conjunction with a bulk electrochemical cell can be employed for the examination of low concentration analyte species. Transparency is due to the thinness of the conducting film (100-500 Å).

Initial development of spectroelectrochemistry was stimulated by the availability of optically transparent electrodes (OTE), which enable light to be passed directly through the electrode and adjacent solution. Electrode transparency is necessary for several spectroelectrochemical techniques. One type of OTE consists of a very thin film

of conductive material such as Pt, Au, SnO_2, C, or Hg-coated Pt, that is deposited on a transparent substrate such as glass or plastic (visible), quartz (UV-visible), or Ge (infrared), depending on the spectral region of interest.

The primary advantage of a spectroelectrochemical technique is that it provides complementary spectral data to the voltage or current response of more conventional electroanalytical techniques. For instance, such parameters as diffusion coefficients and rate constants, which are difficult to determine with conventional analytical measurements, can be easily determined with absorbance measurements.

The advantages of conducting spectroelectrochemical experiments with attenuated total reflection (ATR) geometry were established in the 1960s. Itoh and Fujishima were the first to demonstrate the advantages of performing ATR spectroelectrochemistry in the integrated optical waveguide (IOW) regime. [66,67] They fabricated IOWs that were coated with an electroactive antimony-doped SnO_2 layer. They observed sensitivity enhancements ranging from 20 to 150 for adsorbed films of methylene blue.

Heineman and coworkers (2000) used a model sensor consisting of a cationically selective sol-gel-derived Nafion composite film coated on an indium tin oxide (ITO) electrode, with $Ru(bpy)_3^{2+}$ as model analyte, to demonstrate signal acquisition techniques. [68] They also demonstrated the use of a mediator to detect a nonabsorbing analyte during spectroelectrochemical modulation. They used charge-selective composite film of Nafion-SiO_2 to entrap the mediator, $Ru(bpy)_3^{2+}$. They then

observed the change in modulation amplitude, as determined by ATR, upon addition of the analyte, ascorbate. A larger change was observed for thinner films. [68]

Armstrong *et al* (1997) have reported highly sensitive spectroelectrochemistry of adsorbed films on ITO with the electroactive integrated optical waveguide (EA-IOW). [69] The EA-IOW, a planar waveguide coated with an ITO layer, was found to be about 10^4 fold more sensitive to changes in absorbance occurring during electrochemical events as compared to a single pass transmission spectroelectrochemical experiments, as demonstrated by adsorbed methylene blue. The EA-IOW was also observed to be selective to near-surface events, as it was relatively insensitive to absorbance by solutions of dissolved chromophores at less than 1 mM.

Planar Waveguide

The principle of operation of planar waveguides is the same as that for optical fibers that are circular in cross section. A planar waveguide electrode device is comprised of a thin film of membrane deposited on an optically transparent electrode (OTE), which is supported over a cladding material.

The refractive index of a medium is defined as

Refractive index, $n = \frac{c}{v}$ (13)

where c is the velocity of light in a vacuum and *v* is the velocity of light in a high electronic medium. The refractive index is greater than one because the velocity of light is less in any medium than in a vacuum. That is, light slows down in any medium.

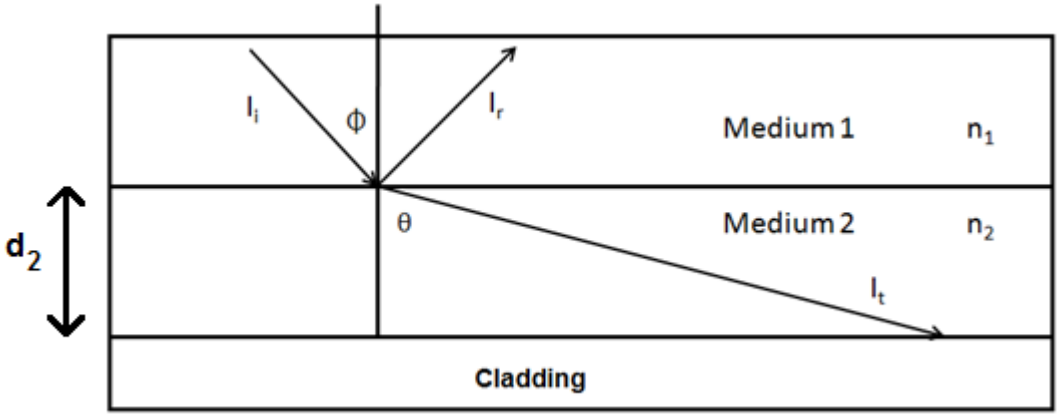

Figure 4: Schematic representation of incident (I_i), reflected (I_r), and refracted (I_t) light associated with the change of propagating medium.

From Snell's law, incident (I_i), reflected (I_r), and transmitted or refracted (I_t) light occurring at the interface of two media are related as follows:

$$\frac{\mathrm{Sin}\theta}{\mathrm{Sin}\Phi} = \frac{n_1}{n_2} \tag{14}$$

$$\frac{I_r}{I_i} = \left(\frac{n_2 - n_1}{n_2 + n_1}\right)^2 \tag{15}$$

where Φ is the angle of incidence, θ is the angle of refraction, n_1 and n_2 are the refractive indices of medium 1 and 2, respectively.

When light enters a waveguide electrode device at an angle less than the critical angle, the light will be contained within the waveguide (cladded) medium, with the exception of a surface or evanescent electric field, which is generally small in distance (100 nm). To achieve this, the refractive indices of the cladding materials (the thin film and the underlying OTE cladding) should be less than the refractive index of the guided material so that the entering light is totally internally reflected and contained within the latter.

The evanescent wave penetrates only a fraction of the wavelength into the sample, allowing measurements to be made in highly scattering liquids. The penetration depth is related to launch angle and the refractive index:

$$d_p = \frac{\lambda}{4\pi n_2}\left[\sin^2\theta - \left(\frac{n_1}{n_2}\right)^2\right]^{-\frac{1}{2}} \quad (16)$$

The true extent of penetration of the evanescent wave is about three times the calculated d_p. [70,71]

Light intensity contained in the evanescent field and subject to attenuation is about 4%. The evanescent field extends from the waveguide surface into the superstrate, probing both the film and any adsorbed analyte close to the waveguide surface. This results in enhanced sensitivity and selectivity of waveguide systems, which ensures us of selective analyses. For example Heineman and coworkers (2000) incorporated planar waveguide technology into a spectroelectrochemical sensor. [72] In the sensor design, potassium ion-exchanged BK7 glass waveguide was over-coated with a thin film of ITO that served as an OTE, and a chemically selective film was spin-coated on top of the ITO film. They investigated the impact of the ITO film on optical properties of the waveguide and on the spectroelectrochemical performance of the sensor. They found that this waveguide spectroelectrochemical sensor results in an enhancement in sensitivity of about 6-fold over the corresponding mid-infrared (MIR) device. The exponential decay (calculated depth of penetration) of the evanescent field provides the

capability to perform spatially selective optical measurements of the environment adjacent to the waveguide surface.

The sensitivity of a waveguide is a function of the total percentage of adsorbed light present in the evanescent field. Using a raw optics model to describe light propagation, this percentage is related to the number of reflections that occur per unit waveguide length, N. The reflection density (number of reflections per unit distance, $\frac{N}{D}$) at the waveguide/film interface for a waveguide of thickness d_2 can be approximated as:

$$\frac{\mathrm{N}}{\mathrm{D}} = (2\mathrm{d}_2\tan\theta + \Delta_{21} + \Delta_{23})^{-1} \quad (17)$$

where Δ_{21} and Δ_{23} are Goos-Hänchen shifts at the waveguide/film and waveguide/substrate interfaces, respectively.

Decreasing waveguide thickness increases the number of reflections, and thus increases the interaction of light in the waveguide with the superstrate above the electrode. Increasing the glass thickness decreases the percentage of total light power in the waveguide contained in the evanescent field, thus decreasing the absorbance sensitivity. Sensitivity enhancement can, therefore, be achieved by decreasing the ITO layer thickness. A decrease of 10 nm would theoretically double sensitivity. However, there is a practical limitation to this, as losses in the waveguide need to be kept to a level where it is possible to measure the outcoupled light intensity after traversing a reasonable electrode area.

Indium tin oxide is a transparent conductor with substantial transmittance in the visible spectrum and near IR regions. This coating can be deposited on a wide range of

materials, which exhibit superior adhesion, compact density, uniformity, and thermal stability. ITO is a highly absorbing medium as compared to other waveguide materials such as the glass substrate and the deposited film, but its attenuation of light at various wavelengths is very small. It also exhibits a high refractive index ($n \approx 2.0$), which shifts the electric field distribution towards the superstrate, increasing the field strength at the ITO/superstrate interface and enhancing optical losses due to absorbance. [73-76] The high refractive index of ITO increases waveguide sensitivity. For efficient propagation of light through the waveguiding structure, the refractive indices of the glass substrate and the thin film should be less than that of the ITO layer. Electric field amplitude is greatest in the glass substrate, which is critical to operation of these devices, as too much power in the ITO layer will lead to unacceptable propagation loss in the waveguide system.

In an electrochemical experiment at a bare ITO electrode with an electroactive probe molecule there is usually little change in the evanescent wave signal observed during the course of the experiment. This is true even for optically active molecules because diffusion allows the surface concentrations to be controlled by the bulk solution concentration. When the ITO is coated with an additional layer restricting diffusion, such as clay, the concentration of the probe molecule within the evanescent wave is a function of the applied potential at the electrochemical surface instead of the bulk solution concentration. Likewise if the optically active compound is adsorbed/attached to the surface then the evanescent wave can measure the

desorption/detachment of the compound. Hence the ITO electrode can be used to probe in situ UV-Vis changes of molecules or microorganisms held close to the electrode surface. The UV-Vis change of microorganisms are expected on oxidation and reduction due to the outer membrane cytochrome c.

Cytochrome C

Electron transfer from a *Shewanella* microbe to an electron sink is believed to occur through a series of cytochromes. While the entire pathway is still unknown, antibody recognition force microscopy showed that the cytochromes OmcA and MtrC are expressed on the exterior surface of living *Shewanella oneidensis* MR-1 cells when Fe(III) was the terminal electron acceptor. OmcA was localized to the interface between the cell and mineral. MtrC displayed a more uniform distribution across the cell surface. Both cytochromes were associated with an extracellular polymeric substance. [38]

OmcA is an 85kDa decaheme outer membrane *c*-type cytochrome. [26] Direct electrochemistry of purified OmcA (harvested from *S. putrefaciens* MR-1) on Fe_2O_3 electrodes was observed using cyclic voltammetry, with cathodic peak potentials of -380 to -320 mV versus Ag/AgCl. Variations in the cathodic peak positions are speculatively attributed to redox-linked conformation changes or changes in molecular orientation. Purified OmcA can exchange electrons with ITO electrodes at higher current densities than with Fe_2O_3. Overall, OmcA can bind to and exchange electrons with several oxides, and thus its utility in fuel cells is not restricted to Fe_2O_3. [26] The native protein includes a lipid-binding site that is presumed to hydrophobically anchor the protein to the outer-

membrane. [77] Although the structure of OmcA is not yet known, it is reasonable to assume that the lipid-binding site would be attached to the outer-membrane, leaving the portion of the protein suited for interaction with the mineral, roughly speaking, on the opposite side. [26]

Wiggington *et al*. [78] used scanning tunneling microscopy to determine that the diameter of an individual cytochrome is 5 to 8 nm. Lower *et al*. [79] estimated that *S. oneidensis* has 4×10^{15} to 7×10^{15} cytochromes per square meter by comparing atomic force microscopy measurements for whole cells to force curves on purified MtrC and OmcA molecules. These values can be used to create a simple, geometric, close-packing arrangement of MtrC or OmcA molecules on a surface. Using this approach, cytochromes could occupy 8 to 34% of the cell surface. This estimate is in agreement with the results obtained from atomic force microscopy. [38]

It is noted that, in nature, OmcA does not operate in isolation. OmcA is known to complex with another outer-membrane decaheme cytochrome, MtrC, in a 2:1 OmcA:MtrC ratio [77]. The complex may operate in a completely different manner than does isolated OmcA. For example, a complete catalytic cycle, with electron transfer to iron oxide followed by ‘‘reloading’’ with electrons from upstream in the electron transport chain, may require a complete complex as well as other as yet unknown proteins or other molecules.

Other reducible minerals include *S. putrefaciens* 200R which attaches to ferrihydrite and magnetite [80], *Shewanella oneidensis* MR-1 is capable of attaching to

calcite surfaces [81] and can recognize the crystal surfaces of goethite and diaspore. [82] Furthermore, MR-1 seemed to be able to modify the molecular arrangement at its outer cell membrane and react to molecular configurations present at the crystal surface. This is a strong argument for microbial recognition of mineral surfaces and microbe response to these surfaces. Indeed, such attachment is required for respiration. In addition to iron mineral reduction, microbes are capable of reducing iron in clay crystals.

The first published report of microbial influence on the oxidation state of structural Fe in smectite was in 1986 by Stucki and Getty [83] when four different *Bacillus* microbes were found to reduce Fe in clay. Following this initial publication, Komadel *et al*. [84] continued with the investigation of microbial reduction of Fe in clay. Three different smectites: ferruginous smectite SWa-1 from Grant County, Washington; API 33a, Garfield nontronite; and API 25, Upton montmorillonite were reduced. However the specific organism responsible for the Fe reduction was never classified.

Gates *et al*. [85] studied the reduction of structural Fe in ferruginous smectites by using a mixture of five *Pseudomonas* species of bacteria and found that a consortium of these microbes was more effective than any of the individual species alone. While using a mixture of microbes elicits itself to further study, current research is normally focused in the establishment of single culture results.

As a result it is thought that a microbe would better attach to a clay surface rather than directly to an electrode.

With this thinking, preliminary clay modified ITO experiments were performed. Placing a thin clay layer on the ITO electrode was in hope of capturing greater microbial electrochemical activity by having a higher concentration of the microbe at the electrode, *i.e.* reducing the distance between microbes and the electrode.

The spectroelectrochemical setup was verified with a clay coating when a thin clay layer was applied and tested with $[Ru(bpy)_3]^{2+}$, as described in Chapter 2. This chapter provides background on clays and results obtained from clay modified electrodes.

Clays have been shown to have open structures favorable for interactions with enzymes and which intercalate redox mediators. The open structure enables clays to serve as host matrices likely to immobilize enzymes onto electrode surfaces. They may make excellent modifications for microbial fuel cells. Electrochemical biosensors have been developed for clays, too. This biosensor success lies in the ability to immobilize a large variety of enzymes within an open bidimensional structure favorable to analyte diffusion. [86]

Properties of Clays

Clays come in a variety of sizes, shapes, layer charge, elemental composition, and spaces between ion exchange sites. Clays are low cost, ubiquitous, have large surface areas [87,88], and can serve as cation-exchangers and catalyst supports. [87,89,90] Due to the very high cation exchange capacity (CEC) (measured in milliequivalents of charge per 100 g), clays exhibit unusual intercalation and swelling

properties that enhance diffusion of molecules through clay films. [87,91,92] Clays also serve as useful support matrices for redox reactions and exhibit many desirable electrochemical properties for the modification of electrodes. [93-96] Clays are highly stable, which results from the high surface area, special structure, and distinguishing features of the particles. Clays are composed of hydrous aluminosilicate layered materials and the exchange of cations occurs in between these aluminosilicate layers. The acidity and interlayer spacing of clays mainly depend on the nature of the exchanged cations.

Uses of Clays

Clays are indispensable in architecture, industry, and agriculture due to their variety of uses and unique properties. They are used in the form of bricks as building materials. They are also used in the manufacture of porcelain, tiles for walls and floor coverings, and pipes for drainage and sewage.

Natural and synthetic clays have been used as inert matrices for the isolation of photocatalytic components in charge storage devices, the encapsulation of semiconductors, and the concentration of analytes. They are also widely used as active participants in reactions. The electrochemical activity of clays plays an important role in the reduction of toxic substances like carbon tetrachloride, nitrobenzene, trichloroethane, and chromium to a less toxic state via electron donation from metal sites within the clay matrix.

One major environmental concern is the transport of contaminants through clays. Investigation on the properties of clays is, therefore, very important. Clay-modified electrodes (CMEs) have been used to understand the clay structural unit and its impact on the transport variety of electroactive probes. For example, CMEs have been used to study the effect of aqueous electrolytes on the diffusion of probe molecules in clay layers. [96] Clays have also been used as barriers in landfills and riverbeds to keep pollutants out of the natural environment. They are also contemplated for use in nuclear waste storage. Although clay barriers are able to contain heavy metals for decades, species like Cl^- diffuse through the barrier with only a slight decrease in the diffusion coefficient. Clays are also used as molecular sieves due to their ability to selectively sort out molecules based on size and charge exclusion processes. Zeolite is a typical example of a molecular sieve due to its very regular pore structure of molecular dimensions.

Also of interest is what happens to clay layers when the clay swells or collapses. Different techniques have been used to monitor the presence of water in clays, which gives information on the swelling of clays. For instance, swelling of clays causes problems in the oil industry. Upon exposure to water or water-based drilling fluid at oil drilling sites, compact clay soaks up the water and swells. When this occurs in a bored hole, the walls of the hole contract around the drill bit or a pipe, which may damage the equipment. Addition of certain polymers seems to inhibit the swelling of the shales. [97-99] However, clays are very useful in the oil industry. For example, less absorbent

bentonites are used as filtering and deodorizing agents in the refining of petroleum and, mixed with other materials, as drilling muds to protect the cutting bit while drilling.

Clays also have the ability to provide a useful matrix to participate in reactions. Modified clays have been used as catalysts for various synthetic processes including Diels-Alder reactions [100-102], polymerization of olefins [103-105], and reactions of hydroxymethyl ferrocenes with acids. [106] Several patents have outlined iron-exchanged silicate matrices as catalysts to reduce nitrogen oxide car emissions. [107-109] In other applications, sensors for trace detection have found increased sensitivity following preconcentration of analytes within a clay film. Kwak and co-workers (2002) demonstrated the use of layered double hydroxides (nano-sized inorganic clay) as a delivery carrier for genes and drugs by hybridizing with DNA and c-antisense oligonucleotide. [110] Montmorillonite and kaolinite clays are also used as dietary supplements in many rural areas to improve energy and stamina and reduce arthritis. [111]

In recent years, polymer-clay composites have become the subject of considerable research efforts due to their remarkable physical and mechanical properties. Dispersing clay platelets into a polymer matrix improves the physical properties of the matrix. Nonionic polymers act as H-bond acceptors (amide and acid moieties) and donors (acid groups). Cationic polymers exhibit strong irreversible interactions with clay, while anionic polymers show only weak or no adsorption. There are three categories of polymer-clay composites. [112] The first consists of conventional

composites, in which the clay particles (tactoids) exist unchanged from their original state of stacked sheets. The matrix polymer is not inserted into the interstices of the clay layers but only interacts with the external surfaces of the clay particles. The second, intercalated nanocomposites, occurs when the polymer enters the clay layer structure in a crystallographically regular fashion. This type of nanocomposite is normally interlayered by occasional molecular layers of the polymer and its properties are typically similar to that of the clay host. Low molecular weight polymers are more effective in intercalation than high molecular weight polymers. Exfoliated nanocomposites are the third category of polymer clay composites, where individual clay platelets are homogeneously dispersed in the polymer matrix. The polymer enters the clay galleries only if there is sufficient enthalpic interaction between the clay and the penetration polymer. Improved toughness, increased tensile strength and tensile modulus, increased flexural strength and flexural modulus, are achieved if platelets are completely exfoliated as compared to the polymer matrix alone. [112]

Pretreatment of smectite clays with polymers having polar functionality at one end of the molecule results in intercalates or exfoliates that are useful as plasticizers. They are also useful for providing increased viscosity and elasticity to thermoplastic and thermosetting polymers, for improving gas impermeability in food wrappers, for electrical components, and for food grade drink containers. [112]

Clays are used as modifiers for high temperature polymers and magnetically altered to develop recoverable sorbents.

Clays and Electrochemistry

Because of the dual measurements used in this study involving electrochemistry, a review is important. Evaluation of transport processes into clay films have been a subject of interest for many years. Electrochemistry is a technique that is extensively used in clay chemistry. Fitch and co-workers have reported studies on the uptake of electroactive compounds into clay films, using clay-modified Pt electrodes. [92,93,95,113-116] There has, however, been a problem of accurately assessing clay-analyte interactions. The present work offer the advantage of conducting in-situ optical and electrochemical studies to properly asses the absorption and redox reaction of $[Ru(bpy)_3]^{2+}$.

Clays form membrane-like films and possess redox properties, hence are able to exhibit many desirable electrochemical properties. Electrochemical activity of clays is a measure of the efficiency of charge transport, either via physical diffusion or via charge hopping. Cations strongly bound to the exchange sites of clay are electroinactive. [117] Ion paired cations present in excess of the CEC are, however, electroactive. These ion pairs are absorbed but not strongly enough to prohibit mobility. Some ion pairs travel to the electrode through interparticle pores. Ion pairs are also responsible for charge shuttling from the electrode to immobile cations located away from the electrode surface. Electron hopping would also explain why some cations are electroactive and others are more strongly electroinactive.

Clay Modified Electrodes

Because CMEs are used in this study, a review of their properties and applications is essential.

Modified electrodes have been studied extensively during the last twenty years because of the possibility of intelligently designing the surface of an electrode to perform desired tasks. Such tasks may consist of selective analysis (enzyme modified electrodes for glucose measurements via the glucose oxidase reactions), enhances flux design (nucleopore membranes), charge storage devices, catalysis, and support matrices for electrocatalysis. [93-96] The vast majority of modified electrode surfaces consist of surface assembled monolayers and polymeric coatings, or modification with inorganic matrices such as clays.

CME was first developed by Ghosh and Bard around 1983. [87] There are two major reasons why studying CMEs are interesting. First, the transport processes observed by CMEs have applications to transport of pollutants in natural environments. For example, the mechanisms by which materials are transported within clay sheets is a fascinating subject which is related to molecular reorganization, membrane sieving, and the effect of localized versus delocalized fields on enhanced transport. The second is related to the possible use of the modified electrode as a device. Modification of electrodes or optrodes with layered clay materials is of interest because one can control the architecture of the surface, which could be designed with specific functionalities or size characteristics.

Physical Properties of Clay Modified Electrodes

In this study, the clay-coated indium tin oxide electrode is employed for system validation with $[Ru(bpy)_3]^{2+}$. This section outlines the physical properties associated with CMEs to obtain insight into the nature of these modified electrodes.

Clays self-adhere to surfaces to which they are attached due to the fact that both the surface and the clays are polar. Polarity of clays is due to isomorphous substitution within the crystal lattice. Simple air drying of the film, oven drying, or spin coating should result in a film that adheres to the polar substrate, most likely through cation or anion bridges.

Understanding the type of structure found in the gel solution gives insight in the drying process that results in the clay film. In a gel state, clays are thought to be linked together by two processes controlled by the face-to-face and the edge-to-face bridging of the clay. The face-to-face interaction is repulsive and is modeled by the classical DLVO theory. When the diffuse double layers are compressed sufficiently, the negative charge of the clay is shielded and the individual clay sheets can rest at an equilibrium distance determined by the overlap of the diffuse double layers. Edge-to-face structure depends predominantly upon the pH of the gel. At low pH, the edges of the platelets are protonated and edge/face interactions can result. Also impacting on the gel structure is the treatment of clay with orthophosphoric acid, which can create edge-to-edge linkages expanding the lateral dimension of the layer. Because of salt effects on the

structure, well-dispersed solutions are most easily obtained when the clay is exchanged with a mono-cation at dilute concentrations. [93]

Air drying pure gel results in loss of all but the surface attached water. If drying is slow, enough time is available for the development of face-to-face orientation. Drying at higher temperatures (550-650 °C for montmorillonites) removes surface hydroxyls causing irreversible collapse, or calcination, with linkages formed between layers. Spin coating does not usually result in face-to-face orientation but it is possible at moderate speed. [93]

Dry films may reswell and this is particularly known for cationic clays. The hydration energy of the salt (the nature of cations associated with the permeating solution), but not the DLVO theory and diffuse double layer effects, determines the extent of swelling. For example, K^+ and Cs^+ result in an un-expanded film since they are easily dehydrated during the intercalation process. Na^+ and Li^+, on the other hand, have high hydration energies and enter the interlayer in their hydrated forms. Generally, interlayer distance increases with decreasing salt concentration. Intercalation reactions, however, proceed layer by layer but not randomly over all layers. The clay's charge and CEC also govern the rate of film swelling and its final state. Highly charged clays have a greater capacity for hydration and thus can support more layers of water. [93,118]

Clays exhibit repetitive structural units on several scales (layer sheets and hexagonal hole arrays). Those structural arrangements are affected by water adsorption. Montmorillonite clays for instance, are able to expand upon exposure to

water. Water is able to penetrate between the layers and expand or swell the clay. There are two types of swelling. Interlayer swelling is when one to four layers of water penetrate between the clay layers and is driven by the concentration gradient. Montmorillonite clays swell due to the interlayer cations pulling in water to become hydrated. The basal spacing between clay layers increases when hydrated, allow more water to enter the layers and further expand the clay. Clays can be expanded from 5 Å to 60 Å by solutions with different salt concentrations. [96,117] Fitch *et al.* (1999) used CMEs to investigate the effects of varying concentrations of bathing electrolytes on clay swelling. [96] They observed that all concentrations of K^+ result in compact clays while low concentrations of Na^+ (below 0.4 M) result in swollen clays, and that incorporation of anions depends on the extent of swelling.

Applications of Clay-Modified Electrodes

Due to the ease of controlling the clay structure, CMEs have many useful applications, some of which are discussed below.

CMEs find applications in molecular electronics, where they can be used for the development of charge storage devices with unidirectional or controlled directional current flow. CMEs can also be used for photocatalysis of water splitting, which requires directionally controlled charge transport. Clays serve as hosts for sensitizers used for water splitting. In addition, clays are used as templates for enzyme-based analytical sensors, which require control of the directionality of charge transfer and the localization of various reagents in specific spatial organization. For example,

bioelectrochemical sensors based on modified CMEs have been used to detect glucose, glucose oxidase, and hydrogen peroxide. [93,111,113,119]

CMEs are used as stripping sensors to protect catalysts from decomposition within an aqueous regime. This is accomplished by the use of the clay to support micelles at the electrode surface and/or by the use of surfactant modified clays to create a liquid gel interface. CMEs are also used as chiral sensors. Clays are used to create a chiral atmosphere at the surface of an electrode. Although clays are not themselves chiral, they impart spatial organization to adsorbing species. The energy of pairing racemates versus enantiomers, combined with the templating effect of the clay, apparently drives the organization of a chiral substrate. The selectivity of the surface to chiral mixtures can be observed electrochemically. [93,96,116]

Certain dyes (*e.g.* methylene blue and thioflavin) are strongly adsorbed to clays; hence they can be used in electrocatalysis to displace exchangeable cations for a facile cation exchange capacity measurement. These dyes are also known to undergo dimerization and/or aggregation processes, which affect the efficiency of charge transfer within the clay. [93]

CMEs can also be used in controlling ion fluxes (diffuse double layer gating). A large atmosphere or Debye length prevents particles from close association driven by van der Waals forces. The inadequate shielding of the charged surfaces keeps the particles apart so that a net potential barrier exists between particles. As the anion atmosphere increases, the double layer repulsion diminishes and the van der Waals

forces take effect. The interplate distance at which a potential minimum is developed will thus vary depending upon the salt concentration. [93,96]

CMEs are formed from either large or small particle size platelets (Figure 5). Large particle size platelets have the ability to slip over each other to form a uniform coating and the platelets are close together at high salt concentrations. The presence of slip planes implies that no stacking defects are present and a diffusing ion must traverse a narrow interlayer pathway. The ion moving through such film is thus impeded due to closure of the channels. Small particle size platelets cannot slide over each other's surfaces and form small stacks instead. The stacks expand and contract in response to Debye length, forming interparticle channels. In this case, the channels are larger in the presence of high salt concentrations. Reduction current is observed to be greater at high salt concentrations for small particle size clay (*e.g.* Laponite) as compared to large particle size clay (*e.g.* SWy-1 montmorillonite). [119]

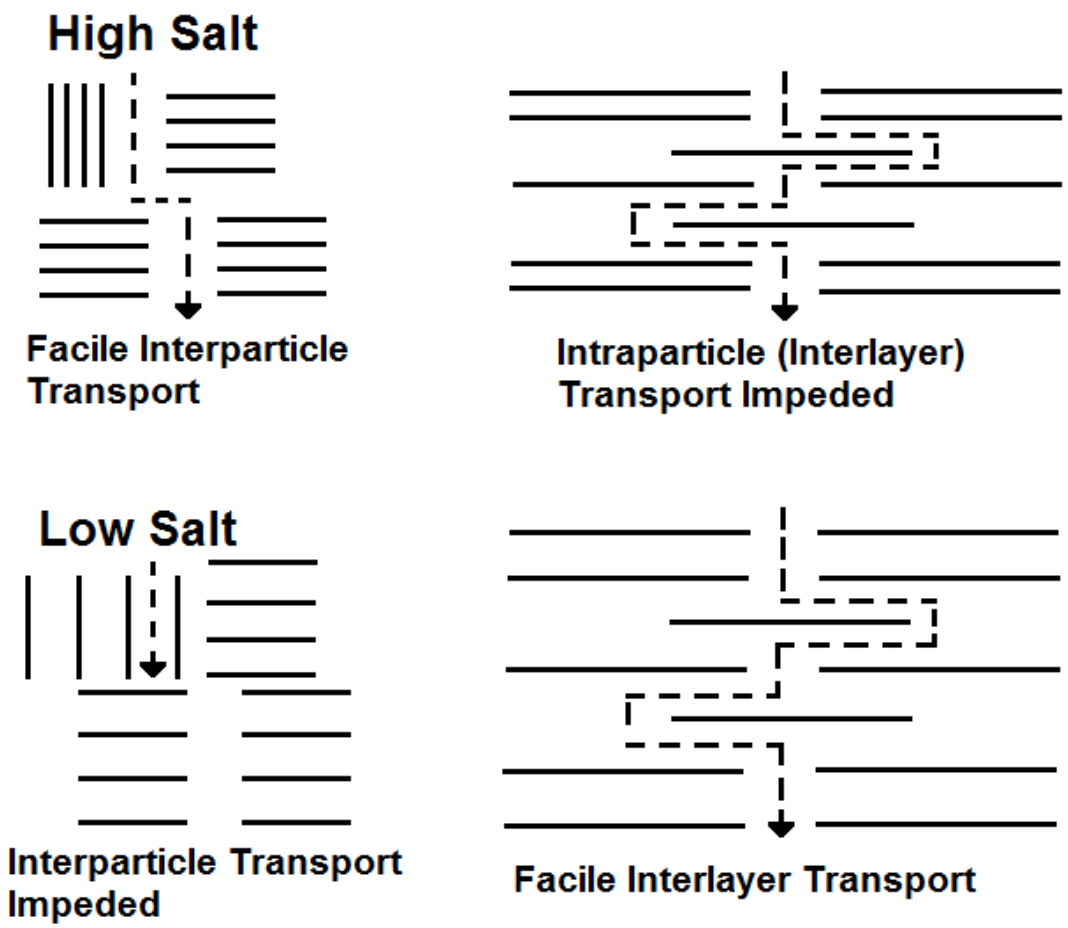

Figure 5: Schematic representation of interparticle and intraparticle (interlayer) transport through small particle size (left) and large particle size (right) platelets. [119]

Summary

The literature review provides all the necessary information needed to be used as a guide in operating the spectroelectrochemical instrument and analyzing experimental results. The next issue is to validate and calibrate the instrument using the extensively studied and well known analyte $Ru(bpy)_3^{2+}$ and compare the experimental results to those published in the literature. Once the instrument is calibrated then testing with the microbe *Shewanella putrefaciens* will begin.

CHAPTER 2

MATERIALS, METHODS, SPECTROELECTROCHEMICAL SYSTEM VALIDATION AND *SHEWANELLA PUTREFACIENS* VALIDATION

This chapter provides a detailed description of chemicals, equipment, and experimental procedures employed in this project.

Chemicals, Microbes, and Materials

Unless otherwise specified, all chemicals were used as received. Nanopure deionized water (Barnsted Nanopure II) with a conductivity of 18 MΩ/cm^3 was used to prepare all solutions and clay suspensions. Chemicals that were used include tris(2,2'-bipyridyl)ruthenium(II) chloride hexahydrate $[Ru(bpy)_3]^{2+}$ (Sigma Aldrich), sodium chloride (Morton International, Chicago), potassium chloride (Fischer Scientific), sodium dithionite (sodium hydrosulfite) (Sigma Aldrich), and tryptic soy broth (TSB) (Sigma Aldrich).

Part I: Growth of *Shewanella putrefaciens*

This chapter details the validation of the entire spectroelectrochemical bacterial experiment. Due to the complexity of the multiple components that needed to be validated, we begin with the bacterial system, follow with the electrochemistry of the bacterial system, and then finish with the spectroelectrochemical system.

The microbe *Shewanella putrefaciens* (MicroBiologics Inc.) was previously prepared and kept frozen at -80 °C in 1 mL vials. Each 1 mL vial was prepared by mixing

500 µL of culture and 500 µL of 20% glycerol solution (each measured with a micropipette) into specially ordered 2 mL sterilized vials (Fisher Scientific). No attempt was made to optimize the harvest with respect to position on the growth curve. The tips used with the micropipette were autoclaved before use. The vial was then sealed with the associated cap and frozen in a -80 °C freezer until being retrieved. When a vial was removed from the freezer it was thawed out and added to TSB media to immediately begin a new culture.

Tryptic soy broth (TSB) solution was prepared with 30 g of dehydrated TSB powder dissolved in 1 L of deionized (DI) water before being autoclaved. Any water evaporated by the autoclave process was replaced by autoclaved DI water. The TSB solution was kept in a sealed 1 L bottle until used.

The TSB media, also known as Soybean-Casein Digest Medium, was originally developed in determining the effectiveness of sulfonamides against pneumococci and other organisms. [120] It was discovered that anaerobes grow well when incubated in TSB under anaerobic conditions. Each 30 g solution of TSB contains 17.0 g of enzymatic digest of casein, 3.0 g enzymatic digest of soybean meal, 5.0 g of sodium chloride, 2.5 g of dipotassium phosphate, and 2.5 g of dextrose with a final pH of 7.3 ± 0.2 at 25 °C. The enzymatic digest of casein and soybean meal are nitrogen sources, dextrose is the carbon energy source, sodium chloride maintains osmotic balance, and dipotassium phosphate is a buffering agent. TSB is suitable for electrochemistry because the molarity

of the 5 g of NaCl results in 0.08 M solution which is an excellent range for electrochemistry.

Shewanella putrefaciens Growth Curve

In order to obtain reproducible results a growth curve of *Shewanella putrefaciens* had to be established. This required optimization of the growth and handling of the microbial population. Aerobic cultures of *Shewanella putrefaciens* were prepared by adding a 1 mL vial of previously prepared *S. putrefaciens* stock solution (kept frozen at -80 ^{o}C) to a 250 mL Erlenmeyer flask filled with 150 mL of TSB. The flask tip was previously flame sterilized. The TSB solution transferred via a 100 mL graduated cylinder was also flame sterilized. All glassware was autoclaved immediately before use. The Erlenmeyer flask was covered with aluminum foil. The aluminum foil was used to cover the flask opening while being autoclaved and remained as the only cover in direct contact with the flask to prevent contamination. The microbes were incubated at room temperature.

The optical density of three separate cultures were taken at various points along the growth curve to determine how long it takes for a culture to grow, seen in Figure 6 along with a growth curve from literature. [121] The growth curve (from initial log phase to stable phase) is in agreement with literature when using TSB as the growth medium. They all follow the same growth trend with an initial lag phase, an exponential growth phase, and a plateau. The literature added lactate to a TSB culture in the growth curve

whereas no lactate was added to our TSB cultures. This indicated *S. putrefaciens* was cultured from the dextrose within the TSB even if lactate is the favored growth media.

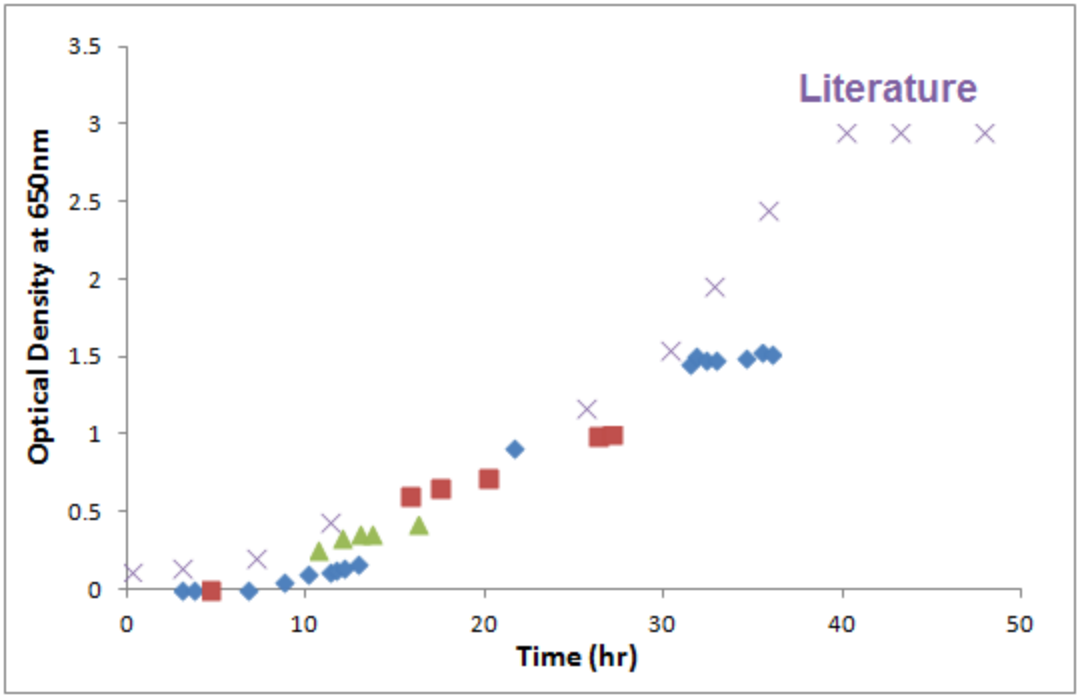

Figure 6: Growth curve of multiple aerobic *Shewanella putrefaciens* cultures grown in 150 mL TSB (red boxes, green triangles, and blue diamonds) and a literature growth curve (purple x's).

Cell Counting Method

The cell density determined in the growth curve (Figure 7) was determined by manually counting the number of cells by using a known volume with a hemocytometer. Two separate aliquots of a *S. putrefaciens* aerobic culture were taken for the OD_{650} and the hemocytometer. The first aliquot was put in a glass cuvette and the OD_{650} was measured with a VWR UV6300PC double-beam spectrophotometer. After the OD_{650} was taken a 10 µL aliquot of the culture was injected onto the hemocytometer under the cover slip. The hemocytometer was imaged at 400x zoom with an Olympus BH2

compound microscope. Multiple images were taken of each culture in various locations around the hemocytometer. The number of cells in these images was then manually counted. The hemocytometer has a known volume (3 nL per image) so that the amount of microbes counted could be divided by the area to give a cell concentration.

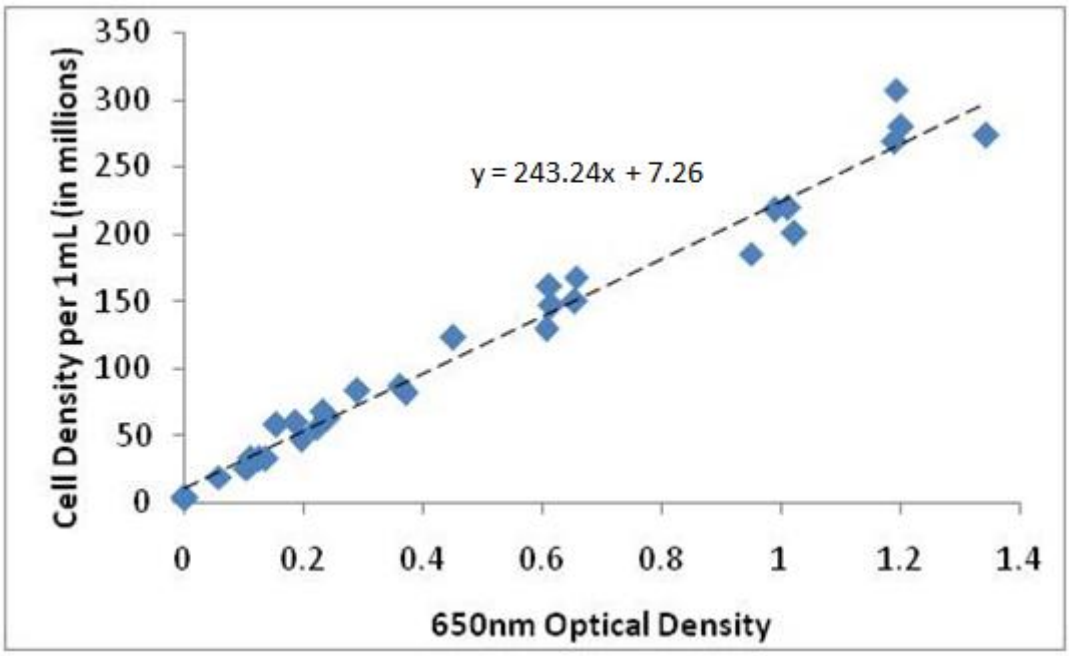

Figure 7: Ratio of OD_{650} to aerobic cell density (millions of cells per 1 mL)

The growth of three unique cultures from Figure 6 are included in Figure 7. The OD_{650} measured in the growth curve is nicely related to the total microbial population as observed in Figure 7.

Shewanella putrefaciens Growth Method

Anaerobic cultures of *Shewanella putrefaciens* were made with variable volumes of TSB solution. The volumes were selected to facilitate harvest of the microbe for further spectroelectrochemical experiments at a target range of optical density. The timing was chosen to facilitate scheduling around other tasks.

After adding the 1 mL vial of *S. putrefaciens* stock the culture was then N_2 purged for 1 hr to create an anerobic environment. The time of N_2 purge for each culture was determined by measuring the amount of dissolved O_2 with an oxygen sensor (Pasco Scientific). The sensor indicated that the amount of dissolved O_2 in the resulting solutions were measured at <0.8 mgO_2/L ($8x10^{-7}$ M) after 1 hr of nitrogen purging (data not shown). The concentration of dissolved oxygen < 1.0 mgO_2/L has been called anaerobic in some literature. [122] The amount of dissolved O_2 did not decrease with additional nitrogen purging.

The aluminum foil on the Erlenmeyer flask was covered with a semi-airtight seal using parafilm (Bemis Co., Neenah, WI). The seal was removed only before immediate injection into the electrochemical cell.

Part II: Electrochemical Optimization for *Shewanella putrefaciens*

In order to perform spectroelectrochemistry on *S. putrefaciens* the electrode loading time had to be optimized. This section describes the method by which the time and applied potential was optimized and verification of the health of the colony within the cell. The spectroelectrochemical cell is first described, then the method of cell harvest, then the loading of the cell, and finally verification of microbial validity.

Spectroelectrochemical Cell Setup

The electrochemical setup utilized a three electrode system (working, reference, and counter electrodes) incorporated into the spectroelectrochemical cell, made from Delrin plastic (Abbott Development Shop). The spectroelectrochemical cell had top and

bottom parts and a measured volume of 11 mL. The ITO slide served as the working electrode, a platinum wire runs through the solution to provide the counter electrode, and a small Ag/AgCl electrode (BASi Inc) was placed between the counter electrode ends and used as the reference electrode. All electrochemical data was determined with a Ag/AgCl reference electrode, which sits 0.22 V relative to the standard hydrogen electrode. [123] The ITO slide was 9 cm x 2 cm in size (refractive index of 1.95) with an area of 4.5 cm x 1 cm in contact with the analyte. [124] Once the spectroelectrochemical cell is fully setup the slide rests on its side instead of laying flat, seen in Figure 8.

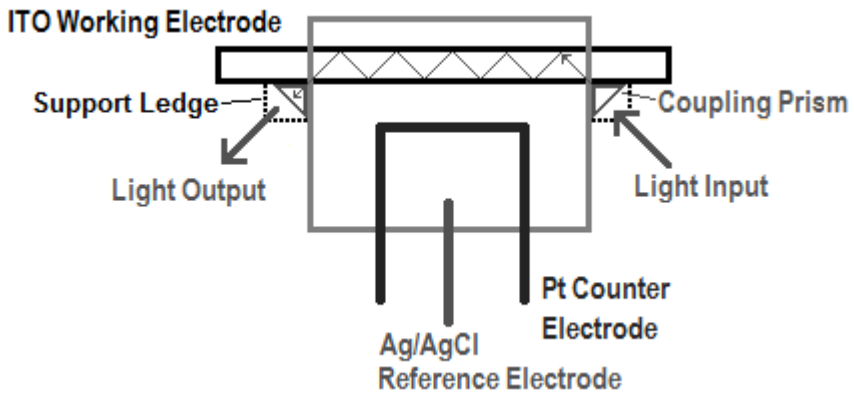

Figure 8: View of spectroelectrochemical cell setup from above. The light is represented by the lines bouncing back and forth through the ITO slide in evanescent wave mode.

Indium Tin Oxide glass slides (Thin Film Devices, Inc.) were washed with 1% alconox, wiped dry, and then wiped with 70% isopropyl alcohol before air drying and equilibrating with air. The side with high resistance (*i.e.* the conductive or electroactive side) was selected using a voltammeter at the ends, where the coupling prisms are placed. The resistance was not recorded. After each experiment the ITO slide was

wiped with 1 % alconox, wiped dry, and then wiped with 70% isopropyl alcohol before being left to air dry. The ITO slides were not stored in any solution.

The ITO was cleaned with isopropyl alcohol before being inserted into a groove (shaped to fit) in the bottom part of the cell. The top and bottom sections of the cell were then fitted in place and screwed together. The ITO working electrode consists of a semiconductor surface. It is known to have a capacitance between 3.36-6 µF/cm^2. [125-127] The capacitance of the electrode is one way to verify the electrochemical setup. The capacitance was determined by obtaining a CV for the bare ITO surface in a TSB solution as shown in Figure 9.

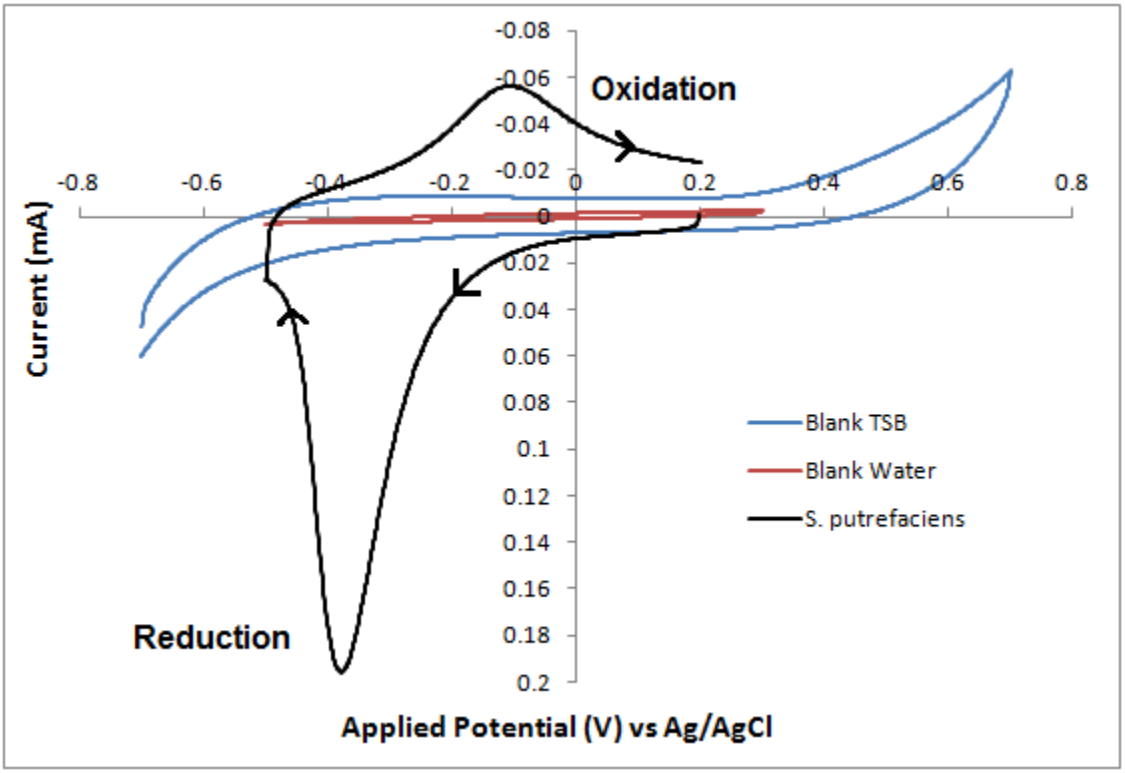

Figure 9: A 100 mV/s CV comparison of a culture of *S. putrefaciens* (grown in 100 mL TSB) compared to an autoclaved solution of TSB and DI water on a bare ITO slide. The *S. putrefaciens* culture had an OD_{650} of 0.706 and +200 mV applied for 2 hr.

The capacitive current observed can be used to determine the capacitance of the electrode by use of the equation:

$$i_c = vC_d \quad (18)$$

where i_c is the capacitive current, v is the scan rate, and C_d is the capacitance of the electrode. The total current in the "box" is twice the capacitive current. So, for example, the TSB was 0.01 mA/100 mV/s = 0.0001 F = 100 µF. The electrode surface is 4.5 cm^2 resulting in a measured capacitance of 22 µF/cm^2 in TSB. The increase in capacitance from the bare electrode in the presence of TSB can be attributed surface adsorption of components of TSB, such as enzymatic digest of casein and papaic soybean digest. The ITO capacitance (1.03 with a range from 0-5 µF/cm^2) is consistent with literature (3.36, 4.6, 6 µF/cm^2). [125,126]

The value obtained in pure water is substantially lower at 2.4 µF/cm^2, consistent with literature reports. This data serves as a reminder that the ITO surface is capable of strongly adsorbing a variety of species, including, as will be seen, the *Shewanella* microbe.

Part III: *Shewanella putrefaciens* in an Electrochemical Cell

Experimental Procedure of Shewanella putrefaciens

Once the spectroelectrochemical cell was assembled, a microbial culture of *Shewanella putrefaciens* was pumped in. Isopropyl alcohol was used to clean the tubing (for pumping the microbial culture) before each experiment. The optical density at 650 nm (OD_{650}) was taken (VWR UV6300PC double-beam spectrophotometer) of the *S.*

putrefaciens culture immediately before the experiment. The OD_{650} was used to determine the microbe concentration. A second optical density measurement was made of the recovered culture and of the original stock culture of bacteria after each experiment.

Once filled, the pump was stopped and the incoming and outgoing tygon tubes clamped shut with 37 cm of tube space filled with culture. Immediately after clamping the input and output tubes, a potential of +0.2 V (vs Ag/AgCl) was applied (via a BASi EC Epsilon potentiostat) for 2 hr before a cyclic voltammogram was taken, if applicable. The CV was scanned at a scan rate of 5 mV/s (unless otherwise noted) and ran from the initial potential of +0.2 V to the switching potential of -0.5 V back to the initial potential of +0.2 V.

After an experiment was complete the culture was pumped out and the electrochemical cell disassembled before the ITO electrode was taken out and left to dry in a vertical position resting longways on its side. The ITO slide was placed on its side in the same manner as when it was in the spectroelectrochemical cell during the experiment. The vertical drying position of the slide was chosen to minimize pooling and drying of loosely attached microbes.

Confirming the Presence of Shewanella putrefaciens

While the tryptic soy broth growth media changes from a see-through orange liquid to a more opaque orange, indicating that something additional is in the broth, it is not enough to simply say that the proper bacteria has been cultured. Cyclic

voltammetry was run on multiple *S. putrefaciens* cultures to demonstrate that the microbes were in the cultured solution. The initial experiment applied a potential (vs. Ag/AgCl) from 0.7 V to -0.7 V back to 0.7 V to test for the range which the microbial redox peaks will show. An initial range was chosen to be 0.2 V to -0.5 V and back to 0.2 V. These values encompass the known potentials for the outer membrane cytochrome c proteins that make up the final position in the electron transport chain for *S. putrefaciens*. The chain is illustrated with Figure 10 obtained from Alanah Fitch.

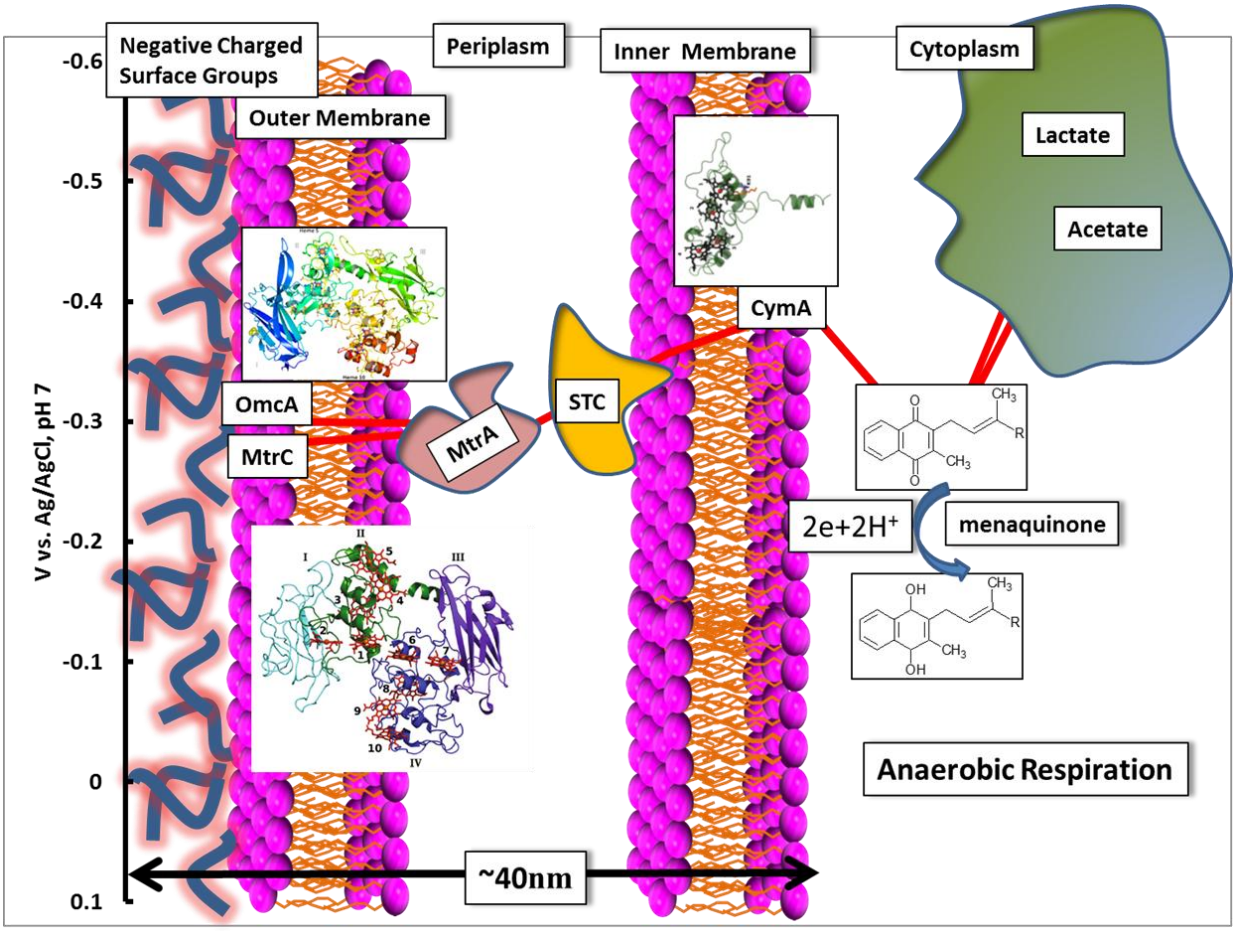

Figure 10: Illustration of the electron transfer chain from the cytoplasm through the inner membrane, periplasm, and outer membrane with certain cytochromes labeled.

The OmcA and MtrC proteins are the active electron transfer species to be observed at the electrode. Their reduction potentials occur around -0.2 to -0.3 V vs Ag/AgCl at pH 7.

The first CV discussed above (Figure 9) was for the TSB solution. Also shown was the effect of a CV on a *S. putrefaciens* culture compared to a sterile tryptic soy broth solution and to deionized water. All of these experiments were performed on a bare ITO slide. The arrows indicate the direction of the applied potential.Neither blank shows any discernable peaks, as expected. In contrast, the *S. putrefaciens* culture has an estimated midpeak potential of -0.24 V against the Ag/AgCl reference electrode. Both the reduction peak (~ -0.38 V) and the oxidation peak (~ -0.1 V) are in agreement with literature values. [12]

The microbial CV was taken after 200 mV of oxidizing potential was applied for 2 hr. Applying this potential increases the size of the redox peaks and can restore electrochemical activity to an aerobic culture of *S. putrefaciens* [7].

The tryptic soy broth shows a capacitive current (the difference in the baseline of the reduction and oxidation peak) somewhat similar to the bacterial CV, unlike the water CV, indicating that the initial baseline for each sample is likely from the tryptic soy broth and not from the microbes. The CV taken in water had a very minimal reading.

Figure 11 shows multiple CVs taken on the same sample. 200 mV were applied from 0 min to 20 min, followed by a CV. Each CV is annotated with the time of applied potential. As the amount of adsorption time increased so did the current.

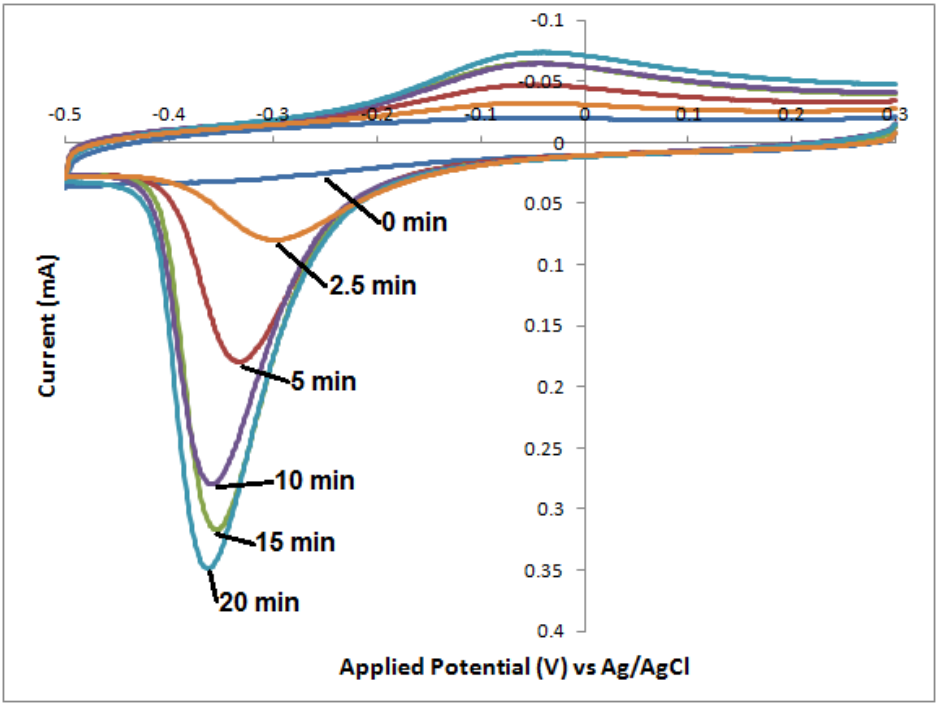

Figure 11: 100 mV/s CVs of *S. putrefaciens* (grown in 150 mL TSB) on a bare ITO electrode with different amounts of time of +200 mV applied potential.

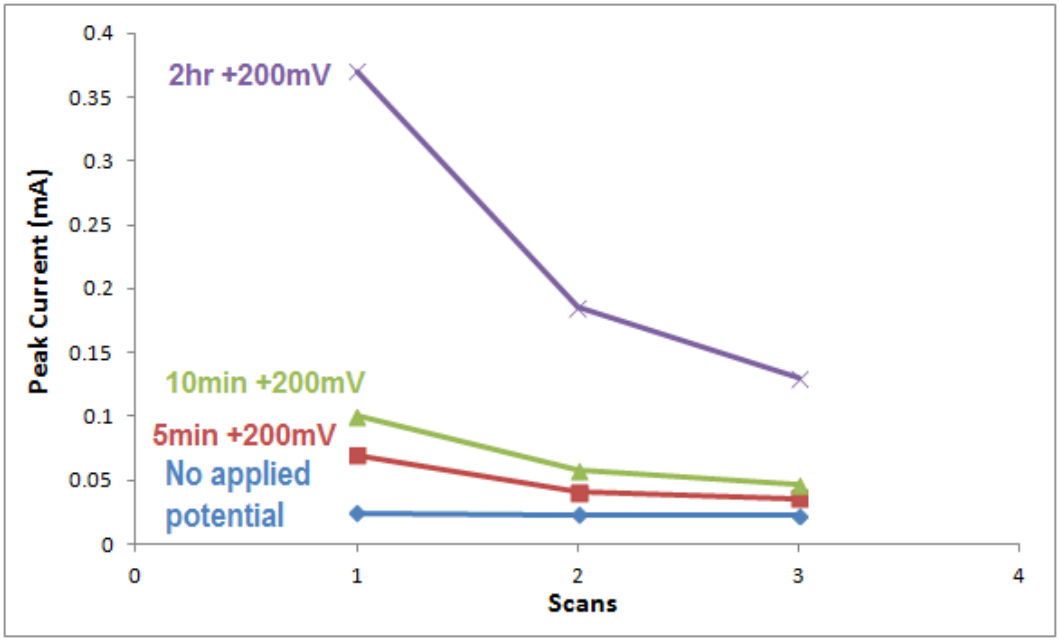

Figure 12: Peak height vs additional CVs. Multiple 100 mV/s CVs were taken after +200 mV (vs Ag/AgCl) was applied.

In a separate set of experiments, multiple consecutive CVs were run on samples (each grown in 150 mL TSB) incubated at +0.2 V for different periods of time (Figure 12). Each set of experiments (4 sets total) had potential applied for a designated time before three CVs were taken back to back without any time between each CV. The first group of cultures did not have any potential applied before the CVs, the second group had 5 min of +200 mV applied, the third group had 10 min of +200 mV applied, and the fourth group had 2 hr of +200 mV applied. The value (in mA) of each reduction peak was plotted for each set of CVs. When a potential is applied it results in an increased peak height for the first CV. The increase in the first CV peak height indicates greater attachment of microorganisms to the electrode with increased incubation time at +0.2 V. Subsequent consecutive CVs show loss of peak current indicating loss of microbial activity from the surface. The loss is non-linear and may, as will be discussed below, be related to the detachment of microorganisms followed by a lag time required to reattach. The data clearly indicates that a minimum of 10 min were required for the first attachment such that back to back CVs would allow insufficient time for reattachment.

This data indicates that the incubation time at +0.2 V will have to be carefully optimized, as explained in the next section.

Determination of Experimental Parameters

Experimental parameters must be determined for system optimization before any experiments may be performed on *S. putrefaciens*. These parameters include the potential to be applied, length of time of applied potential, scan range of a CV, and if a

culture can be reused. This is to ensure a large enough population is attached to the electrode so that it is able to be interrogated with the optical equipment.

Literature reports that measured current densities increase when the applied potential increases from -0.1 V through +0.4 V during the growth of *S. putrefaciens* wild-type NCTC 10695. [19] No CV signals were detected at electrodes poised at -0.1 V or 0 V during biofilm growth, which can be attributed to the absence of the interaction with bacteria on the electrode surface. [19] Literature also reports non-permanent attachment of *S. putrefaciens* cells and no complete biofilm coverage [19], which agrees with our experimental results. Cell swimming speed was also observed to increase when whole cells of *Shewanella* species (*S. oneidensis* MR-1, *S. amazonensis* SB2B, and *S. putrefaciens* CN32) were exposed to varying electrode potentials. [21] *S. oneidensis* MR-1 [17] and *S. lohica* PV-4 [19] also show dependence of activity on applied electrode potential.

A potential of +200 mV was applied for oxidation of the microbes. This potential was chosen as it has been demonstrated to result in electrochemical activity from *S. putrefaciens*. [124] Previously mentioned CVs covered the location of the redox peaks so all future scans were chosen to be from 200 mV to -500 mV at 5 mV/s. This is so the applied potential of 200 mV aligned with the starting potential of the CV.

After a culture was prepared it could be harvested only once due to air exposure. Decreased electrochemical activity (Figure 13) was monitored by the capacitance ratio (CR).

$$C_r = \frac{i_{r0.15} - i_{o0.15}}{i_{r-0.45} - i_{o-0.45}} \quad (19)$$

where C_r is the capacitance ratio, $i_{r0.15}$ is the reduction current at 0.15 V, $i_{o0.15}$ is the oxidative current at 0.15 V, $i_{r\text{-}0.45}$ is the reduction current at -0.45 V, and $i_{o\text{-}0.45}$ is the oxidative current at -0.45 V. The CR of a CV was measured by dividing the capacitance at 0.15 V by the capacitance at -0.45 V, illustrated by the arrows in Figure 13. The locations where the capacitance was measured were determined from data in Table 1. Table 1 shows ratios of capacitance values at different potentials of the "Fresh" graph in Figure 13. The ratio of 0.15 V/-0.45 V had the highest value. Activity measured by this ratio, seen in Figure 14 and Table 2, indicated that the culture could only be sampled once even if the culture was nitrogen purged when the seal was broken. As such, all experiments were performed on a fresh *Shewanella* culture.

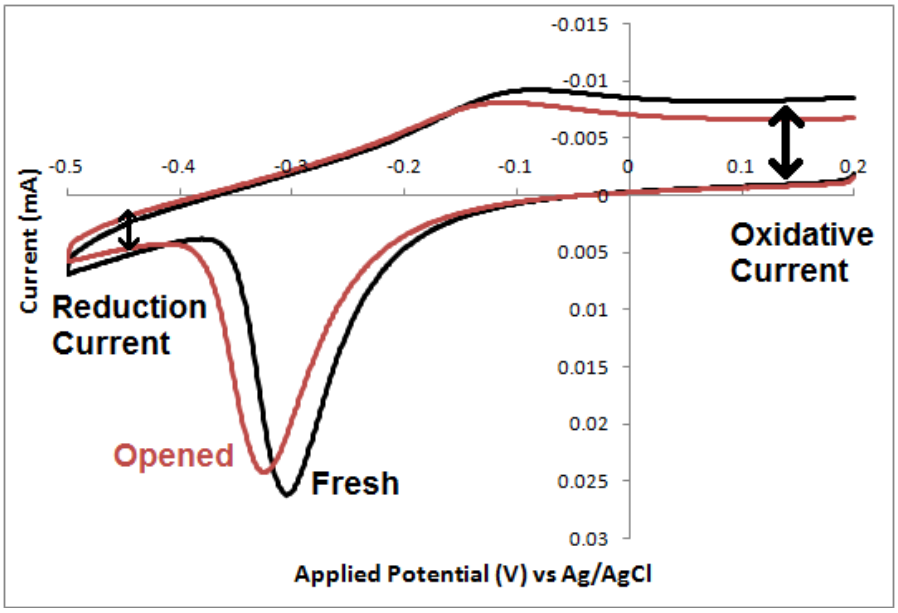

Figure 13: Comparison of a fresh culture and the same culture (grown in 100 mL TSB; OD_{650} 0.328) after being nitrogen purged after being opened. 2 hr of +0.2 V potential was applied before each 5 mV/s CV. The black arrows at 0.15 V and -0.45 V are where the capacitance ratio is calculated.

Scan Range (V)	Capacitance Ratio
0.15/-0.45	2.73
0.15/-0.4	2.36
0.2/-0.45	2.49
0.2/-0.4	2.16

Table 1. Different capacitance ratios from Fresh Culture in Figure 13

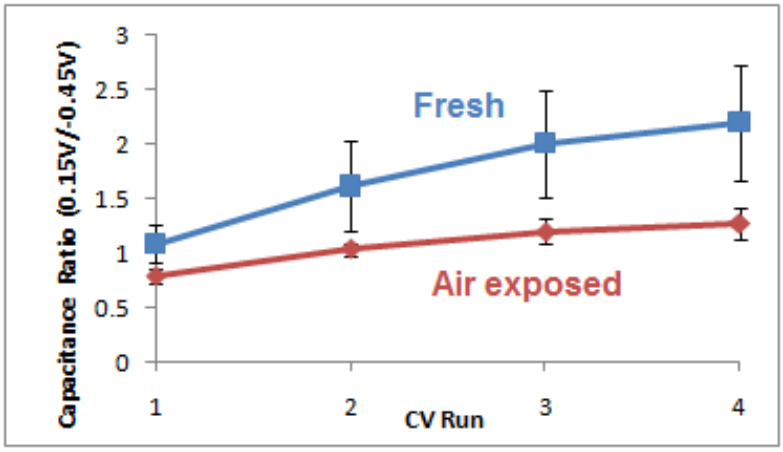

Figure 14: Comparison of CV capacitance ratio from a fresh *Shewanella* culture (grown in 150 mL TSB) and after it was exposed to air for 2 hr. +200 mV of potential was applied for 20 min before each 5 mV/s CV with 4 CVs ran in a row for each experiment.

Capacitance Ratio (0.15 V/-0.45V)		
Fresh Culture	Air exposed	Ratio (Air/Fresh)
2.73	2.13	0.78
2.54	2.48	0.98
3.49	2.43	0.70
2.52	2.10	0.83
Average: 2.82	Average: 2.28	Average: 0.82

Table 2. 5 mV/s CV capacitance ratio (0.15 V/-0.45 V) of four different experiments after 2 hr of +0.2 V applied potential.

The time for microbial cell loading with applied potential was optimized at 2 hr using the capacitance ratio method. The total time for loading was tested by application of three different potential regimes (Figure 15).

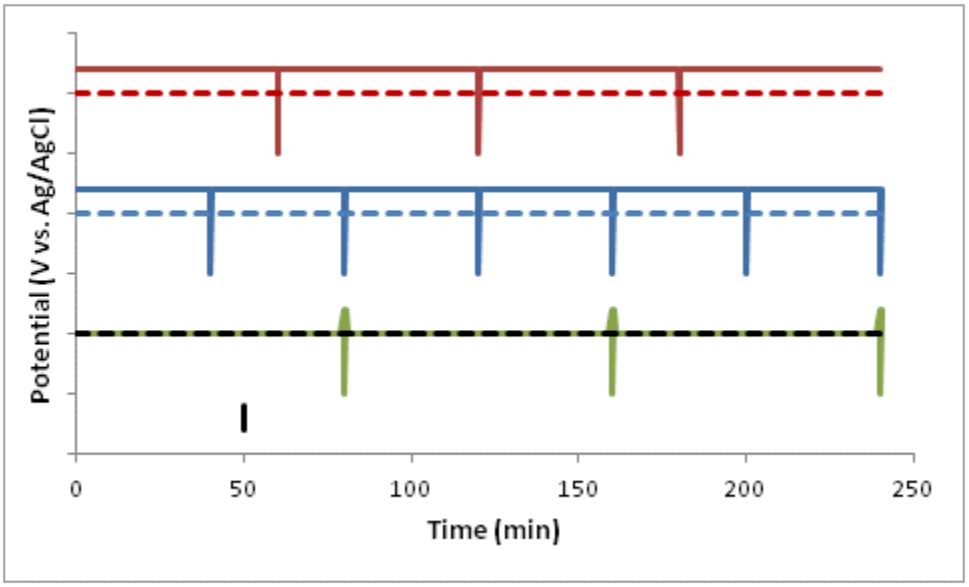

Figure 15: 0.2 V loading time before each CV. The potential shown in the solid lines is relative to zero potential (dotted lines). The CV is observed as an excursion in negative potential. The small black line is a 0.2 V scalar.

The CR for experiments with incubation at 0.2 V all showed enhancement relative to the control experiment (Figure 16). The control experiment (lower trace in Figures 15 & 16) showed minimal increase in anodic capacitance. When incubated at 0.2 V there was an enhancement in capacitive ratio (upper traces Figures 15 and 16). Experiments 1 and 2 both had a total time of 4 hr at 0.2 V. Based on these experiments it was determined that by the 2 hr mark the CV capacitance ratio had reached a point of diminishing returns, seen in Figure 16. The greater the number of interruptions the lower the CR, indicating the CV excursion to -0.5 V had the ability to disrupt establishment of microbial films on the electrode.

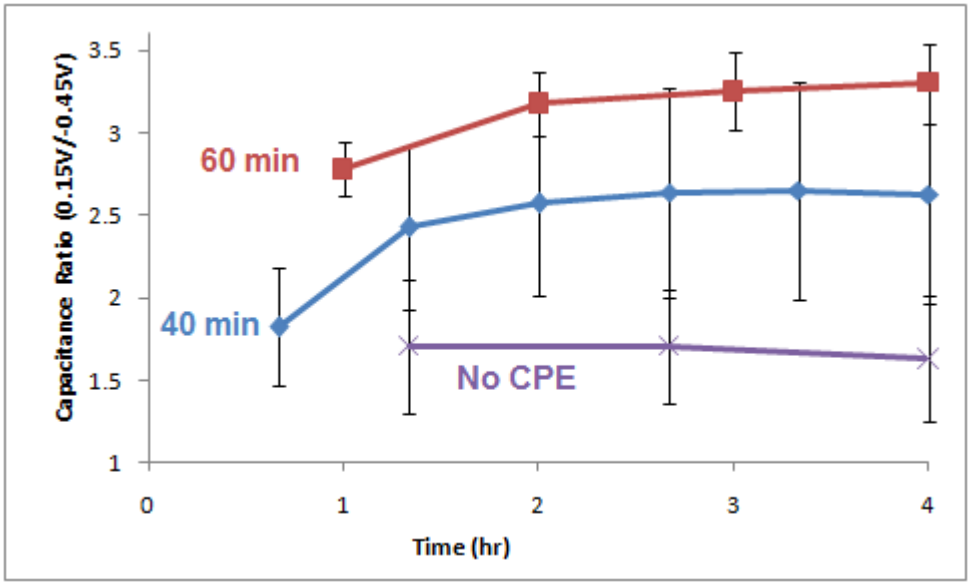

Figure 16: +0.2 V potential was applied for a determined amount of time before a 5 mV/s CV was taken. The CV capacitance ratio was plotted against the total time elapsed. 3 replicates were taken for each set of conditions.

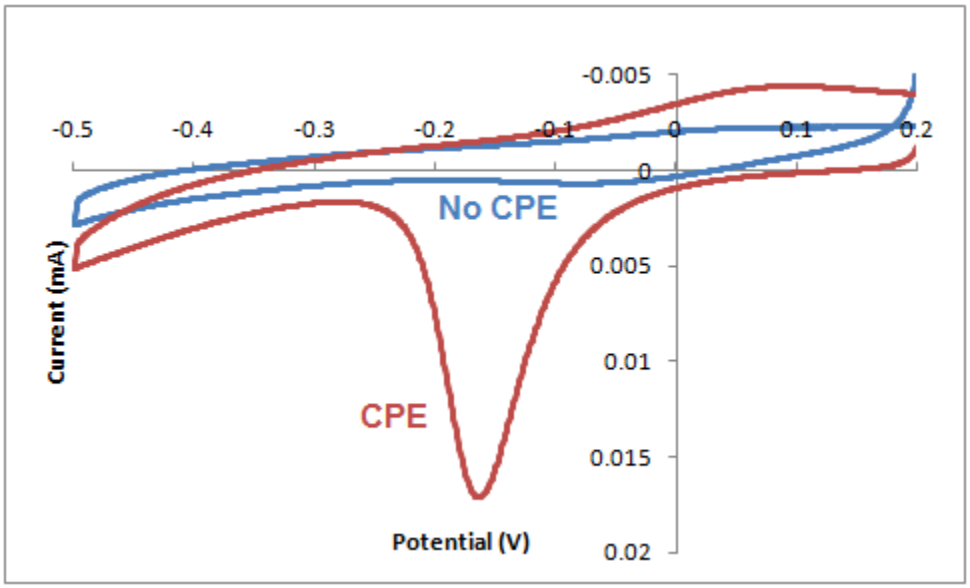

Figure 17: 2 hr of +0.2 V potential was applied before the CPE CV while 2 hr without any potential preceded the CV marked No CPE. Both CVs at 5 mV/s scan rate.

The effect of 2 hr of +0.2 V applied potential can be seen in Figure 17, which shows two CV plots of *S. putrefaciens*: one after being in the spectroelectrochemical cell for 2 hr without any applied potential (No CPE) and another under the same conditions

except for +0.2 V of applied potential for 2 hr (CPE). A much larger set of reduction and oxidation peaks can be seen after the applied potential whereas no applied potential provides a much smaller set of redox peaks.

Shewanella putrefaciens Does Not Exude Mediators

Figure 9 showed not only capacitance features associated with the microbial population but also two distinct electron transfer events (peaks). These are attributed to the microorganisms themselves and not to any exuded mediators. This was demonstrated in the next experiment. The microbes were centrifuged out of a *S. putrefaciens* culture and the remaining supernatant was tested. Figure 18 compares a CV of this supernatant against the *S. putrefaciens* CV from Figure 9. If extracellular mediators were in the culture then they would remain in the supernatant and thus any redox peaks could be attributed to them. The microbe-free solution in Figure 18 has the reduction scan with a rising current past -0.4 V and a broad return current centered between -0.25 and -0.10 V. The oxidative location does not correspond to the CV observed in Figure 9 where the oxidative peak is clearer and located at -0.10 V. This indicated that either no mediators are in the culture or that the mediators were centrifuged out along with the microbes. The data suggests that the electron transfer electrochemistry is related to direct contact of the microbes with the electrode.

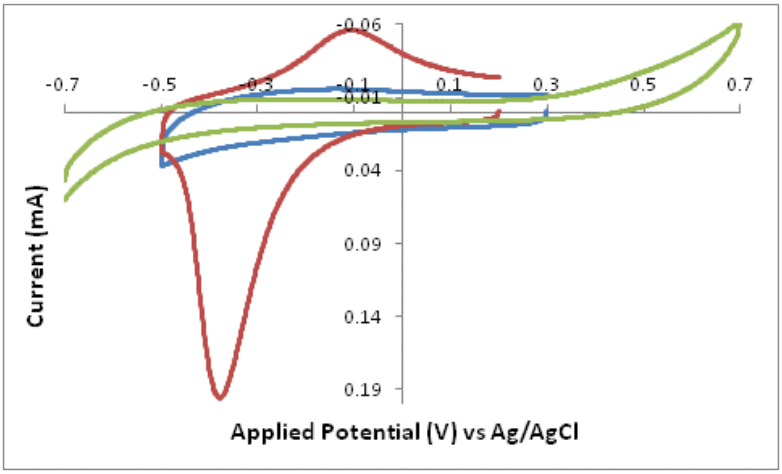

Figure 18: CV of *S. putrefaciens* from Figure 9 (red graph), the sterile TSB solution from Figure 9 (green graph), and a *S. putrefaciens* growth culture after the microbes are centrifuged out (blue graph). Scan rates at 100 mV/s for each CV.

Surface Confined Microbes are Responsible for Electrochemistry

A large number of the microbes attached during conditioning at 0.2 V can be retained even when the electrochemical cell solution is replaced with microbe free TSB as shown in Figure 19.

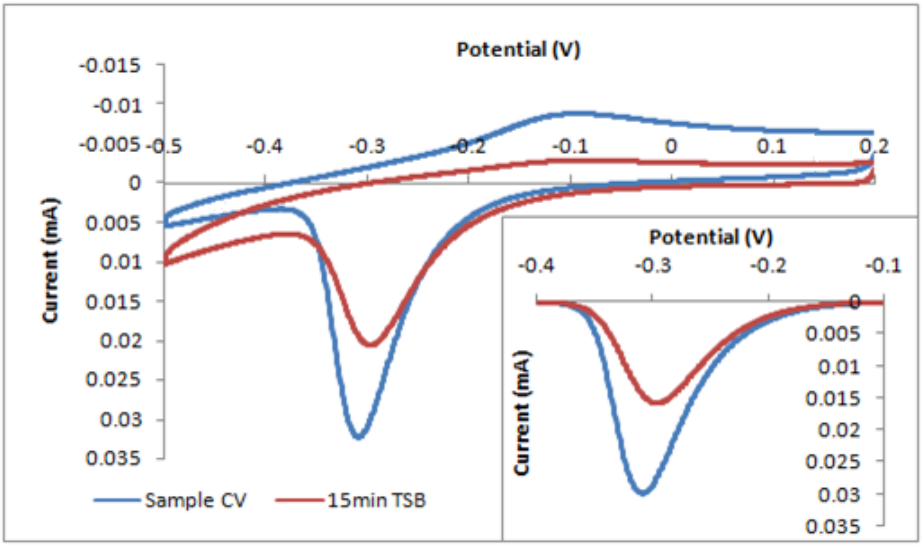

Figure 19: Both CV scans are of *S. putrefaciens* after 2 hr of +0.2 V applied potential at a 5 mV/s scan rate on a bare ITO slide. 15 min TSB had replacement of the bulk solution with sterile N_2 purged TSB to remove unattached microorganisms. Insert: baseline corrected reduction peaks.

The experiment labeled “15 min TSB” in Figure 19 had the *S. putrefaciens* solution subjected to an applied potential of +0.2 V for 2 hr. Sterile, nitrogen purged, TSB was slowly pumped into the electrochemical cell (~10 mL/min, the slowest rate for the pump in use) during the final 15 min. The time was determined by the volume flow rate and the total volume of the electrochemical cell. The experiment was designed to remove the bulk solution (containing any possible mediators) without disturbing any adsorbed microbes. After this was completed a CV was run at 5 mV/s, shown as "15 min TSB" in Figure 19. The presence of the reduction peak indicates the *S. putrefaciens* microbes remain attached to the working electrode during rinsing. The insert in Figure 19 is of the reduction peaks after baseline correction. It shows both experiments have a similar, non-symmetric, shape, albeit different peak heights. The asymmetry indicates the possibility of multiple electron transfer events. There is a loss of the diffusional components which may be attributed to mediators.

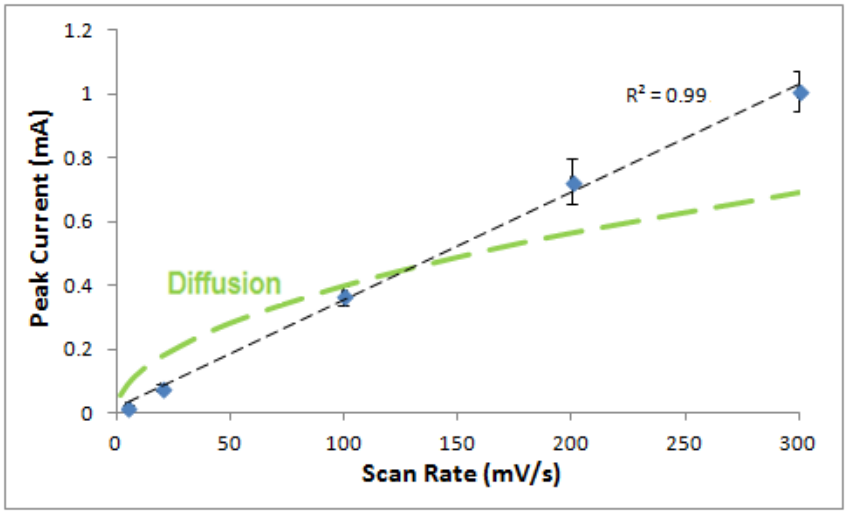

Figure 20: Graph of scan rate vs peak reduction current. The corresponding R^2 value is included with the linear trendline. The green dashed line represents a theoretical diffusion curve.

Figure 20 shows the magnitude of the Faradaic reduction peak is linearly dependent upon scan rate. This is consistent with a surface confined reaction, as a diffusion process results in the peak height increasing by the square root of the scan rate, represented by the dashed line in Figure 20. This result is further proof direct electron transfer (instead of mediated electron transfer) during the reduction process is operative.

Shewanella putrefaciens Microscope Imaging Procedure

After an experiment the ITO slide was removed from the spectroelectrochemical cell and air dried. Two cover slips were then placed on top of the ITO slide and it was imaged at 400x with an Olympus BH2 compound microscope using confocal microscopy. Twelve images were taken of each ITO slide after an experiment. These images were taken in the upper, center, and lower regions of the left, center, and right areas of the ITO slide for nine regions in total with two images taken in each of the three center regions, shown in Figure 21. This was to cover each region of the slide in order to offset any discrepancies that may occur across the slide, particularly at the jointure of the cover slips (the gray boxes in Figure 21). Discrepancies arising from the operation of the spectroelectrochemical cell may arise from the location of the input and exit ports, the location of the potential gradients in the cell due to placement of the counter and reference electrode, and gravity. The input port directly pumped solution at the ITO slide. To prevent mechanical detachment of attached microbes the flow rate was kept at the lowest possible rate allowed by the pump. The output port was located above the

left side of the ITO slide. During and after each experiment the slide was on its side so that gravity was pulling the opposite direction of the output (*i.e.* down through the slide).

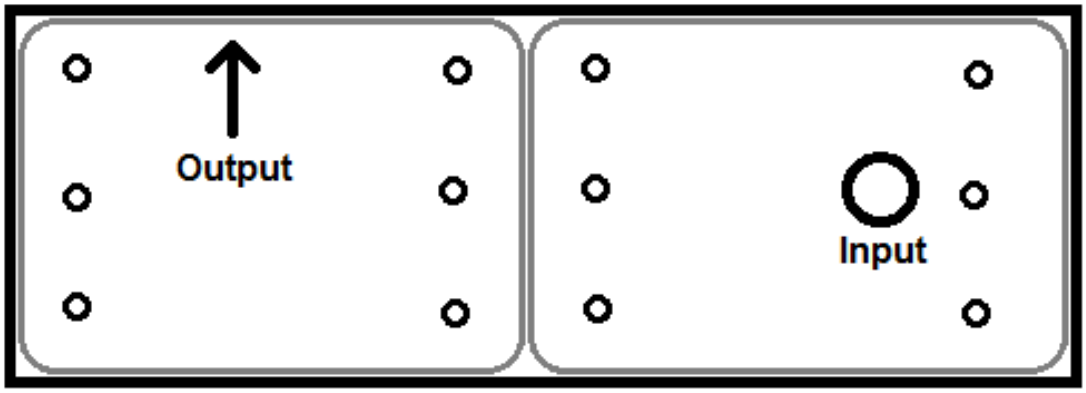

Figure 21: Relative locations of where microscope images were taken on the ITO slide are represented by 12 small circles. All images were taken of the experimental area. The input location is represented by a large circle and the output is above the arrow. The gray boxes represent the cover slips placed on the ITO slide during imaging.

Dried cells on the ITO slide were either manually counted or analyzed by NIH ImageJ software. The NIH ImageJ program was used to set the contrast between the microbes and the background so that the microbes could be made measurable. The program calculates the percent area of the microbes vs total area. The percentage was related to the number of cells present by manual count of select samples. The NIH ImageJ program was validated by comparing it to manually counted results (Figure 22).

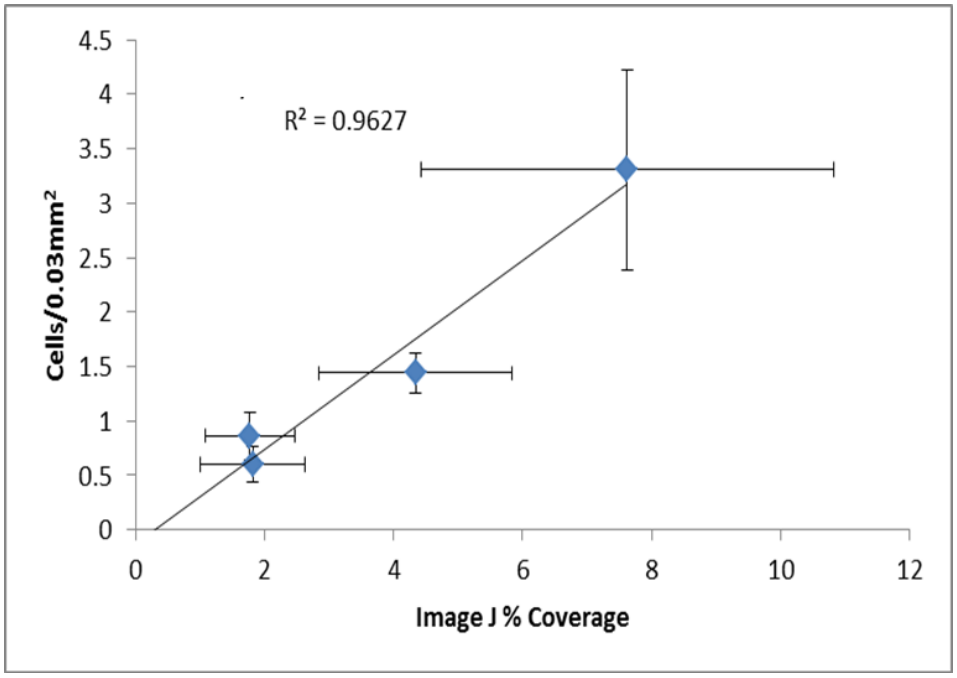

Figure 22: Comparison of cell counts between the ImageJ program and manual counting.

Shewanella putrefaciens Imaging Results

Images of the ITO electrode were taken after each experiment to count how many cells remained on the electrode. Each experiment had images taken in multiple places around the electrode to account for possible variation in electrochemical cell potential, seen in Figure 23. A sample image taken after an experiment is shown in Figure 24. There was found to be minimal difference in the average microbe density across the electrode relative to the error in the replicate manual counts, as shown in Figure 25.

Upper Left	Upper Center	Upper Right
Center Left	Center	Center Right
Lower Left	Lower Center	Lower Right

Figure 23: Locations of where the ITO electrode was imaged.

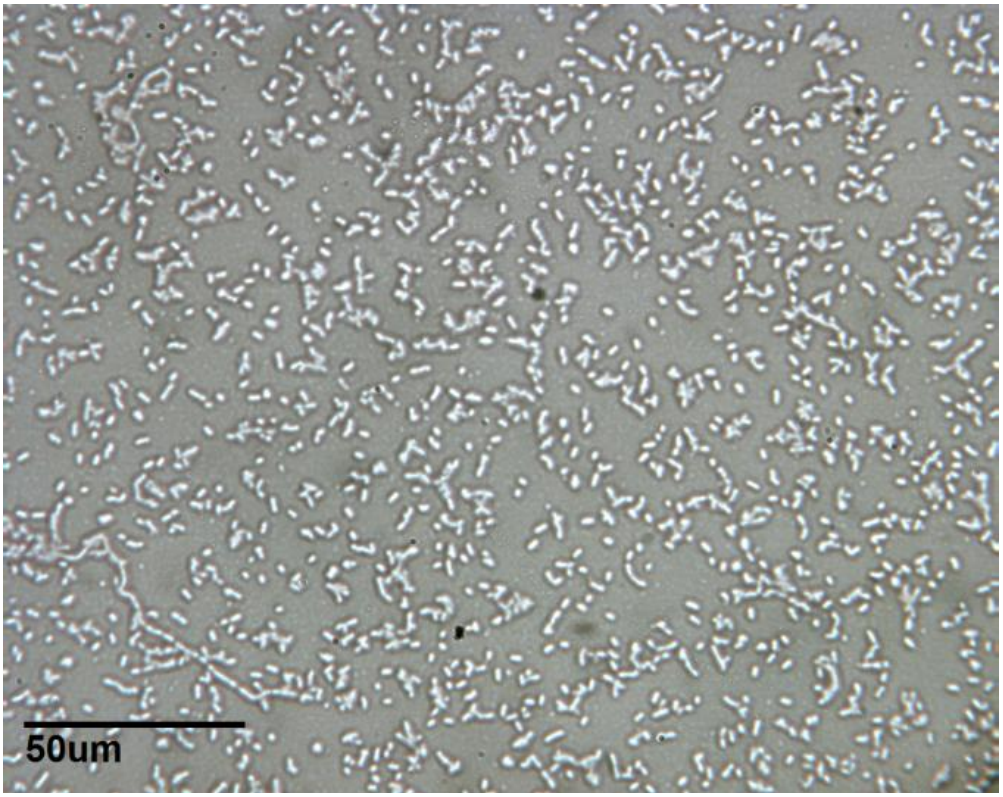

Figure 24: Sample image of an ITO electrode after an experiment.

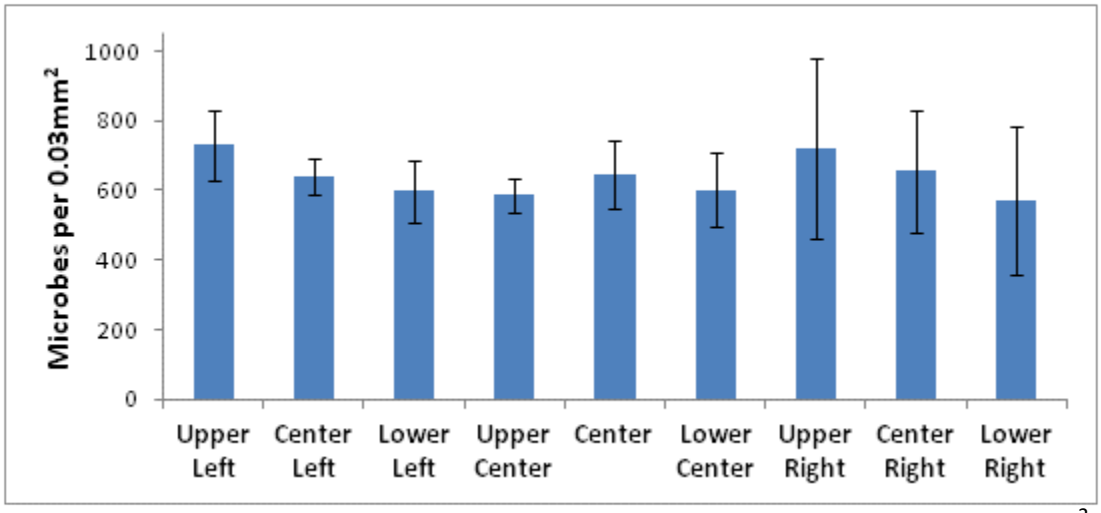

Figure 25: Average number of microbes from 3 experiments (counted per 0.03 mm^2) according to where the images were taken on the electrode (seen in Figure 23).

Figure 26 shows the amount of microbes that were manually counted on the ITO electrode after each type of experiment. Controlled Potential Electrolysis (CPE) means 2

hr of +0.2 V potential was applied before the CV (if taken) and imaging. Those marked No CPE had no potential applied while the microbes were in the electrochemical cell for 2 hr. After the applied potential half of experiments had a CV taken before imaging.

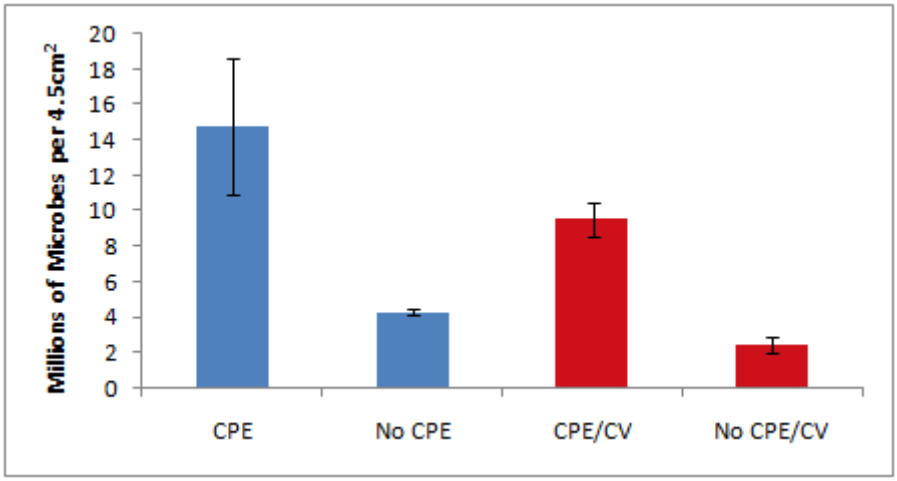

Figure 26: The amount of microbes imaged in a 4.5 cm^2 area on the ITO electrode. Those marked CPE had 2 hr of +0.2 V potential applied before imaging. The red bars had a CV taken. 3 replicates were taken for each set of conditions with an average OD_{650} of 0.35 for around 92 million microbes/mL and 1 billion total microbes.

More microbes attached to the electrode when +0.2 V of potential was applied for 2 hr, as seen from the first two bars in Figure 26. The bar labeled "CPE" had 2 hr of applied potential while the bar labeled "No CPE" had no applied potential. The applied potential experiment had 14.8 ± 3.8 million microbes vs 4.31 ± 0.14 million microbes for no applied potential. The total cell count was obtained by averaging the cell counts in the sampled microscopic areas scaling to the total area. The increased attachment of *S. putrefaciens* microbes under applied positive potential is in agreement with the CV and CR data shown above. [19]

A second series of experiments examined the effect of a single CV on electrode coverage by microbes. The red bars in Figure 26 had the electrode held at +0.2 V for half

the experiments while the other half did not have any applied potential. All of these experiments had a CV taken after the 2 hr (with or with applied potential) before being imaged. As in the preceding experiment, the cell count was higher when potential was applied (9.6 ± 0.96 vs. 2.4 ±0.5 million cells). By comparison to the preceding experiment nearly 5 million cells are dislodged during the CV. In both cases, *i.e.* with or without applied potential, around 65% of microbes remained on the electrode after a CV. This corresponds with Figure 12, which noted that multiple CVs resulted in lower current, likely from microbes no longer being on the surface. The peak magnitude drop was of a similar magnitude as the loss of cells (ca. 50%).

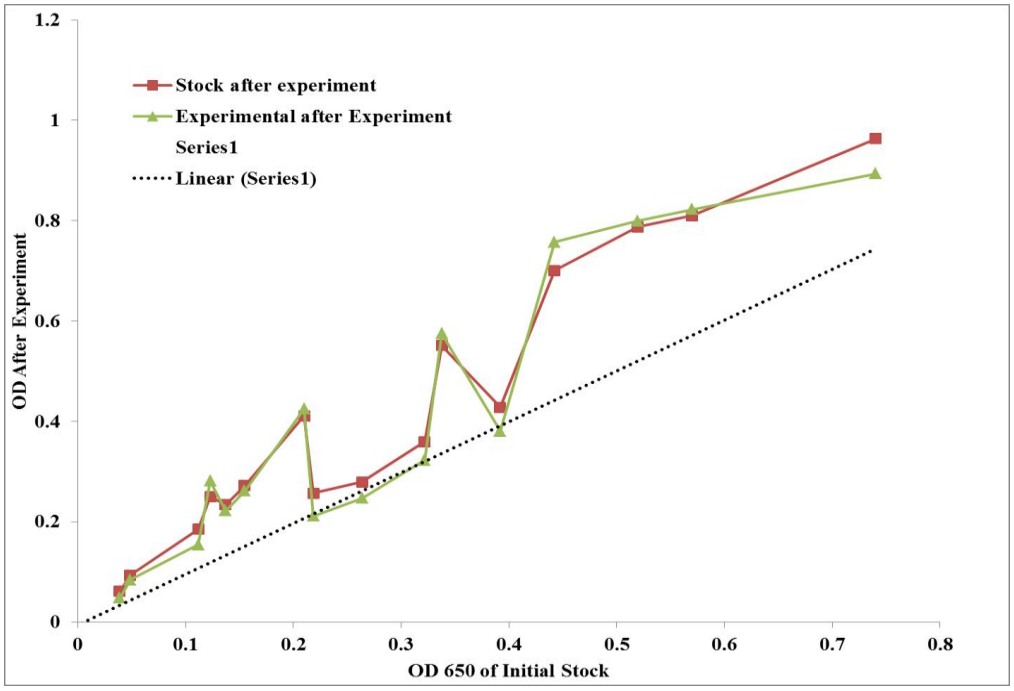

Figure 27: Plot of the OD_{650} of the unused stock culture vs. the experimented sample (both taken from the original stock culture) after the experiment is complete with the x-axis being the OD_{650} of the original stock culture.

The previous experiments indicate that the cells are affected by application of electrode potential both in loading and in ejection under a negative potential scan. In order to determine if the viability of the cells was altered by the experiment the following experiment was performed. Figure 27 shows how the OD_{650} changes in multiple separate experiments. The x-axis is the original stock OD_{650} culture taken before the experiment begins. The Stock after experiment is the same stock culture (which remained in the original stock flask during the experiment, *i.e.* it was not tested) after the experiment and the Experimental after Experiment is the culture that was tested in the spectroelectrochemical cell. The tested culture has an OD_{650} similar to the untested culture. The intent was to determine if the difference in OD_{650} could be used to calculate the amount of microbes that attach to the ITO electrode. Unfortunately the results did not prove this and were unusable in this regard.

Part IV: Optical Setup and Parameter Verification

System Description

The system allows for spectral measurements both in the transmission and ATR modes. The ATR mode (evanescent field discussed above) is a multiple reflection arrangement that provides substantial enhancement in sensitivity and selectivity (Figure 8). In the transmission mode, the light path is a single pass, which is perpendicular to the ITO electrode device. However, transmission spectroelectrochemistry may lack sufficient sensitivity to probe thin films because the light runs through the entire

solution instead of just near the surface, which can result in not being able to measure the surface changes due to them being too small compared to the rest of the solution.

High refractive index (RI) fluid (Cargille, RI = 1.517) was applied to each end of the ITO to hold the coupling prisms in place. Schott SF6 coupling prisms (RI = 1.84, Karl Lambrecht, Chicago, IL) were put in place on each end of the ITO slide and the assembled cell was then placed on a mount. The position of the mount and the orientation of the fiber optic cables were such that the incident angle of light was 29.9°. This is the angle at which the maximum possible intensity output is obtained at a wavelength of 460 nm, as previously determined. [124] No attempt was made to optimize the output for any of the wavelengths determined to be diagnostic for the microorganisms (see below).

The light enters the ITO waveguide via Schott SF6 coupling prism. Once in the ITO it is totally internally reflected until it is refracted out through the outcoupling prism, visualized in Figure 28. Total internal reflection (TIR) occurs because the refractive index of the ITO waveguide medium is higher than the refractive indices of the glass substrate and the film-analyte superstrate.

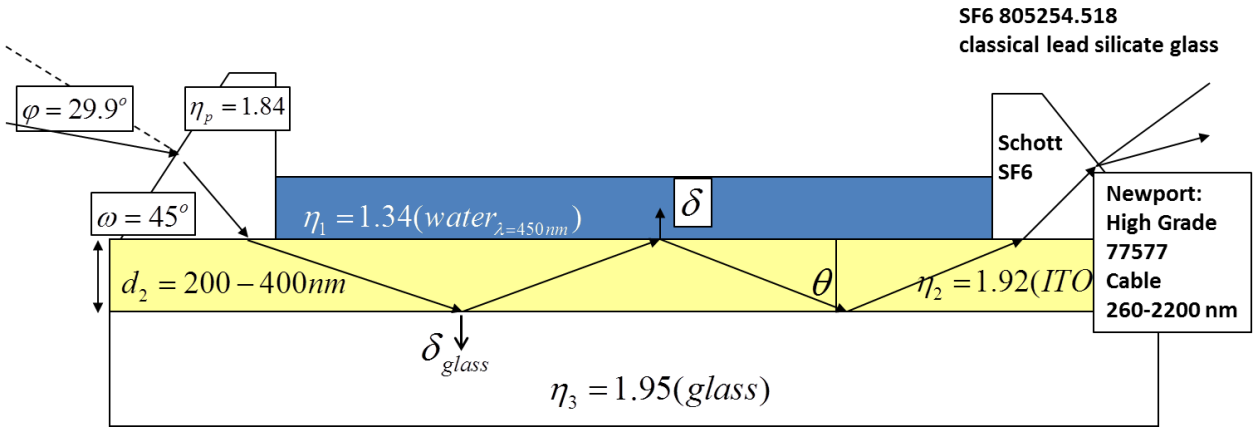

Figure 28: Visualization of how light enters through the incoupling prism, reflects through the ITO substrate, and exits through the outcoupling prism. Representative angles (φ,ω,θ), refractive indexes (η), and penetration depth (δ) listed. The thickness of the ITO (d_2) is 200-400 nm.

The depth of penetration can be calculated from the various experimental parameters and appropriate ATR equations. (See for example, Agyeman Ph.D. 2007.) Agyeman [124] calculated the penetration depth in the presence of a clay superstrate to be ~100 nm. In the presence of water the depth has been calculated to be ~42 nm at 460 nm. This depth is well below the diffusion depth sampled in most electrochemical experiments.

$$x \sim \sqrt{2Dt} \qquad (20)$$

For the CV experiments described above (1.4 V at 0.005 V/s = 280 s, and a typical diffusion coefficient of 10^{-6} cm^2/s) the depth of electrochemical sampling is expected to be ca. 0.02 cm or 200 µm. The dimensions of *S. putrefaciens* are reported to be ca. 0.5 to 2 µm, which lies well within the electrochemical sampling volume. The electrochemistry described above suggests that *S. putrefaciens* attaches to the surface.

If so, then the sampling region includes the inner and outer membrane (~40 nm thick), where the reactive proteins are located.

The optical window is controlled by the various components present. Light from a 75 watt Xe arc lamp (Newport Corp; transmittance range: 200-2400 nm) was directed to a Schott SF6 coupling prism (transmittance range: 300-2500 nm) via fiber optic cables (Oriel Corp Model 77577 output & 77578 receiver; transmittance range: 260-2200 nm for both). The light enters the ITO waveguide within which it is totally internally reflected until it is refracted out through the outcoupling prism. Total internal reflection (TIR) occurs because the refractive index of the ITO waveguide medium is higher than the refractive indices of the glass substrate and the film-analyte superstrate. The light exiting the planar waveguide via the exit prism was collected by a second fiber optic cable and directed to an Ocean Optics USB2000 detector (detector range: 200-1100 nm) to be displayed by the OOIBASE32 program (Ocean Optics Inc).

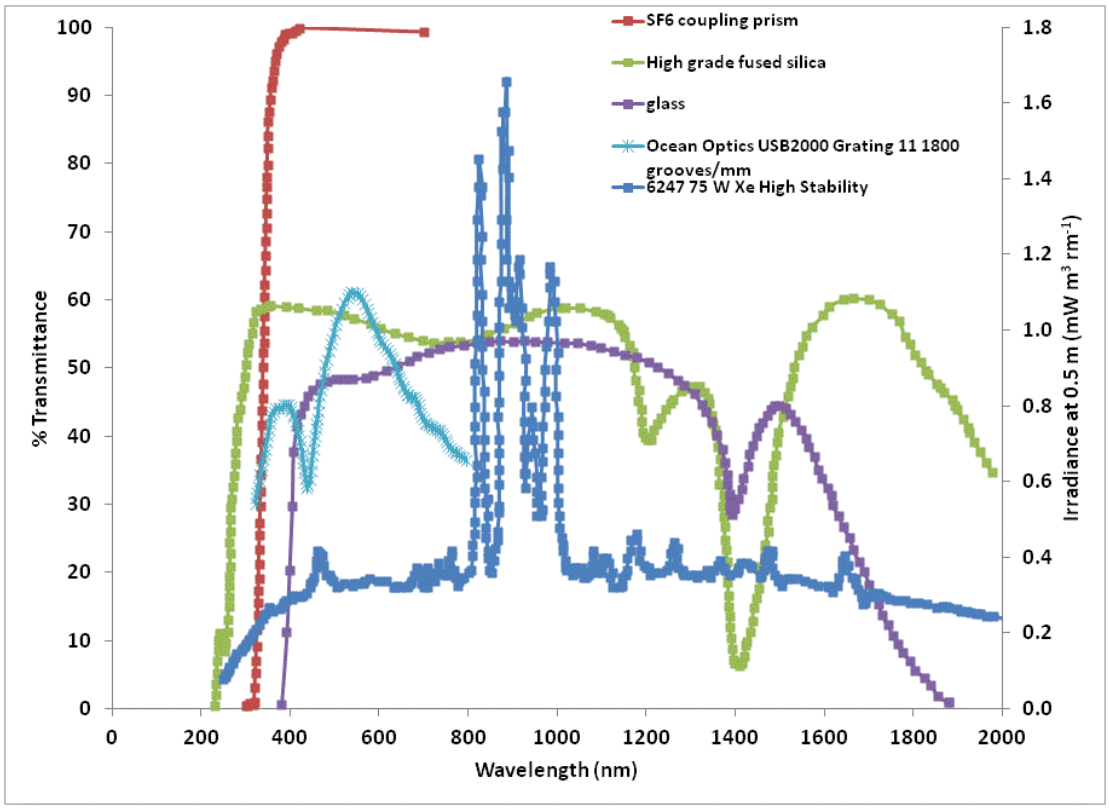

Figure 29: Optical range of individual parts used in the spectroelectrochemical cell setup.

As shown in Figure 29, in principle, the optical range is curtailed by the glass substrate to the ITO electrode at low wavelength. The upper wavelength region appears to be curtailed primarily by the Ocean Optics grating used. For data acquired <400 nm or >700 nm the total amount of light collected is low and it is anticipated that noise will be correspondingly increased.

Data was acquired using a single spectra collection, at typically 10 ms integration time. More details on the spectra collection rate will be given when discussing the Shewanella experiments.

Validation of surface confinement via tris(2,2')ruthenium(II) ($Ru(bpy)_3^{2+}$)

The spectroelectrochemical cell was tested with tris(2,2')ruthenium(II) chloride to verify the system can simultaneously measure evanescent wave light spectra and electrochemistry. This section reports on that validation.

The choice of an appropriate chemical to validate the spectroelectrochemical system performance is of great importance since the criteria below have to be met. First, the analyte (usually a complex ion) must have different oxidation states such that one oxidation state absorbs much more strongly than the other at an accessible wavelength. Second, the complex ion or its ligands must be able to partition into the selective film (in this case a thin layer of montmorillionite clay) and be pre-concentrated. Third, the complex ion must be relatively stable in both oxidation states. Fourth, the complex ion must be electrochemically active and exhibit facile electrochemical behavior at the ITO electrode. Finally, the redox potential of the complex ion couple must be accessible within the electrochemical potential window of the ITO electrode.

The validation of the electrochemical and optical measurements made with the homebuilt spectroelectrochemical system was tested with the reversible tris(2,2'-bipyridyl)ruthenium(II)chloride hexahydrate ($[Ru(bpy)_3]^{2+}$) complex. This method tested both the evanescent wave mode of the light spectroscopy and the electrode setup.

Tris(2,2'-bipyridyl)ruthenium(II)chloride hexahydrate was chosen as the model analyte for this validation work since it is the best candidate that satisfies all of the

above mentioned. The redox couple, $[Ru(bpy)_3]^{2+}$ / $[Ru(bpy)_3]^{3+}$, has well defined and reversible electrochemical behavior. $[Ru(bpy)_3]^{2+}$ absorbs strongly at 460 nm whereas there is no absorption by $[Ru(bpy)_3]^{3+}$. It is expected that both $[Ru(bpy)_3]^{2+}$ and $[Ru(bpy)_3]^{3+}$ will be ion-exchanged and intercalated into the interlayers of a clay film due to the clay having an anionic charge and the complex having a cationic charge. The clay film is used to confine the complex to the surface of the electrode. The structure of $[Ru(bpy)_3]^{2+}$ is propeller-shaped and matches the geometry of the hexagonal holes of the clay, allowing for better intercalation within the clay matrix. [128-131]

A thin clay coating was placed on an ITO slide before the slide was placed into the electrochemical cell. A fresh clay coating was used for each replicate of this validation experiment. The clay coating was applied by first cleaning the ITO slide with isopropyl alcohol, laying it on a flat surface, then pipetting 500 µL of a 1 g/L Sodium Wyoming montmorillonite (SWy-1) (obtained from the Source Clay Minerals Repository at Purdue University, Indiana) clay solution and letting the solution evaporate, leaving behind a thin clay layer. The amount of clay present was not optimized for this experiment.

After the spectroelectrochemical cell was assembled with the thin clay layer on the ITO slide, a solution containing 0.1 mM $[Ru(bpy)_3]^{2+}$ and 0.01 M NaCl was pumped into the electrochemical cell. $[Ru(bpy)_3]^{2+}$ was absorbed into the clay layer and after some time had passed was then measured in the visible light region when a sweeping potential (*i.e.* a CV) was applied. The applied potential oxidized the $[Ru(bpy)_3]^{2+}$ to

$[Ru(bpy)_3]^{3+}$. The oxidation occurred at 1.13 V and all experiments had the applied potential sweep from 0.9 V to 1.3 V back to 0.9 V at a scan rate of 0.01 V/s. When sweeping negative the $[Ru(bpy)_3]^{3+}$ was reduced back to $[Ru(bpy)_3]^{2+}$. The reduction was confirmed both by the current and the observed absorbance.

One aspect of using $[Ru(bpy)_3]^{2+}$ in this experiment was making sure enough time had elapsed for the molecule to saturate the clay film. As the $[Ru(bpy)_3]^{2+}$ concentration in the clay film increased so did the peak height of the cyclic voltammogram (Figure 30) while the magnitude of light absorption change increased (Figure 31). The absorbance appeared to remain constant after an hour of saturation while the CV increased in current through two hours, indicating the absorbance samples a smaller solution depth than the CV. Figures 30 and 31 are spectra from the same experiment, which illustrates how this experimental set-up can measure light and electrochemical spectra at the same time.

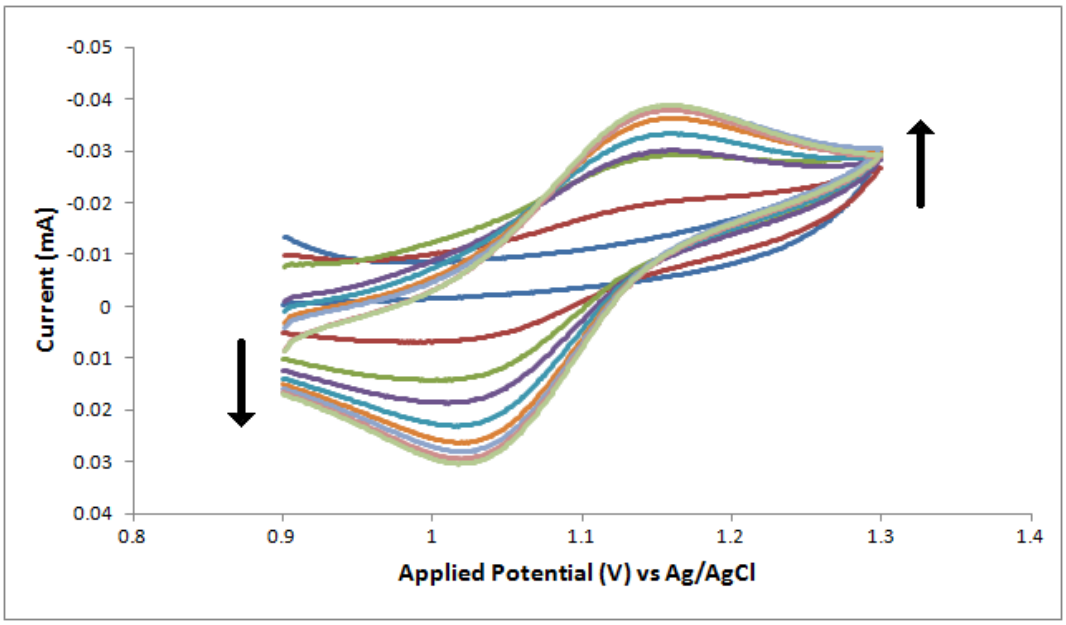

Figure 30: The measured CV current (scan rate: 10 mV/s) increases over time as 0.1 mM $[Ru(bpy)_3]^{2+}$ in 0.01 M NaCl saturates the clay film. The arrows indicate the direction each peak is increasing as time progresses. Samples were taken at 30 min, 60 min, and 70 min with 10 min increments thereafter to 120 min.

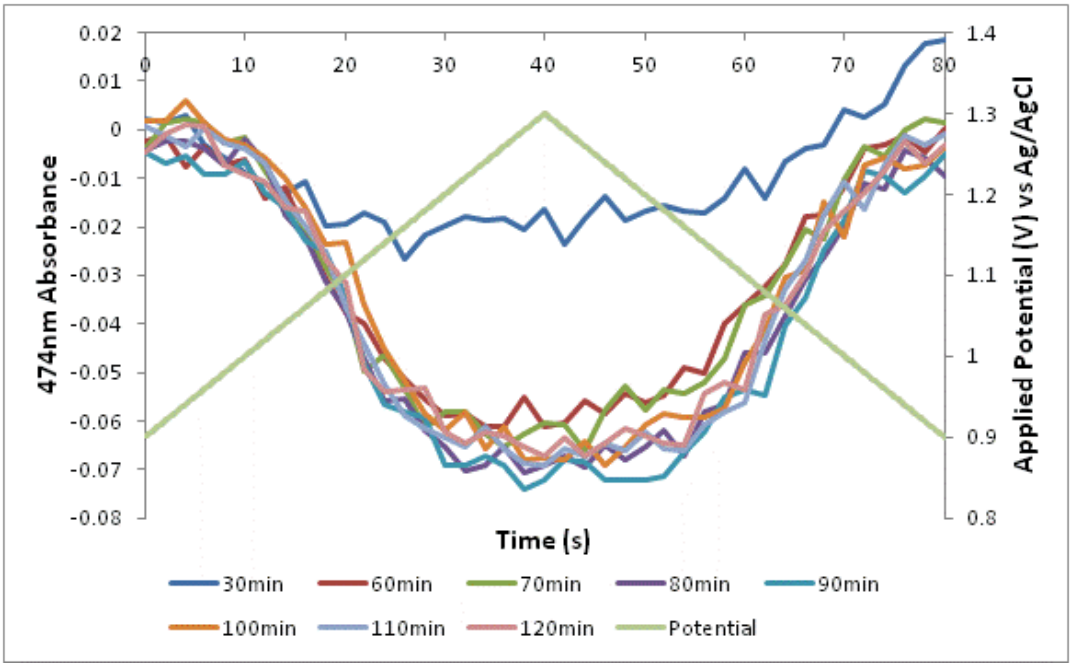

Figure 31: The measured 474 nm light absorbance over time. Each light spectrum was taken the same time as each CV in Figure 7. Light spectra data points were taken every 2 sec. The applied potential (from 0.9 to 1.3 to 0.9 V) is on the right y-axis, relating how the light spectra changes with applied potential.

The light absorbance plateaus earlier than the current, seen in Figure 32. In order to visualize the data better each value was normalized to 1 = minimum signal. This result was not investigated further.

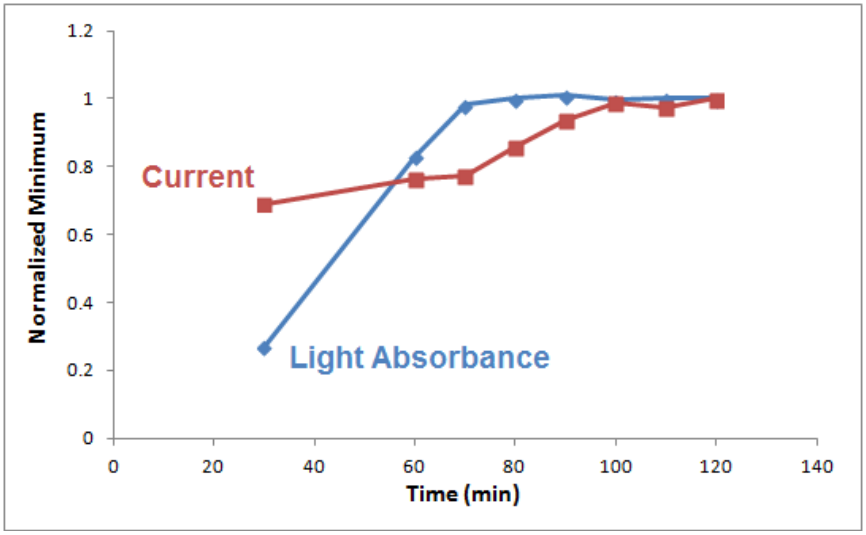

Figure 32: Values of the current and light absorbance from Figures 7 and 8 after being normalized to 1 = minimum signal.

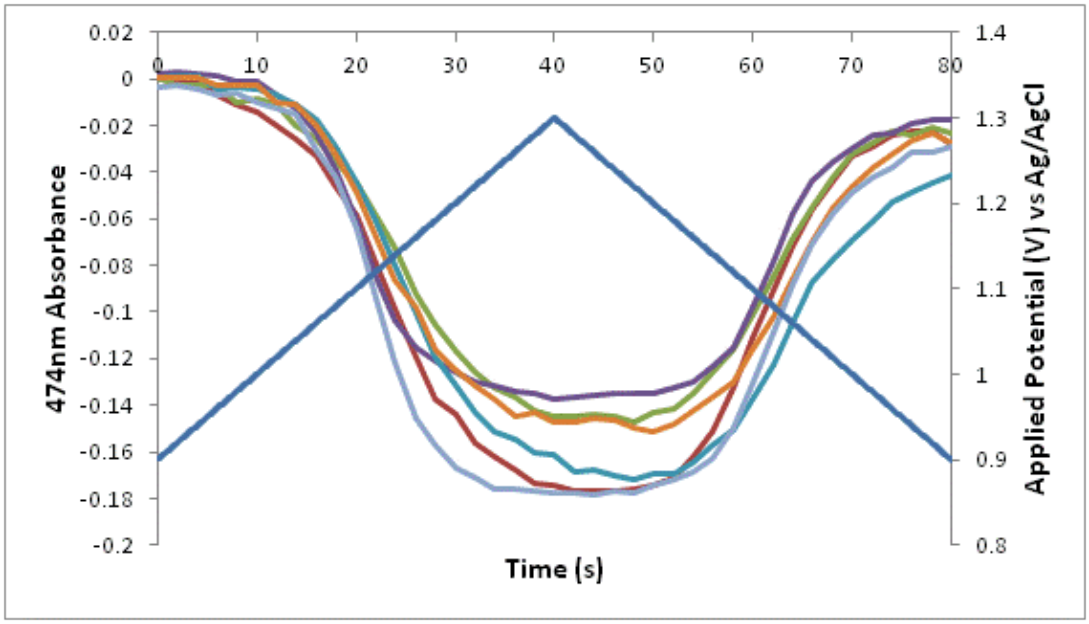

Figure 33: An overlay of the final 474 nm absorbance change taken from separate $[Ru(bpy)_3]^{2+}$ experiments. The applied potential (from 0.9 to 1.3 to 0.9 V) is on the right y-axis.

The $[Ru(bpy)_3]^{2+}/[Ru(bpy)_3]^{3+}$ based experiment was repeated multiple times with the final light absorbance of each day plotted in Figure 33. The variation in the light absorbance at the switching potential is noticeable at -0.159 (± 0.018). This was attributed to variation in clay film formation consistent with earlier reports. [132-134] The results from the $[Ru(bpy)_3]^{2+}$ experiments agree with literature values [21] and validate the spectroelectrochemical setup.

This experiment validates that the fact that this setup only samples surface confined species, albeit the light absorbance samples a smaller depth than the CV. This is relevant as the microbe *Shewanella putrefaciens* can be tested at the ITO surface rather than the entire bulk solution.

Validation with Cytochrome c

S. putrefaciens has cytochrome c in its outer membrane (OM), which absorbs specific wavelengths based on whether it is oxidized or reduced. [135] Studying the absorbance wavelength should provide another method to determine the redox state of the microbes. To verify the spectral signature expected from the cytochrome c of the microbial OM wall, experiments were performed with pure cytochrome c.

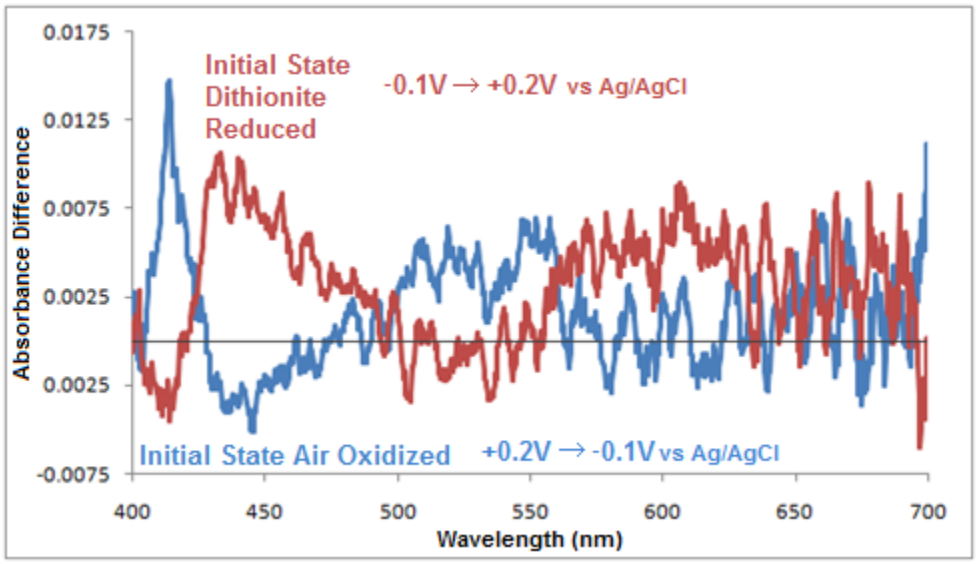

Figure 34: Purified equine heart cytochrome c light difference spectra (I_o obtained at E_i and I obtained at the switching potential, E_s). The spectra labeled "oxidized" refers to an oxidized sample of cyt c that was subsequently reduced. The spectra labeled "reduced" refers to a reduced sample of cyt c that was subsequently oxidized.

In Figure 34 a 3 µM purified equine heart cytochrome c (Sigma Aldrich) in 0.1 M KCl solution was run in evanescent wave mode in the spectroelectrochemical cell. Air oxidized and sodium dithionite (Mallinckrodt Baker, Inc) reduced cytochrome c were tested for comparison. In the case of the air oxidized cytochrome c a difference spectra was obtained at E_i +0.2 V (oxidized state) and E_s -0.5 V (vs. Ag/AgCl) (reduced state). In the case of the chemically reduced (dithinonite) cytochrome c, a difference spectra where I_o was obtained at -0.1 V vs Ag/AgCl (reduced state), and I was obtained at +0.2 V vs Ag/AgCl (oxidized state). The resulting spectra display the Soret reduction band (for air oxidized) and the Soret oxidation band (for dithionite reduced) bacteria. [135,136]

There are some differences between our experiment in Figure 34 vs literature results. [136] The absorbance of our experiment was much lower. Figure 34 has a peak

absorbance difference of ~0.015 for the Soret band around roughly 414nm. Literature has the peak absorbance difference of ~0.5 in the same Soret band region. The difference is likely from using evanescent wave mode, which only measures ~100 nm above the ITO surface. Literature, however, had the cytochrome c observed in a transmission experiment while it was immobilized at the electrode surface in a 30 µm thick biofilm of *Geobacter sulfurreducens* grown over 96 hr. [136] The lower net signal in the evanescent wave mode accentuates signal to noise issues related to the CD (uncooled) detector. The signal-to-noise ratio could be increased with increased integration time and waveform summation, and/or averaged number of CV scans. The breadth of the reduction peak is larger than in literature. [136] Literature has the spectral peak at 410-418 nm while Figure 34 ranges from 420-475 nm.

It will be noted, that consistent with the lower expected intensity of light collected at longer wavelengths that the noise level increases substantially. Although the noise level is large, the signal between 400-500 nm is clearly resolved from the baseline noise at the level of ± 3 standard deviations. There is significant change in the 500-600 nm region associated with the Q bands. The Q band peaks at 523 nm and 552 nm are not resolved from each other. A potential reason for unresolved peaks is adsorption to the electrode surface.

A ΔA limit of detection is calculated to be from the noise near 450 nm of 0.0016 absorbance units. From these values the signal limit of detection is calculated to be ± 0.005 absorbance units.

Part V: Application of the Spectroelectrochemical System to *Shewanella putrefaciens*

The entire spectroelectrochemical system was applied to the study of the microbe *Shewanella putrefaciens*. The setup was tested for its ability to observe the Soret band of the intact microorganism. The experimental protocol is shown in Figure 35.

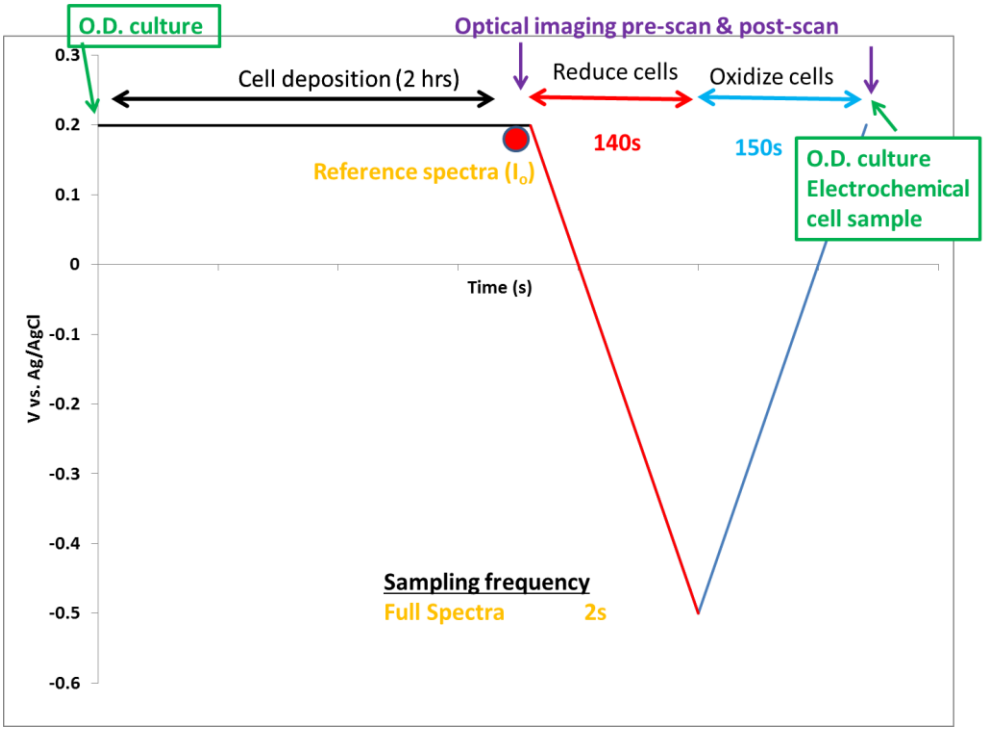

Figure 35: Visualization of the *S. putrefaciens* procedure. 2 hr of cell deposition at 0.2 V followed by a 5 mV/s CV scan to -0.5 V and back. Light spectra captured once a minute during the 2 hr deposition and every 2 sec during the CV. OD_{650} taken before and after the experiment. Imaging of the dried ITO slide was taken after the experiment.

The evanescent signal was captured from 200 nm to 900 nm during the entire experiment, however only the region from 400 nm to 700 nm was analyzed. Light spectra were captured once a minute during the 2 hr of applied potential (for 120 spectra) and every 2 sec during a 5 mV/s CV (for 140 spectra). A new light spectra

reference, I_o, was captured before the CV began and CV absorbance is reported with respect to this new reference. All light spectra were converted to absorbance relative to the initial spectra taken at the start of each respective scan. This procedure is visualized in Figure 35.

An example of the utility of the combined electrochemical evanescent wave spectroscopic method is shown with Figure 36. The goal is to combine optical and electrochemical measurements. With an applied potential of +200 mV (vs. Ag/AgCl) for 2 hr both the current and light absorbance can be measured. Figure 36 only displays absorbance at 695 nm for ease of viewing (even though absorbance from 400 nm to 700 nm was analyzed). The magnitude of the maximum current is consistent with that obtained by a working microbial fuel cell at 0.2 $\mu A/cm^3$. [137]

The spectral trace for 695 nm, assumed to measure total microbial attachment, shows an initial attachment phase, during which the current is accelerating. The peak current begins to decrease ca. 2000 s, but the rate of decrease alters at ca. 3000 s. The rate of current loss (possibly due to cell death) diminishes at the same time that new cells are seen to arrive at the electrode.

The peak in the light spectra around 3000 s is significantly after the sharp current increase. Since the light spectra only measures within ~100 nm of the electrode surface it may be that the microbes initially interact with the electrode without being in direct contact. It is also possible that the first attached microbes may result in an increased

amount of microbes, almost serving as a catalyst, resulting in microbes rapidly attaching in large groups instead of a slow, consistent rate of attachment.

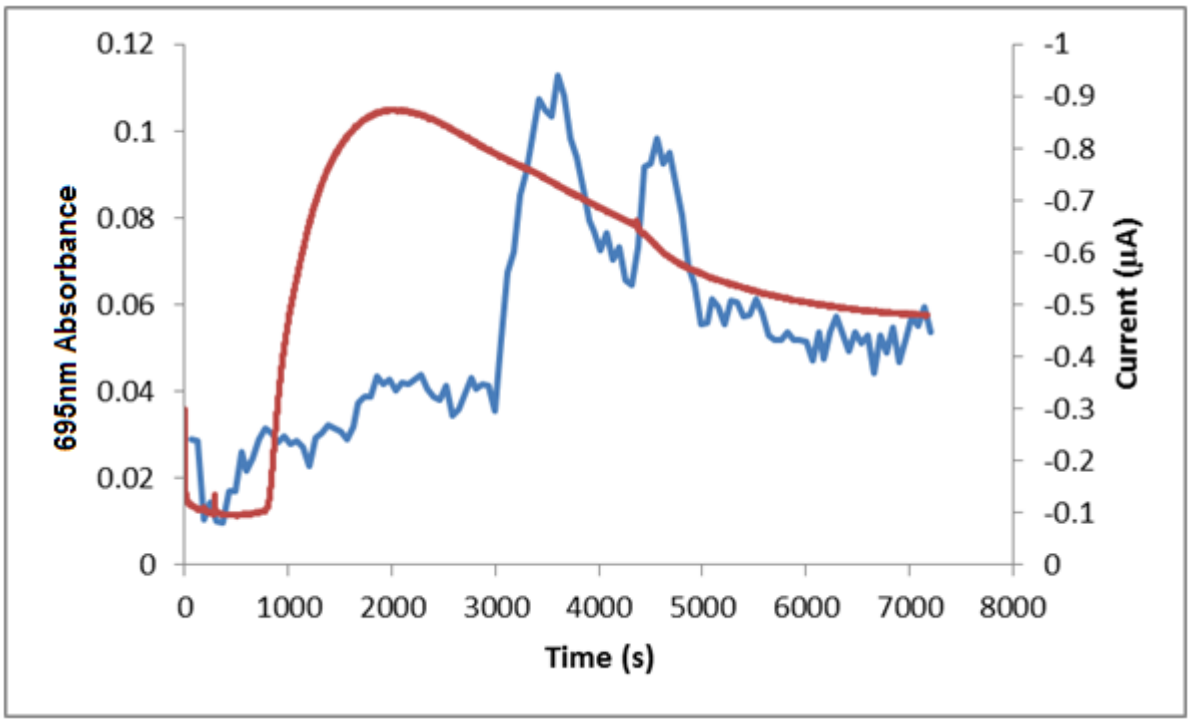

Figure 36: Current (red line) and absorbance at 695 nm (blue line) measured during +200 mV (vs. Ag/AgCl) of applied potential.

Spectra were also acquired during the CV taken after loading in the electrochemical call at 0.2 V for 2 hr, similar to the $[Ru(bpy)_3]^{2+}$ and cytochrome c experiments described above. See Figure 37. Each graph uses its respective reference spectra, I_o, obtained after two hours of +0.2 V applied potential. The blue lines are the average spectra of multiple separate experiments obtained at the switching potential of the CV. The red lines illustrate the average spectra obtained at the end of the CV. 18 different experiments were averaged at 5 mV/s and 8 different experiments were

averaged at 100 mV/s. 3 different experiments were averaged for both 200 mV/s and 300 mV/s.

Every experiment showed absorbance peaks around 422 nm and 570 nm. The 422 nm peak, the location of the Soret region, was nearly twice as large for the 5 mV/s scan rate compared to the 100 mV/s and 200 mVs scan rate. This suggests that more material was reduced when a longer time was allowed for electron transfer. Another difference between the 5 mV/s and higher scan rates is a return to initial conditions. At high scan rates the absorbance at the final potential did not change much from that obtained at the switching potential, consistent with a lack of re-oxidation. At 5 mV/s it can be observed that more of the material is capable of being re-oxidized.

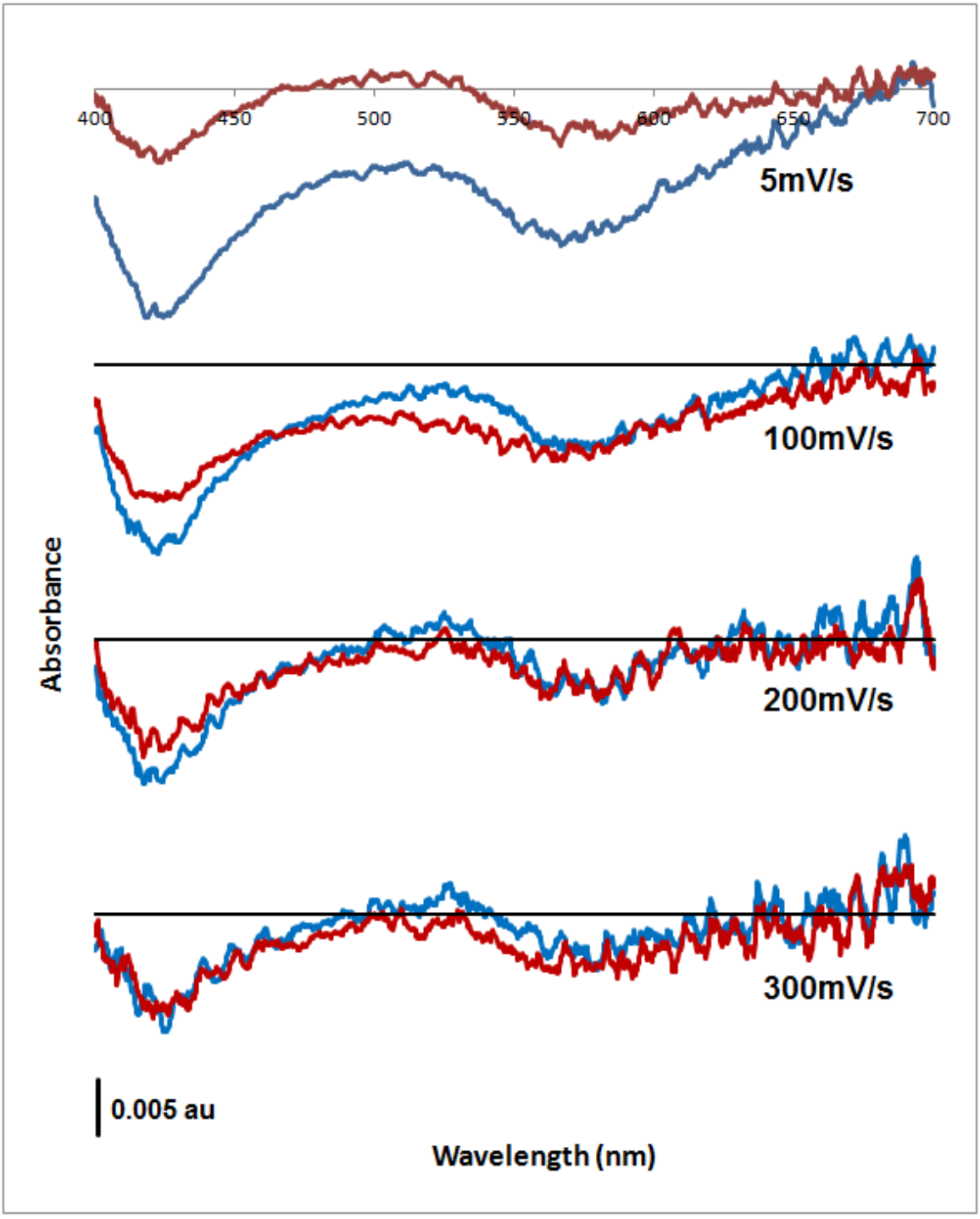

Figure 37: Averaged light spectra taken during a CV with different scan rates. Each scan rate was offset for clarity. For each scan rate the blue line was taken at the switching potential and the red line was taken at the end of the CV. Both used the respective initial spectra as the reference spectra. The 5 mV/s had a standard deviation of 0.01 A, 100 mV/s had 0.003 A, 200 mV/s had 0.0025 A, and 300 mV/s had 0.002 A.

Each averaged spectra in Figure 37 were taken either at the switching or initial potential of a CV. The current is expected to increase with scan rate.

$$i = (VC)\nu \frac{n^2F^2}{RT} \left\{ \frac{\exp^{\left[\left(\frac{nF}{RT}\right)\left(E-E^o\right)\right]}}{\left(1+\exp^{\left[\left(\frac{nF}{RT}\right)\left(E-E^o\right)\right]}\right)^2} \right\} \quad (21)$$

The total current is expected to increase linearly with scan rate, *v*. The first term is the moles present, the second the scan rate, the third constants, and the final term is exponential decay on either side of the peak. The charge passed is the integrated current. It is expected to be constant with scan rate. At faster scan rates *v* increases and the current increases. The total time however decreases such that

$$\sum idt \quad (22)$$

drops correspondingly.

The total charge during the reduction half of each CV (*i.e.* the area under the curve) was calculated with equation 23 and shown in Table 3.

$$Q = \sum idt \quad (23)$$

In equation 23 Q is the total charge, i is the current, and dt is the change in time. The total charge produced was fixed for each scan rate, which is expected for a surface confined species. However when adjusted for the scan rate each experiment had a similar total charge (~0.5 μC), indicating that the same amount of charge transfer occurs at all measured scan rates. This is in contrast to the absorbance signal. The magnitude of

the absorbance change decreased as scan rate increased. This would suggest that absorbance is responding inequivalently to current, which would suggest it gives different, complementary information.

Scan Rate (mV/s)	Total Charge/Scan Rate (μC/(mV/s))
5	0.572
100	0.593
200	0.557
300	0.575

Table 3. Values from Figure 37. The "Total Charge/Scan Rate" is the total amount of charge during the reduction half of each corresponding CV divided by the scan rate.

The effect of scan rate can be seen more clearly in Figures 38 and 39. Figure 38 re-plots the switching potential spectrum from Figure 37. This shows the slower the scan rate the greater the change in absorbance. Likely as the slower scan rate has more reduction time. Figure 39 shows the spectrum previously shown in Figure 37. The spectra maintained the same order as observed at the switching potential. One notable difference is that the 5 mV/s end spectrum decreased by a greater amount than the spectrum obtained at the switching potential. This is likely due to the greater re-oxidation time. Table 4 shows the time each scan rate spent being reduced and re-oxidized. Overall it appears spectra changed a greater amount when more time is spent under applied potential, whether oxidized or reduced.

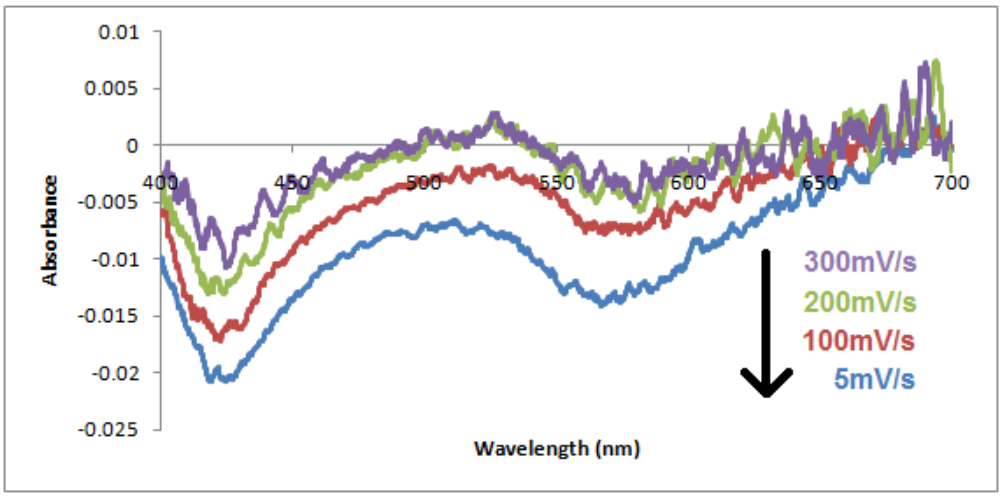

Figure 38: The average absorbance at the CV switching potential for different scan rates. Data shown in Table 3.

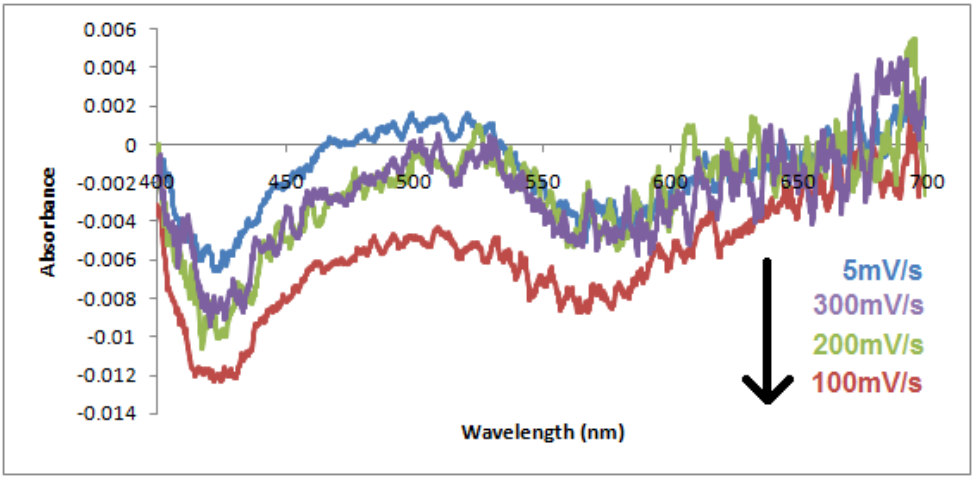

Figure 39: The average absorbance at the end of a CV for different scan rates. Data shown in Table 3.

Scan Rate (mV/s)	Reduction Time (sec)	Re-Oxidation Time (sec)
5	120	80
100	6	4
200	3	2
300	2	1.33

Table 4. CV time spent being reduced and re-oxidized based on formal potential.

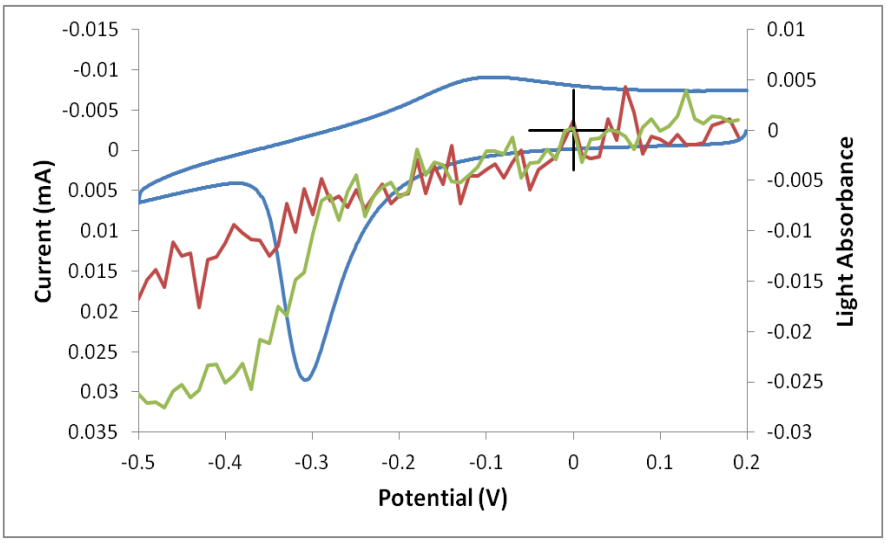

Figure 40: 650 nm (red line) and 419 nm (green line) absorbance during a 5 mV/s CV. The 650 nm and 419 nm absorbance are on the secondary y-axis.

Figure 40 shows the change in absorbance at 650 nm and 419 nm during a single CV. The absorbance at 419 nm was chosen as it is attributed, in this experiment, to the cytochrome c Soret band (see Figure 34). 650 nm was chosen for the same reason that it is commonly used to monitor cell culture growth. It lies outside of the Soret and Q band region. As a result it should be a generic monitor of attachment as compared to oxidation state. As the CV sweeps negative to a reducing potential both absorbances decreased as microbial reduction and detachment was believed to occur. The 419 nm absorbance decreases during the reduction peak and seems to stop decreasing after the peak returns to baseline. If the 419 nm absorbance only changes during the reduction peak then the wavelength may be indicative of an electron transfer event. The 650 nm absorbance steadily decreases during reduction. It is believed that the detachment of microbes would result in less light being reflected, thus decreasing absorbance. The trendline associated with each wavelength indicated that the different light spectra may

measure different events. It is unknown whether the detachment is related to the microbe being reduced or happens due to reaching a potential and is unrelated to electron transfer.

Part VI: Preliminary Experiments Using Thin Clay Films

Preparation of Montmorillonite Clay Suspension

Exploratory experiments were performed with the microorganisms at clay-modified electrodes. The goal was to determine the impact of a small barrier (clay) that is a natural component of microbial environments, on electrochemical activity. Standard clay (Sodium Wyoming Montmorillonite (SWy-1), Source Clay Minerals Repository at Purdue University, Indiana) was prepared by adding about 15 g of powdered clay to 0.5 L of deionized water and stirring periodically for 48 hr. The suspension was then centrifuged at a relative centrifugal force of about 26.5 xg for 6 hr using a Marathon 2100R centrifuge (Fisher Scientific). The supernatant, which contained about 5 g/L clay with a particle size less than 0.2 µm, was decanted and stored in vials. A known volume of this solution was taken and diluted to 1 g/L and stored in a separate vial. The concentration of the clay suspension was estimated by drying a known volume in a pre-weighed beaker and determining the mass of the dried clay.

Preparation of ITO Slide and Clay Film

For experiments that have clay on the ITO slide, the clay coating was applied by first cleaning the ITO slide with isopropyl alcohol, laying it on a flat surface, letting it air

dry, then pipetting 500 µL of a 1 g/L clay solution onto the center of the ITO slide and letting the solution dry overnight, leaving behind a thin clay layer.

Shewanella putrefaciens on a Clay Modified Electrode

A limited amount of experiments were performed with a thin clay layer on an ITO electrode as the majority were performed without a clay coating. Due to the minimal amount of clay modified electrode (CME) experiments the only reportable results are from preliminary testing. This section reports on the experiments utilizing a CME.

The shape of a CV taken on a CME was similar to one taken on a bare electrode, seen in Figure 41. The CME also showed the magnitude of the Faradaic reduction peak is linearly dependent upon scan rate just like the bare electrode experiments, shown in Figure 42. This is consistent with a surface confined reaction, as a diffusion process results in the peak height increasing by the square root of the scan rate, represented by the dashed line in Figure 42. This result indicates direct electron transfer (instead of mediated electron transfer) during the reduction process is operative even in the presence of a thin clay film. When a 500 uL suspension of 5 g/L clay is spread over the surface of the ITO slide it resulted in a clay film thickness of 1.2 µm, as estimated from previous work for the same electrochemical cell and ITO setup. [124]

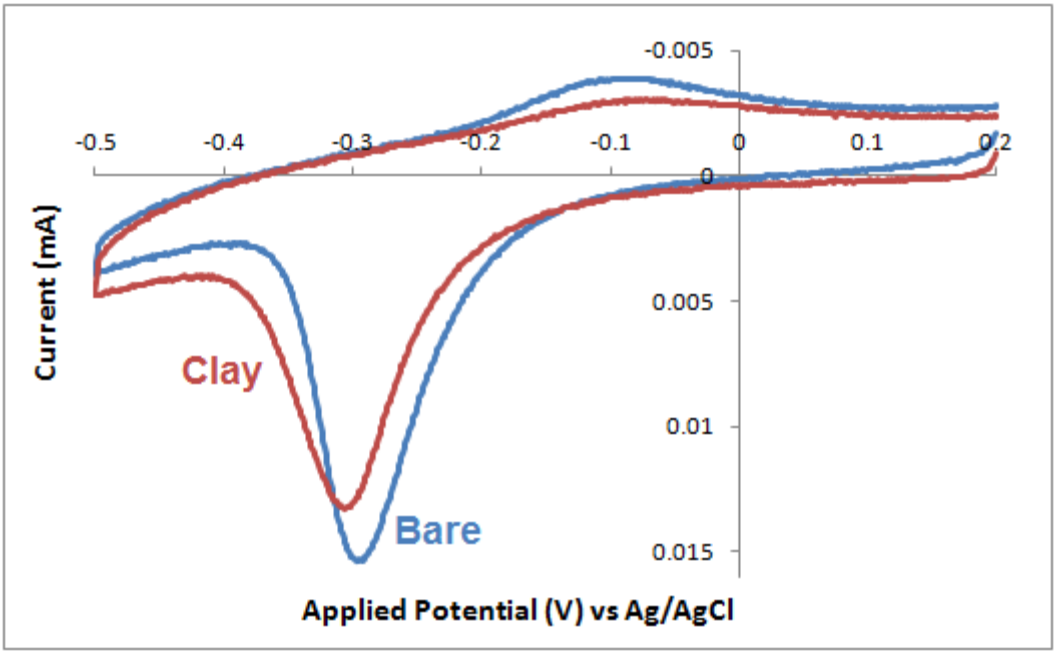

Figure 41: Two separate experiments of 5 mV/s *S. putrefaciens* CVs after 2 hr of 200 mV applied potential. One taken with a thin clay layer on the ITO electrode (denoted as "Clay", OD_{650} 0.799) and one without clay on a bare ITO electrode (denoted as "Bare", OD_{650} 0.483).

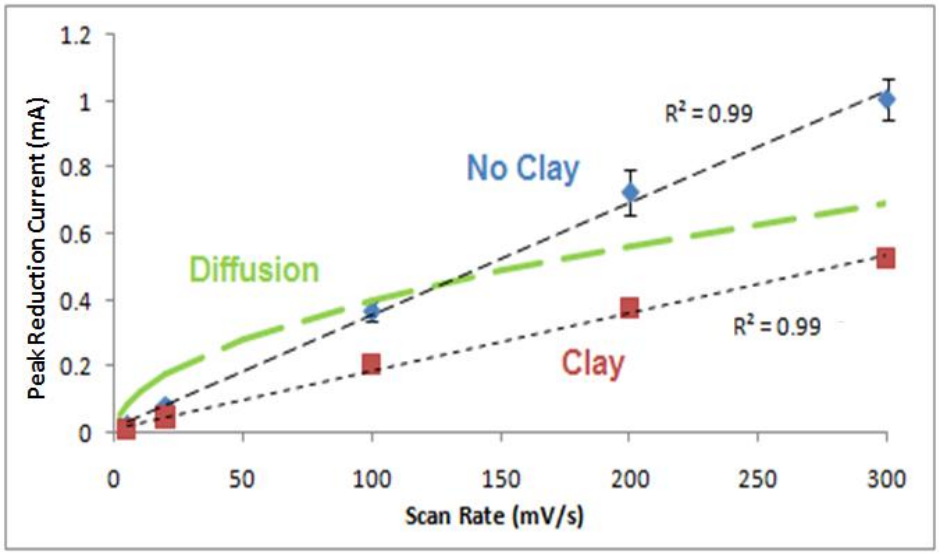

Figure 42: Graph of scan rate vs peak reduction current with and without clay. Corresponding R^2 values are included with each linear trendline. The green dashed line represents a theoretical diffusion curve.

Taking a CV without applying 200 mV potential can result in much smaller peaks, as shown in Figure 43. The purple line, labeled “Bacteria No Applied Potential”, was taken without 200 mV of potential being applied. Contrasting that is the black line, which has much larger peaks, as it was taken after 10 min of 200 mV potential being applied. The results shown in Figure 43 are on a clay coated ITO slide, indicating that the bacteria can be detected even with a thin clay layer on an electrode. The line labeled “Clay Water” was tested with DI water with the same set up. This line is similar in nature to the “Clay TSB” line, which was taken when an autoclaved tryptic soy broth solution was pumped into the cell. All CVs in Figure 43 were taken with the same clay coating. A difference between Figures 11 and 43 is that the CV for water is similar to the tryptic soy broth CV in Figure 43, unlike in Figure 11.

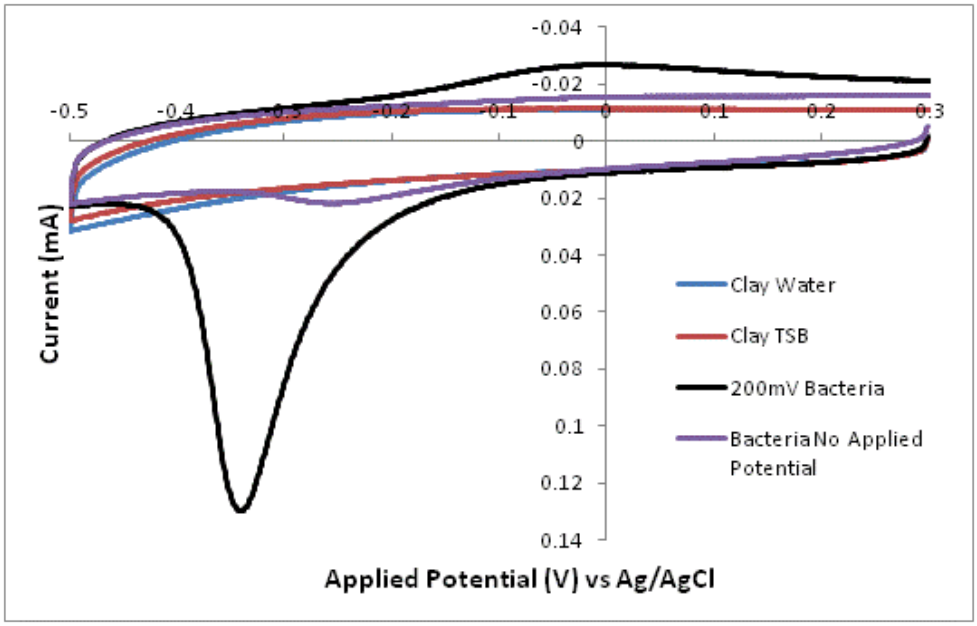

Figure 43: 100 mV/s CV spectra of *S. putrefaciens* compared to a sterile TSB solution and DI water on a clay coated ITO slide. 200 mV was applied for 10 min for the "200 mV Bacteria". No potential was applied for "Bacteria No Applied Potential".

CHAPTER 3

CONCLUSION AND FUTURE WORK

Conclusion

The combination of these experiments indicates that anaerobically grown *S. putrefaciens* attaches to the ITO electrode and undergoes reduction, detachment, and begins reattachment during the CV, though reattachment is incomplete. Attachment was enhanced when a +0.2 V potential was applied. This was expected as literature also indicates that *Shewanella* can recover the ability to transfer electrons to an electrode by having a positive potential applied for an extended time. Without any mediators, planktonic cells, or other electroactive species available the only source of electron transfer would be from the microbes themselves. Scan rate affects the change in light absorbance due to the change in time spent reducing and oxidizing. Evanescent wave spectroscopy can detect purified cytochrome C along with the redox changes of cytochrome C (between ~410-430 nm) and the detachment of microbes (around 650 nm).

Future Work

Further experiments can be performed to further elucidate the optimal conditions for *Shewanella putrefaciens* growth and methodology. When microbes were frozen for future use the culture was captured in the growth phase without regard to OD_{650}. Determining the optimal OD_{650} for freezing could be determined based on how

long it takes a new culture to reach the desired OD_{650} after inoculation. This can be beneficial as frozen samples at different OD_{650} values can be available for when different culture times are needed based on when the experiment will be performed.

Likewise the volume of the TSB used was not optimized. Running growth curves on different volumes of TSB may indicate if the volume alters the time required to reach a certain OD_{650}. This can be combined with a frozen sample mentioned above to prepare a culture overnight and have it ready to be tested at a specific time with a predetermined OD_{650}.

Varying the applied potential, along with the how long it is applied, can affect the necessary attachment time. Literature has demonstrated the effectiveness of up to +0.4 V of applied potential. [19] Testing a greater range may determine when increased potential no longer increases effectiveness but rather poisons the microbe.

The *S. putrefaciens* was always tested with the light source on so it is unknown if the light had an effect on the electrochemistry. Running the electrochemical experiments without any light would determine if there is an electrochemical difference between having the light source on or off.

Increasing the sampling rate of the light spectra to match the sampling rate of the electrochemistry would provide a more in depth examination of data. The light spectra were sampled at a lower rate due to the time intensive nature of deconvoluting the data. Arranging a better system to work through the spectral data would allow for more measurements and have them directly match up with the electrochemistry for

each point throughout the experiment. Likewise the number of light spectra averaged could be changed, which may smooth the change in light absorbance over the course of the experiment and reduce the associate standard deviation.

Using a different microbe in the spectroelectrochemical setup can provide results to analyze the effect of the setup on the experiments. Other microbes are known to be electroactive, such as different members in the genus *Shewanella*, [6] *Pseudomonas,* [6] or *Geobacter*. [82] Likewise instead of using a pure culture of only one microbe, a culture of multiple microbes can be tested to determine if multiple species increase columbic yield. Gates *et al*. [85] demonstrated that a mixture of five *Pseudomonas* species of bacteria was more effective at reducing ferruginous smectites than any of the individual species alone.

S. putrefaciens has been demonstrated to utilize direct electron transfer with no electron mediators found. Adding a mediator may have an effect on experimental results. Having another electron transfer pathway may increase the rate of electron transfer, the current, or possibly even alter the cytochrome concentration within the outer membrane of the microbe. An increase in electron transfer may be seen as sharper, narrower redox peaks and faster changes in light absorbance.

Adding a layer of clay to the ITO slide may affect the attachment and/or electron transfer efficiency of the microbes. Preliminary results indicate a similar shape of a CV though with smaller redox peaks. Adjusting the amount of clay added can determine the ideal clay thickness. Likewise the clay can be changed between montmorillonite,

nontronite, a different clay, or some mixture of clays with the intent of maximizing microbial attachment without reducing current. Adding a mediator may help increase current if it can move through the clay layer to increase electron transfer.

Ultimately testing *S. putrefaciens* in a microbial fuel cell will demonstrate the amount of current that can be produced for electricity generation. The food source used for the microbes could be wastewater or other naturally occurring materials. By using waste products the MFC could generate electricity while performing bioremediation.

REFERENCE LIST

[1] Logan BE, Hamelers B, Rozendal R, Schröder U, Keller J, Freguia S, Aelterman P, Verstraete W, Rabaey K. Microbial fuel cells: methodology and technology. *Environ. Sci. Technol.* 2006, 40, 5181-5192.

[2] Lovley DR. Microbial fuel cells: novel microbial physiologies and engineering approaches. *Curr. Opin. Biotechnol*. 2006, 17, 327-332.

[3] Bennetto HP, Box J, Delaney GM, Mason JR, Roller SD, Stirling JL, Thurston CF. Redox-mediated electrochemistry of whole micro-organisms: from fuel cell to biosensors. In: Turner AFT, Karube I, Wilson GS, editors. Biosensors: fundamentals and applications. Oxford: Oxford University Press. 1987, 291–314.

[4] Chaudhuri SK, Lovley DR. Electricity generation by direct oxidation of glucose in mediatorless microbial fuel cells. *Nat. Biotechnol.* 2003, 21, 1229-1232.

[5] Xiong Y, Shi L, Chen B, Mayer MU, Lower BH, Londer Y, Bose S, Hochella MF, Fredrickson JK, Squier TC. High-affinity binding and direct electron transfer to solid metals by the *Shewanella oneidensis* MR-1 outer membrane c-type cytochrome OmcA. *J. Am. Chem. Soc.* 2006, 128, 13978-13979.

[6] Tayhas G, Palmore R, Whitesides GM. Microbial and enzymatic biofuel cells. In: Himmel ME, Baker JO, Overend RP editors. Enzymatic conversion of biomass for fuels production. Washington, D.C.: American Chemical Society, 1994, 271–290.

[7] Kim BH, Ikeda T, Park HS, Kim HJ, Hyun MS, Kano K, Takagi K, Tatsumi H. Electrochemical activity of an Fe(III)-reducing bacterium, *Shewanella putrefaciens* IR-1, in the presence of alternative electron acceptors. *Biotechnology Techniques.* 1999, 13, 475-478.

[8] Kim BH, Kim HJ, Hyun MS, Park DH. Direct electrode reaction of Fe(III) reducing bacterium, *Shewanella putrefaciens. J Microb Biotech.* 1999, 9, 127–131.

[9] Kim HJ, Hyun MS, Chang IS, Kim BH. A microbial fuel cell type lactate biosensor using a metal-reducing bacterium, *Shewanella putrefaciens. J Microbiol Biotechnol.* 1999, 9, 365–367.

[10] Palmore GTR, Bertschy H, Bergens SH, Whitesides GM. A methanol/dioxygen biofuel cell that uses NAD+-dependant dehydrogenases as catalysts: application of an electro-enzymatic method to generate nicotinamide adenine dinucleotide at low over potential. *J Electroanal Chem.* 1998, 443, 155–161.

[11] Siebel D, Bennetto HP, Delaney GM, Mason JR, Stirling JL, Thurston CF. Electron-transfer coupling in microbial fuel cells: 1. Comparison of redox-mediator reduction rates and respiratory rates of bacteria. *J Chem Tech Biotechnol.* 1984, 34B, 3–12.

[12] Kim HJ, Park HS, Hyun, MS, Chang IS, Kim M, Kim BH. A mediator-less microbial fuel cell using a metal reducing bacterium *Shewanella putrefaciens. Enzyme and Microbial Technology.* 2002, 30, 145-152.

[13] Rabaey K, Lissens G, Siciliano SD, Verstraete W. A microbial fuel cell capable of converting glucose to electricity at high rate and efficiency. *Biotechnol. Lett.* 2003, 25, 1531-1535.

[14] Wang X, Feng Y, Ren N, Wang H, Lee H, Li N, Zhao Q. Accelerated start-up of two-chambered microbial fuel cells: Effect of anodic positive poised potential. *Electrochimica Acta*. 2009, 54, 1109-1114.

[15] Hyun MS, Kim BH, Chang IS, Park HS, Kim HJ, Kim GT, Park DH. Isolation and identification of metal-reducing bacterium, *Shewanella putrefaciens* IR-1. *Kor J Microbiol.* 1999, 37, 206–212.

[16] Torres CI, Krajmalnik-Brown R, Parameswaran P, Marcus AK, Wanger G, Gorby YA, Rittmann BE. Selecting anode-respiring bacteria based on anode potential: phylogenetic, electrochemical, and microscopic characterization. *Energy Environ. Sci*. 2009, 43, 9519–9524.

[17] Cho EJ, Ellington AD. Optimization of the biological component of a bioelectrochemical cell. *Bioelectrochemistry.* 2007, 70, 165–172.

[18] T Goto, T Matsuno, M Hishinuma-Narisawa, K Yamazaki, H Matsuyama, N Inoue, I Yumoto. Cytochrome c and bioenergetic hypothetical model for alkaliphilic *Bacillus* spp. *Journal of Bioscience and Bioengineering*. 2005, Vol 100, Issue 4, 365-379.

[19] Carmona-Martinez AA, Harnisch F, Kuhlicke U, Neu TR, Schroder U. Electron transfer and biofilm formation of *Shewanella putrefaciens* as function of anode potential. *Bioelectrochemistry*. 2012, 93, 23-29.

[20] Carmona-Martínez AA, Harnisch F, Fitzgerald LA, Biffinger JC, Ringeisen BR, Schröder U. Cyclic voltammetric analysis of the electron transfer of *Shewanella oneidensis* MR-1 and nanofilament and cytochrome knock-out mutants. *Bioelectrochemistry.* 2011, 81, 74–80.

[21] Harris HW, El-Naggar MY, Bretschger O, Ward MJ, Romine MF, Obraztsova AY, Nealson KH. Electrokinesis is a microbial behavior that requires extracellular electron transport. *Proc. Natl. Acad. Sci. U.S.A.* 2010, 107, 326–331.

[22] Liu H, Matsuda S, Kato S, Hashimoto K, Nakanishi S. Redox-responsive switching in bacterial respiratory pathways involving extracellular electron transfer. *ChemSusChem.* 2010, 3, 1253–1256.

[23] Liu H, Matsuda S, Kawai T, Hashimoto K, Nakanishi S. Feedback stabilization involving redox states of c-type cytochromes in living bacteria. *Chem. Commun.* 2011, 47, 3870–3872.

[24] Aelterman P, Freguia S, Keller J, Verstraete W, Rabaey K. The anode potential regulates bacterial activity in microbial fuel cells. *Appl. Microbiol. Biotechnol*. 2008, 78, 409.

[25] Bond DR, Lovley DR. Electricity production by *Geobacter sulfurreducens* attached to electrodes. *Appl. Environ. Microbiol.* 2003, 69, 1548-1555.

[26] Eggleston CM, Voros J, Shi L, Lower BH, Droubay TC, Colberg PJS. Binding and direct electrochemistry of OmcA, an outer-membrane cytochrome from an iron reducing bacterium, with oxide electrodes: A candidate biofuel cell system. *Inorganica Chimica Acta.* 2008, 361, 769-777.

[27] Heidelberg JF, Paulsen IT, Nelson KE, Gaidos EJ, Nelson WC, Read TD, Eisen JA, Seshadri R, Ward N, Methe B, Clayton RA, Meyer T, Tsapin A, Scott J, Beanan M, Brinkac L, Daugherty S, DeBoy RT, Dodson RJ, Durkin AS, Haft DH, Kolonay JF, Madupu R, Peterson JD, Umayam LA, White O, Wolf AM, Vamathevan J, Weidman J, Impraim M, Lee K, Berry K, Lee C, Mueller J, Khouri H, Gill J, Utterback TR, McDonald LA, Feldblyum TV, Smith HO, Venter JC, Nealson KH, Fraser CM. Genome sequence of the dissimilatory metal ion-reducing bacterium *Shewanella oneidensis*. *Nat. Biotechnol.* 2002, 20, 1118-1123.

[28] Methé BA, Nelson KE, Eisen JA, Paulsen IT, Nelson W, Heidelberg JF, Wu D, Wu M, Ward N, Beanan MJ, Dodson RJ, Madupu R, Brinkac LM, Daugherty SC, DeBoy RT, Durkin AS, Gwinn M, Kolonay JF, Sullivan SA, Haft DH, Selengut J, Davidsen TM, Zafar N, White O, Tran B, Romero C, Forberger HA, Weidman J, Khouri H,

Feldblyum TV, Utterback TR, Van Aken SE, Lovley DR, Fraser CM. Genome of *Geobacter sulfurreducens*: metal reduction in subsurface environments. *Science.* 2003, 302, 1967-1969.

[29] Gorby YA, Lovley DR. Electron Transport in the Dissimilatory Iron Reducer, GS-15. *Appl. Environ. Microbiol.* 1991, 57, 867-870.

[30] Beliaev AS, Saffarini D, *Shewanella putrefaciens* mtrB encodes an outer membrane protein required for Fe(III) and Mn(IV) reduction. *J. Bacteriol.* 1998, 180, 6292-6297.

[31] Field SJ, Dobbin PS, Cheesman MR, Watmough NJ, Thomson AJ, Richardson DJ. Purification and magneto-optical spectroscopic characterization of cytoplasmic membrane and outer membrane multiheme c-type cytochromes from *Shewanella frigidimarina* NCIMB400. *J. Biol. Chem.* 2000, 275, 8515-8522.

[32] Myers CR, Myers JM. Cell surface exposure of the outer membrane cytochromes of *Shewanella oneidensis* MR-1. Lett. Appl. Microbiol. 2003, 37, 254-258.

[33] Gaspard S, Vazquez F, Holliger C. Localization and solubilization of the Iron(III) reductase of *Geobacter sulfurreducens*. *Appl. Environ. Microbiol*. 1998, 64, 3188-3194.

[34] Seeliger S, Cord-Ruwisch R, Schink B. A periplasmic and extracellular c-type cytochrome of *Geobacter sulfurreducens* acts as a ferric iron reductase and as an electron carrier to other acceptors or to partner bacteria. *J. Bacteriol*. 1998, 180, 3686-3691.

[35] Magnuson TS, Isoyama N, Hodges-Myerson AL, Davidson G, Maroney MJ, Geesey GG, Lovley DR. Isolation, characterization and gene sequence analysis of a membrane-associated 89 kDa Fe(III) reducing cytochrome c from *Geobacter sulfurreducens*. *Biochem. J.* 2001, 359, 147-152.

[36] Park DH, Kim BH, Growth Properties of the Iron-Reducing Bacteria. *Shewanella putrefaciens* IR-1 and MR-1 Coupling to Reduction of Fe(III) to Fe(II). *The Journal of Microbiology*. 2001, 39**,** No 4, 273-278.

[37] Bretschger O, Cheung ACM, Mansfeld F, Nealson KH. Comparative Microbial Fuel Cell Evaluations of *Shewanella* spp. *Electroanalysis*. 2010, 22, No 7-8, 883-894.

[38] Lower BH, Yongsunthon R, Shi L, Wildling L, Gruber HJ, Wigginton NS, Reardon CL, Pinchuk GE, Droubay TC, Boily JF, and Lower SK. Antibody Recognition Force Microscopy Shows that Outer Membrane Cytochromes OmcA and MtrC are

Expressed on the Exterior Surface of *Shewanella oneidensis* MR-1. *Applied and Environmental Microbiology.* 2009, Vol. 75, No 9, 2931-2935.

[39] Rivera M, Wells MA, Walker FA. Cation-promoted cyclic voltammetry of recombinant rat outer mitochondrial membrane cytochrome *b5* at a gold electrode modified with mercaptopropionic acid. *Biochem.* 1994, 33, 2161–2170.

[40] Millo D , Harnisch F, Patil SA, Ly HK, Schröder U, Hildebrandt P. In situ spectroelectrochemical investigation of electrocatalytic microbial biofilms by surface-enhanced resonance Raman spectroscopy, *Angew. Chem. Int. Ed.* 2011, 50, 2625–2627.

[41] Strycharz SM, Malanoski AP, Snider RM, Yi H, Lovley DR, Tender LM. Application of cyclic voltammetry to investigate enhanced catalytic current generation by biofilm-modified anodes of *Geobacter sulfurreducens* strain DL1 vs. variant strain KN400. *Energy Environ. Sci.* 2011, 4, 896–913.

[42] Inoue K, C. Leang, Franks AE, Woodard TL, Nevin KP, Lovley DR. Specific localization of the c-type cytochrome OmcZ at the anode surface in current-producing biofilms of Geobacter sulfurreducens. *Environ. Microbiol. Rep.* 2011, 3, 211–217.

[43] Kim BH, Park HS, Kim HJ, Kim GT, Chang IS, Lee J, Phung NT. Enrichment of microbial community generating electricity using a fuel-cell-type electrochemical cell. *Appl. Microbiol. Biotechnol*. 2004, 63, 672-681.

[44] Malvankar NS, Vargas M, Nevin KP, Franks AE, Leang C, Kim BC, Inoue K, Mester T, Covalla SF, Johnson JP, Rotello VM, Tuominen MT, Lovley DR. Tunable metallic-like conductivity in microbial nanowire networks. *Nat. Nanotechnol.* 2011, 6, 573–579.

[45] Reguera G, McCarthy KD, Mehta T, Nicoll JS, Tuominen MT, Lovley DR. Extracellular electron transfer via microbial nanowires. *Nature* 2005, 435, 1098–1101.

[46] El-Naggar MY, Wanger G, Leung KM, Yuzvinsky TD, Southam G, Yang J, Lau WM, Nealson KH, Gorby YA. Electrical transport along bacterial nanowires from *Shewanella oneidensis* MR-1. *Proc. Natl. Acad. Sci. U.S.A.* 2010, 107, 18127–18131.

[47] Gorby YA, Yanina S, McLean JS, Rosso KM, Moyles D, Dohnalkova A, Beveridge TJ, Chang IS, Kim BH, Kim KS, Culley DE, Reed SB, Romine MF, Saffarini DA, Hill EA, Shi L, Elias DA, Kennedy DW, Pinchuk G, Watanabe K, Ishii SI, Logan B, Nealson KH, Fredrickson JK. Electrically conductive bacterial nanowires produced by *Shewanella oneidensis* strain MR-1 and other microorganisms. *Proc. Natl. Acad. Sci. U.S.A.* 2006, 103, 11358–11363.

[48] Myers JM, Nealson KH. Bacterial Manganese Reduction and Growth with Manganese Oxide as the Sole Electron Acceptor. *Science.* 1988, 240, 1319-1321.

[49] Park DH, Zeikus JG. Electricity generation in microbial fuel cells using neutral red as an electronphore. *Appl Environ Microbiol.* 2000, 66, 1292–1297.

[50] Jiang X, JHu J, Fitzgerald LA, Biffinger JC, Xie P, Ringeisen BR, Lieber CM. Probing electron transfer mechanisms in *Shewanella oneidensis* MR-1 using a nanoelectrode platformand single-cell imaging. *Proc. Natl. Acad. Sci. U.S.A.* 2010, 107, 16806–16810.

[51] Marsili E, Baron DB, Shikhare ID, Coursolle D, Gralnick JA, Bond DR. *Shewanella* secretes flavins that mediate extracellular electron transfer. *Proc. Natl. Acad. Sci. U.S.A.* 2008, 105, 3968–3973.

[52] Rabaey K, Boon N, Höfte M, Verstraete W. Microbial phenazine production enhances electron transfer in biofuel cells. *Environ. Sci. Technol.* 2005, 39, 3401-3408.

[53] Hong, Yi G, Jun GUO, Xu C, Zhi Y, Sun Mei, Guo P. Humic substances act as electron acceptor and redox mediator for microbial dissimilatory azoreduction by *Shewanella decolorationis* S12. *J. Microbiol. Biotechnol.* 2007, 428–437.

[54] Lovley DR, Coates JD, Blunt-Harris EL, Phillips EJP, Woodward JC. Humic substances as electron acceptors for microbial respiration. *Nature.* 1996, 382, 445.

[55] Turick CE, Tisa LS, Caccavo JF. Melanin production and use as a soluble electron shuttle for Fe(III) oxide reduction and as a terminal electron acceptor by *Shewanella algae* BrY. *Appl. Environ. Microbiol.* 2002, 68, 2436–2444.

[56] Turick CE, Beliaev AS, Zakrajsek BA, Reardon CL, Lowy DA, Poppy TE, Maloney A, Ekechukwu AA. The role of 4-hydroxyphenylpyruvate dioxygenase in enhancement of solid-phase electron transfer by *Shewanella oneidensis* MR-1. *FEMS Microbiol. Ecol.* 2009, 68, 223–225.

[57] Lies DP, Hernandez ME, Kappler A, Mielke RE, Gralnick JA, Newman DK. *Shewanella oneidensis* MR-1 uses overlapping pathways for iron reduction at a distance and by direct contact under conditions relevant for biofilms. *Appl. Environ. Microbiol.* 2005, 71, 4414–4426.

[58] von Canstein H, Ogawa J, Shimizu S, Lloyd JR. Secretion of flavins by *Shewanella* species and their role in extracellular electron transfer. *Appl. Environ. Microbiol.* 2008, 74, 615–623.

[59] Biffinger JC, Fitzgerald LA, Ray R, Little BJ, Lizewski SE, Petersen ER, Ringeisen BR, Sanders WC, Sheehan PE, Pietron JJ, Baldwin JW, Nadeau LJ, Johnson GR, Ribbens M, Finkel SE, Nealson KH. The utility of *Shewanella japonica* for microbial fuel cells, *Bioresour. Technol.* 2010, 102, 290–297.

[60] Velasquez-Orta SB, Head IM, Curtis TP, Scott K, Lloyd JR, Von Canstein H. The effect of flavin electron shuttles in microbial fuel cells current production. *Appl. Environ. Microbiol.* 2010, 85, 1373–1381.

[61] Bouhenni RA, Vora GJ, Biffinger JC, Shirodkar S, Brockman K, Ray R, Wu P, Johnson BJ, Biddle EM, Marshall MJ, Fitzgerald LA, Little BJ, Fredrickson JK, Beliaev AS, Ringeisen BR, Saffarini DA. The role of *Shewanella oneidensis* MR-1 outer surface structures in extracellular electron transfer. *Electroanalysis.* 2010, 22, 856–864.

[62] Jiao Y, Qian F, Li Y, Wang G, Saltikov CW, Gralnick JA. Deciphering the electron transport pathway for graphene oxide reduction by *Shewanella oneidensis* MR-1. *J. Bacteriol.* 2011, 193, 3662–3665.

[63] Newton GJ, Mori S, Nakamura R, Hashimoto K, Watanabe K. Analyses of current-generating mechanisms of *Shewanella loihica* PV-4 and *Shewanella oneidensis* MR-1 in microbial fuel cells. *Appl. Environ. Microbiol.* 2009, 75, 7674–7681.

[64] Li SL, Freguia S, Liu SM, Cheng SS, Tsujimura S, Shirai O, Kano K. Effects of oxygen on *Shewanella decolorationis* NTOU1 electron transfer to carbon-felt electrodes. *Biosens. Bioelectron.* 2010, 25, 2651–2656.

[65] Harnisch F, Rabaey K. The diversity of techniques to study electrochemically active biofilms highlights the need for standardization, *ChemSusChem.* 2012, 5, 1027-1038

[66] Itoh K, Fijishima A. An Application of Optical Waveguide to Electrochemistry: Construction of Optical Waveguide Electrodes. *J. Phys. Chem.* 1988, 92, 7043-7045.

[67] Bradshaw JT, Mendes SB, Saavedra SS. Waveguide Spectroscopy, Improvements Make it Feasible to Obtain Absorbance Spectra of Thin Films and Submonolayers for Thin-Film Characterization and Chemical and Biochemical Sensing. *Anal. Chem. A Pages.* 2005, 29-36.

[68] DiVirgilio-Thomas JM, Heineman WR, Seliskar CJ. Spectroelectrochemical Sensing Based on Multimode Selectivity Simultaneously Achievable in a Single Device. 6. Sensing with a Mediator. *Anal. Chem.* 2000, 72, 3461-3467.

[69] Dunphy DR, Mendes SB, Saavedra SS, Armstrong NR. The Electroactive Integrated Optical Waveguide: Ultrasensitive Spectroelectrochemistry of Submonolayer Adsorbates. *Anal. Chem.* 1997, 69, 3086-3094.

[70] Chih T, Jao H-J, Wang CM. Glucose sensing based on an effective conversion of O_2 and H_2O_2 into superoxide anion radical with clay minerals. *J Electroanal Chem*. 2005, 581, 159–166.

[71] Mousty C, Cosnier S, Lopez MS-P, Lopez-Cabarcos E, Lopez-Ruiz B. Rutin Determination at an Amperometric Biosensor. *Electroanalysis*. 2007, 19, 253–258.

[72] Ross SE, Seliska CJ, Heineman WR. Spectroelectrochemical Sensing Based on Multimode Selectivity Simultaneously Achievable in a Single Device. 9. Incorporation of Planar Waveguide Technology. *Anal. Chem.* 2000, 72, 5549-5555.

[73] Saavedra SS, Reichart WM. Integrated Optical Attenuated Total Reflection Spectrometry of Aqueous Superstrates Using Prism-Couple Polymer Waveguides. *Anal. Chem.* 1990, 62, 2251-2256.

[74] Currel G. *Analytical Instrumentation Performance Characteristics and Quality*; John Wiley & Sons, Inc.: England, 2000, pp 67-241.

[75] Robinson JW. *Undergraduate Instrumentation Analysis*, 5th Ed.; Mercel Dekker, Inc.: New York, 1995, pp 386-766.

[76] Strobel HA, Heineman WR. *Chemical Instrumentation: A Systematic Approach*, 3rd Ed.; John Wiley & Sons, Inc.: New York, 1989, pp 302-1112.

[77] Shi L, Chen B, Wang Z, Elias DA, Mayer MU, Gorby YA, Ni S, Lower BH, Kennedy DW, Wunschel DS, Mottaz HM, Marshall MJ, Hill EA, Beliaev AS, Zachara JM, Fredrickson JK, Squier TC. Isolation of a high-affinity functional protein complex between OmcA and MtrC: Two outer membrane decaheme c-type cytochromes of *Shewanella oneidensis* MR-1. *J. Bacteriol.* 2006, 188, 4705-4714.

[78] Wigginton NS, Rosso KM, Lower BH, Shi L, Hochella MF. Electron tunneling properties of outer-membrane decaheme cytochromes from *Shewanella oneidensis*. *Geochim. Cosmochim. Acta* 2007, 71, 543–555.

[79] Lower BH, Shi L, Yongsunthon R, Droubay TC, McCready DE, Lower SK. Specific bonds between an iron oxide surface and outer membrane cytochromes MtrC and OmcA from *Shewanella oneidensis* MR-1. *J. Bacteriol.* 2007, 189, 4944–4952.

[80] Roberts JA, Fowle DA, Hughes BT, Kulczycki E. Attachment Behavior of *Shewanella putrefaciens* onto Magnetite under Aerobic and Anaerobic Conditions. *Geomicrobiology Journal*. 2006, 23, 631-640

[81] Luttge, A., and Conrad, P. G., 2004, Bacterial control of calcite dissolution kinetics: Applied and Environmental Microbiology, v. 70, p. 1627–1637.

[82] Luttge A, Zhang L, Nealson KH. Mineral Surfaces and their Impications for Microbial Attachment: Results from Monthe Carlo Simulations and Direct Surface Observations. *American Journal of Science*. 2005, 305, 766-790

[83] Stucki J.W. and Getty P.J. Microbial reduction of iron in nontronite. In: Agronomy Abstracts, 1986 annual meetings of the Soil Science Society of America. 1986, 279

[84] Komadel P., Stucki J.W. and Wilkinson H.T. Reduction of structural iron in smectites by microorganisms. The Sixth Meeting of the European Clay Groups Sevilla, 1987, 322-324.

[85] Gates W.P., Wilkinson H.T. and Stucki J.W. Swelling properties of microbially reduced ferruginous smectite. *Clays and Clay Minerals*. 1993, 41, 360-364.

[86] Mousty C. Biosensing applications of clay-modified electrodes: a review. *Anal Bioanal Chem.* 2010, 396, 315-325.

[87] Vo-Dinh T, Cullum B. Biosensors and biochips: advances in biological and medical diagnostics. *Fresenius J Anal Chem*. 2000, 366, 540–551.

[88] Baeumner AJ. Biosensors for environmental pollutants and food contaminants. *Anal Bioanal Chem.* 2003, 377, 434–445.

[89] Ahuja T, Mir IA, Kumar D, Rajesh. Biomolecular immobilization on conducting polymers for biosensing applications. *Biomaterials*. 2007, 28, 791–805.

[90] Cosnier S. Biosensors based on electropolymerized films: new trends. Anal Bioanal Chem. 2003, 377, 507–520.

[91] Cosnier S. Affinity biosensors based on electropolymerized films. *Electroanalysis*. 2005, 17, 1701–1715.

[92] Cosnier S. Recent advances in biological sensors based on electrogenerated polymers: A review. *Anal Lett.* 2007, 40, 1260–1279.

[93] Tripathi VS, Kandilalla VB, Ju H. Preparation of ormosil and its applications in the immobilizing biomolecules. *Sens Actuators B*. 2006, 114, 1071–1082.

[94] Jin W, Brennan JD. Properties and applications of proteins encapsulated within sol–gel derived materials. *Anal Chim Acta.* 2002, 461, 1–36.

[95] Kandimalla VB, Tripathi VS, Ju H. Immobilization of biomolecules in sol-gels: biological and analytical applications. *Crit Rev Anal Chem.* 2006, 36, 73–106.

[96] Gupta R, Chaudhury NK. Entrapment of biomolecules in sol-gel matrix for applications in biosensors: problems and future prospects. Biosens Bioelectron. 2007, 22, 2387–2399.

[97] Walcarius A, Kuhn A. Ordered porous thin films in electrochemical analysis. *Trends Anal Chem.* 2008, 27, 593–603.

[98] Walcarius A. Template-directed porous electrodes in electroanalysis. *Anal Bioanal Chem.* 2010, 396, 261-272

[99] Feng J-J, Xu J-J, Chen H-Y. Synergistic effect of zirconium phosphate and Au nanoparticles on direct electron transfer of hemoglobin on glassy carbon electrode. *J Electroanal Chem*. 2005, 585, 44–50.

[100] Geng LN, Wang X, Li N, Xiang MH, Li K. Characterization of hemoglobin immobilized on gamma-zirconium phosphate. *Colloids Surf.* 2004, 34, 231–238

[101] Park S, Chung TD, Kang SK, Jeong R-A, Boo H, Kim HC. Glucose sensor based on glucose oxidase immobilized by zirconium phosphate. *Anal Sci*. 2004, 20, 1635–1638.

[102] Yang F, Ruan C, Xu J, Lei C, Deng J. An amperometric biosensor using toluidine blue as an electron transfer mediator intercalated in α-zirconium phosphate-modified horseradish peroxidase immobilization matrix. *Fresenius J Anal Chem*. 1998, 361, 115–118.

[103] Zhang Y, Chen X, Yang W. Direct electrochemistry and electrocatalysis of myoglobin immobilized in zirconium phosphate nanosheets film. (2008) *Sens Actuators B.* 2008, 130, 682–688.

[104] Stucki JW. Properties and Behaviour of Iron in Clay Minerals. In: Bergaya F, Theng BKG, Lagaly G (ed) Handbook of clay science. *Elsevier*. 2006, 423–475.

[105] Mousty C. Sensors and biosensors based on clay-modified electrodes - new trends. *Appl Clay Sci.* 2004, 27, 159–177.

[106] Gianfreda L, Rao MA, Sannino F, Saccomandi F, Violante A. Enzymes in soil: preperties, behavior and potential applications. *Dev Soil Sci* 2002, 28B, 301–327.

[107] Mousty C, Therias S, Forano C, Besse J-P. Anion-exchanging clay-modified electrodes: synthetic layered double hydroxides intercalated with electroactive organic anions. *J Electroanal Chem*. 1994, 374, 63–69

[108] Therias S, Mousty C, Forano C, Besse JP. Electrochemical transfer at anionic clay modified electrodes: case of 2,2'-azinobis(3-ethylbenzothiazoline-6-sulfonate). *Langmuir*. 1996, 12, 4914–4920.

[109] Morlat-Therias S, Mousty C, Palvadeau P, Molinie P, Leone P, Rouxel J, Taviot-Gueho C, Ennaqui A, de Roy A, Besse JP. Concomitant Intercalation and Decomplexation of Ferrocene Sulfonates in Layered Double Hydroxides. *J Solid State Chem*. 1999, 144, 143–151.

[110] Kwak SY, Jeong YJ, Park JS, Choy JH. Bio-LDH nanohybrid for gene therapy. *Solid State Ionics*. 2002, 151, 229-234.

[111] Therias S, Lacroix B, Schollhorn B, Mousty C, Palvadeau P. Electrochemical study of ferrocene and nitroxide derivatives intercalated in Zn-Cr and Zn-Al layered double hydroxides. *J Electroanal Chem*. 1998, 454, 91–97.

[112] Forano C, Vial S, Mousty C. Nanohybrid Enzymes - Layered Double Hydroxides: Potential Applications. *Curr NanoSci*. 2006, 2, 283–294.

[113] Cosnier S, Gondran C, Senillou A, Graetzel M, Vlachopoulos N. Mesoporous TiO2 films: New catalytic electrode fabricating amperometric biosensors based on oxidases. *Electroanalysis*. 1997, 9, 1387–1392.

[114] Besombes JL, Cosnier S, Labbé P. Improvement of poly(amphiphilic pyrrole) enzyme electrodes via the incorporation of synthetic laponite-clay-nanoparticles. *Talanta*. 1997, 44, 2209–2215.

[115] Besombes JL, Cosnier S, Labbé P, Reverdy G. Improvement of the analytical characteristics of an enzyme electrode for free and total cholesterol via laponite clay additives. *Anal Chim Acta*. 1995, 317, 275–280.

[116] Cosnier S, Mousty C, Gondran C, Lepellec A. Entrapment of enzyme within organic and inorganic materials for biosensor applications: Comparative study. (2006) *Mater Sci Eng C*. 2006, 26, 442–447.

[117] Poyard S, Jaffrezic-Renault N, Martelet C, Cosnier S, Labbé P, Besombes JL. A new method for the controlled immobilization of enzyme in inorganic gels (laponite) for amperometric glucose biosensing. *Sens Actuators B*. 1996, 33, 44–49.

[118] Shyu S-C, Wang CM. Characterizations of Iron-Containing Clay Modified Electrodes and Their Applications for Glucose Sensing. *J Electrochem Soc*. 1988, 145, 154–158.

[119] Senillou A, Jaffrezic N, Martelet C, Cosnier S. A laponite clay-poly(pyrrole-pyridinium) matrix for the fabrication of conductimetric microbiosensors. *Anal Chim Acta*. 1999, 401, 117–124.

[120] McCullough NB. Laboratory tests in the diagnosis of brucellosis. *Amer. J. of Public Health*. 1949, 39, 866-869.

[121] Wang H., Hollywood K., Jarvis R.M., Lloyd J.R., and Goodacre R. (2010) Phenotypic Characterization of *Shewanella oneidensis* MR-1 under Aerobic and Anaerobic Growth Conditions by Using Fourier Transform Infrared Spectroscopy and High-Performance Liquid Chromatography Analyses. *Applied and Environmental Microbiology*. 2010, 76, 18, 6266-6276.

[122] Castle RJ and Nemeth-Harn PEJ. Aerobic Vs. Anaerobic. 2007-04-10. http://www.wwdmag.com/aeration/aerobic-vs-anaerobic

[123] R.G. Bates and J.B. MacAskill, "Standard Potential of the Silver-Silver Chloride Electrode", *Pure & Applied Chem*. Vol. 50, pp. 1701—1706.

[124] Evanescent Wave Spectroelectrochemical Studies on Clay Film: Structure, Topography, and Utilization. Diss. Agyeman, Augustine Ofori. Loyola University Chicago, 2007. 2007. 3295441.

[125] Moulton S.E., Barisci J.N., Bath A., Stella R., and Wallace G.G. (2005) Investigation of Ig.G Adsorption and the Effect on Electrochemical Responses at Titanium Dioxide Electrode. Langmuir, 21 (1) p. 316-322.

[126] Poortinga A.T., Bos R., and Busscher H.J. (2001) Reversibility of Bacterial Adhesion at an Electrode Surface. Langmuir, 17 (9), p. 2851-2856.

[127] Wang WY and Wang CM. Nanocystalline Tin-Oxide Modified Electrodes and Their Electrochemical Characterization. *J. Chin. Chem. Soc.* 2000, 47, 2, 405-414.

[128] Barhoumi H, Maaref A, Rammah M, Martelet C, Jaffrezic N, Mousty C, Vial S, Forano C. Urea biosensor based on Zn3Al–Urease layered double hydroxides nanohybrid coated on insulated silicon structures. *Mater Sci Eng C*. 2006, 26, 328–333.

[129] Shan D, Mousty C, Cosnier S, Mu S. A New Polyphenol Oxidase Biosensor Mediated by Azure B in Laponite Clay Matrix. *Electroanalysis.* 2003 15, 1506–1512.

[130] Guadagnini L, Ballarin B, Mignani A, Scavetta E, Tonelli D. Microscopy techniques for the characterization of modified electrodes in the development of glucose biosensors. Sens Actuators B. 2007, 126, 492–498.

[131] Wang J. Electrochemical Glucose Biosensors. *Chem Rev*. 2008, 108, 814–825

[132] Fitch A, Du J, Gan H, Sucki JW. Effect of Clay Charge on Swelling: A Clay-Modified Electrode Study. *Clays and Clay Minerals*. 1995, 43, 5, 607-614.

[133] Fitch A. Clay-Modified Electrodes: A Review. *Clays and Clay Minerals*. 1990, 38, 4, 391-400.

[134] Macha SM and Fitch A. Clays as Architectural Units at Modified-Electrodes. *Mikrochim. Acta.* 1998, 128, 1-18.

[135] Kwan P, Schmitt D, Volosin AM, McIntosh CL, Seo DK, Jones AK. Spectroelectrochemistry of cytochrome C and azurinimmobilized in nanoporous antimony-doped tin oxide. *Chem. Commun.* 2011, 47, 12367-12369.

[136] Liu Y, Kim H, Franklin RR, Bond DR. Linking Spectral and Electrochemical Analysis to Monitor c-type Cytochrome Redox Status in Living *Geobacter sulfurreducens* Biofilms. *Chem Phys Chem.* 2011, 12, 2235-2241.

[137] Betschger O, Cheung ACM, Mansfeld F, Nealson KH. Comparative Microbial Fuel Cell Evaluations of *Shewanella* spp. *Electroanalysis.* 2010, 22, 7-8, 883-894.

VITA

Jonathan L. Muscolino was born and raised in the southwest suburbs of Chicago, Illinois. He attended Lyons Township High School before enrolling at Loyola University Chicago where he earned a Bachelors of Science in Chemistry degree. In 2007 he attended a chemistry Research Experience for Undergraduates at Virginia Commonwealth University. After completing his undergraduate degree in 2010 he enrolled in the graduate chemistry program at Loyola University Chicago where he researched in the lab of Dr. Alanah Fitch.